東海大學化學研究所

碩士學位論文

Department of Chemistry Tunghai University

Master Thesis

Novel hole transporting materials with electron withdrawing moiety for perovskite solar cells

以拉電子基為核心架構之新型電洞傳輸材料應用於鈣鈦礦太陽能電池

陳羿君

Yih-Chun Chen

指導教授：張源杰 博士

Advisor: Yuan Jay Chang, Ph.D.

中華民國一百零六年七月

July, 2017

ACKNOWLEDGEMENTS

First of all, I appreciate that Professor Chin-Hsin Chen's, Chin-Wei Lu's, Diyan Wang's and Yuan Jay Chang's effort and comment as part of my presentation committee.

Next, I would like to thank Professor Yuan Jay Chang for accepting me as an undergraduate intern student and graduate student, for letting me have the opportunity to gain further insight into organic chemistry and solar cell development. I'm also grateful to him for introducing me to the laboratory of Professor Tahsin J. Chow and Shin-Sheng Sun in Academia Sinica, and providing me such a good experimental environment to learn in.

Furthermore, I'm also thankful for the guidance of Professor Yuan Jay Chang, leading me to independently face problems, study from mistakes and find solutions. I also learned how to deal with problems and cultivate patience and concentration. In addition, I have to thank Professor Hao Ming Chen and his student Bo An Chen for providing material and teaching me fabrication of perovskite solar cells. Besides, I also want to thank Ching-Ting Chien, Yan-Duo Lin, Po-Ting Chou, Bo-Yu Ke and Tingyu Li, the seniors from Academia Sinica, and every member of Jay's lab, for helping me to solve experimental problems and for accompanying me through hard times during my Master degree.

Finally, the person that I am grateful to the most are my parents, being there to support me so that I could finish my Master degree without any worry. I appreciate all the help from everyone again, I could not be here without all of you. Thank you.

ABSTRACT

Seven novel hole transporting materials, **Yih-1~7**, based on electron withdrawing core had been designed and synthesized. Cruciform-shaped core is widely used in hole transporting layer for perovskite solar cells, according to the well-known material, **Spiro-OMeTAD**. Therefore, **Yih-3~7** were synthesized, which are based on cruciform-shaped core, 1,1,2,2-tetraphenylethene, dibenzo[g,p]chrysene and 10'H-spiro[fluorene-9,9'-phenanthren]-10'-one, and modified with different donors, bis(4-methoxyphenyl)amine and 10-(4-(hexyloxy)phenyl)-10H-phenothiazine. Compared with cruciform-shaped core, planar core is springing up in recent years, due to strong intermolecular interaction, which indicates a great potential to show high hole mobility instead of adding additives. On account of this concept, **Yih-1** and **Yih-2** were synthesized based on anthracene-9,10-dione, modified with two different donors, bis(4-methoxyphenyl)aniline and bis(4-methoxyphenyl)amine. Most of the **Yih-** series HTMs show the absorption bands in the visible region, which could act as both light harvesting and hole transporting layers in perovskite solar cells. In addition, all of their HOMO levels are lower than that of **spiro-OMeTAD**, which could enhance the open circuit voltage (V_{oc}) value. Most of their thermal stability are on par with **spiro-OMeTAD**, especially for **Yih-4** and **Yih-6**. The performance of devices based on **Yih-** series HTMs are anticipated to reach the certain values.

List of Publications

1. **Yih-Chun Chen**, Yan-Zuo Lin, Yu-Ting Cheng, Yuan Jay Chang,* "Synthesis of novel isophorone-based dyes for dye-sensitized solar cells" *RSC Advances*, **2015**, *5*, 96428-96436.

2. **Yih-Chun Chen**, Motonori Watanabe*, Yuh-Sheng Wen, Yuan Jay Chang*, "Crystal structure of racemic 2,7-dibromo-10'H-spiro[fluorene-9,9'-phenanthren]-10'-one" *IUCrData*, **2017**, *2*, x170301.

TABLE OF CONTENTS

List of Figures

List of Tables

List of NMR Spectra

Chapter 1 Introduction

1-1 Energy Demand and Solar Cell Applications

We already know that energy has been a vital issue of global concern over these past few years, and global warming and extreme climate change has become a crisis of great magnitude for Earth. In addition to this, it is predicted that we will run out of fossil fuel in about 50 years. Figure 1 shows the world marketed energy consumption through 2040 projected by the International Energy Administration. [1] It is clear that fossil fuels, i.e. natural gas, coal, and liquid fuels, still account for the main energy generation currently. The problems with direct usage of fossil fuels are well known. They are not only non-renewable but also cause environmental problems in relation to the emission of the greenhouse gas, CO_2. In 2015, World Meteorological Organization (WMO) announced that the annual average of carbon dioxide concentrations in the atmosphere had exceeded 400 ppm, beyond any record of history.

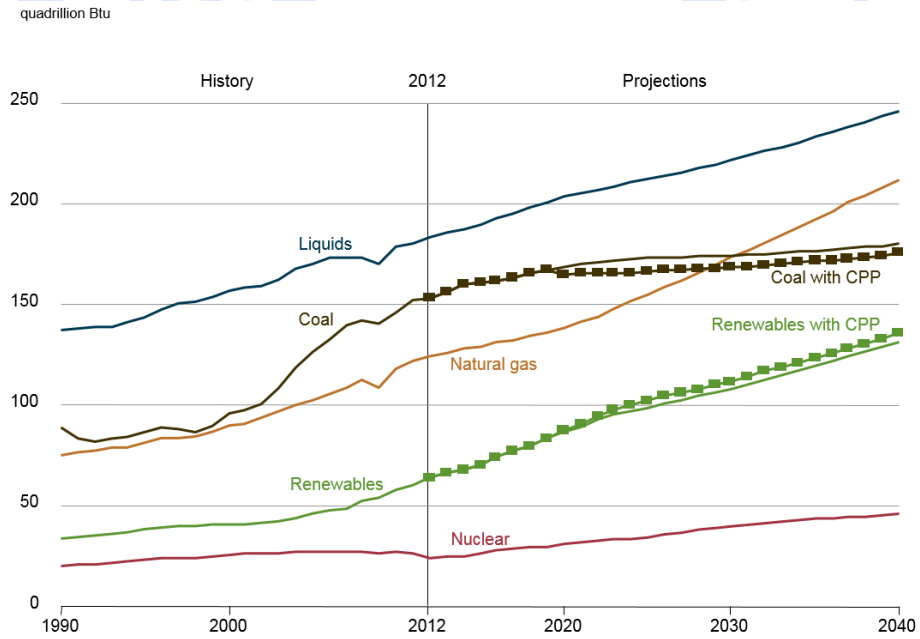

Figure 1. World energy consumption by energy source, 1990–2040.

(CPP = Clean Power Plan) [1]

In recent years, scientists have focused on green energy, which is more sustainable and environmentally friendly. Examples include wind power, hydroelectric power, fuel cells, geothermal energy, solar energy, biomass energy and ocean energy. Among these, solar energy is attracting worldwide attention due to its potential to generate power.

The main source of energy on the Earth is sunlight. The estimated energy of direct sunlight on the surface of the Earth is about 1.68×10^{24} joules per year. If we can utilize just 0.1% of this with 10% power conversion efficiency of solar cells, the converted power could satiate human consumption for one year.

Thus far, the use of solar energy is not as widespread as one might imagine; in fact, it's still in its early stages of development. In addition to the weak intensity of sunlight, night hours without sunlight is another problem we have to overcome. Currently, the most important task is to find a breakthrough that will both increase power conversion efficiency as well as reduce cost. It seems that solar energy is our best hope in respect to future energy generation.

1-2 The History of Solar Cells

A solar cell is a photovoltaic device which can convert sunlight into electricity. This phenomenon was first discovered in AD 1839 by Alexandre Edmond Becquerel, the physicist from France. When exposed to light, due to the non-uniformity internal of materials, such as semiconductor or a combination of a semiconductor and a metal, the excited electrons and the holes which are lost electrons will move in the opposite direction, and generate a potential difference. This phenomenon was termed "Photovoltaic Effect". [2]

The first photovoltaic cell which has practical value was fabricated by silicon doped with a certain amount of impurities in 1954 at Bell Laboratories. [3] Although

silicon is the second-rich element on the Earth, its challenging purification renders it a relatively expensive material. In order to reduce the cost and enhance efficiency, scientists have been working towards researching new-types of solar cells in recent years, with huge technological advances having been made, we have already seen three generations of solar cells developed.

At present, silicon solar cells still account for a great proportion of market share because of their high efficiency. Silicon is an atom with four valence electrons, which will become a n-type semiconductor (electron donor) after doping Arsenic or Phosphorus with five valence electrons, and become p-type semiconductor (electron acceptor) after doping Boron with three valence electrons. When exposed to light, electrons will be excited by photons to produce a pair of electrons-electron holes, and electrons will move to n-type semiconductor and electron holes will move to p-type semiconductor, only to become a loop via the outer circuit (Figure 2). This is general working principle of solar cells.

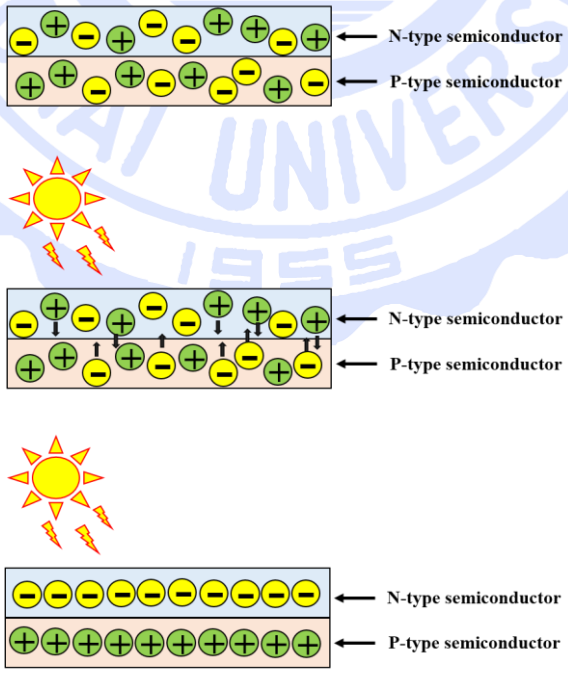

Figure 2. General working principle of solar cells

1-3 Different Types of Solar Cells

Solar cells developed to now can be divided into three generations. The first generation is silicon solar cells, the second generation is thin film solar cells, and the third generation is new concept solar cells (Figure 3). The most important parameter of solar cells is power conversion efficiency. For decades, silicon-based solar cells have formed the mainstream of solar cells market with higher efficiency up to 25%, but another crystalline material made of perovskite solar cells is rapidly catching up to this.

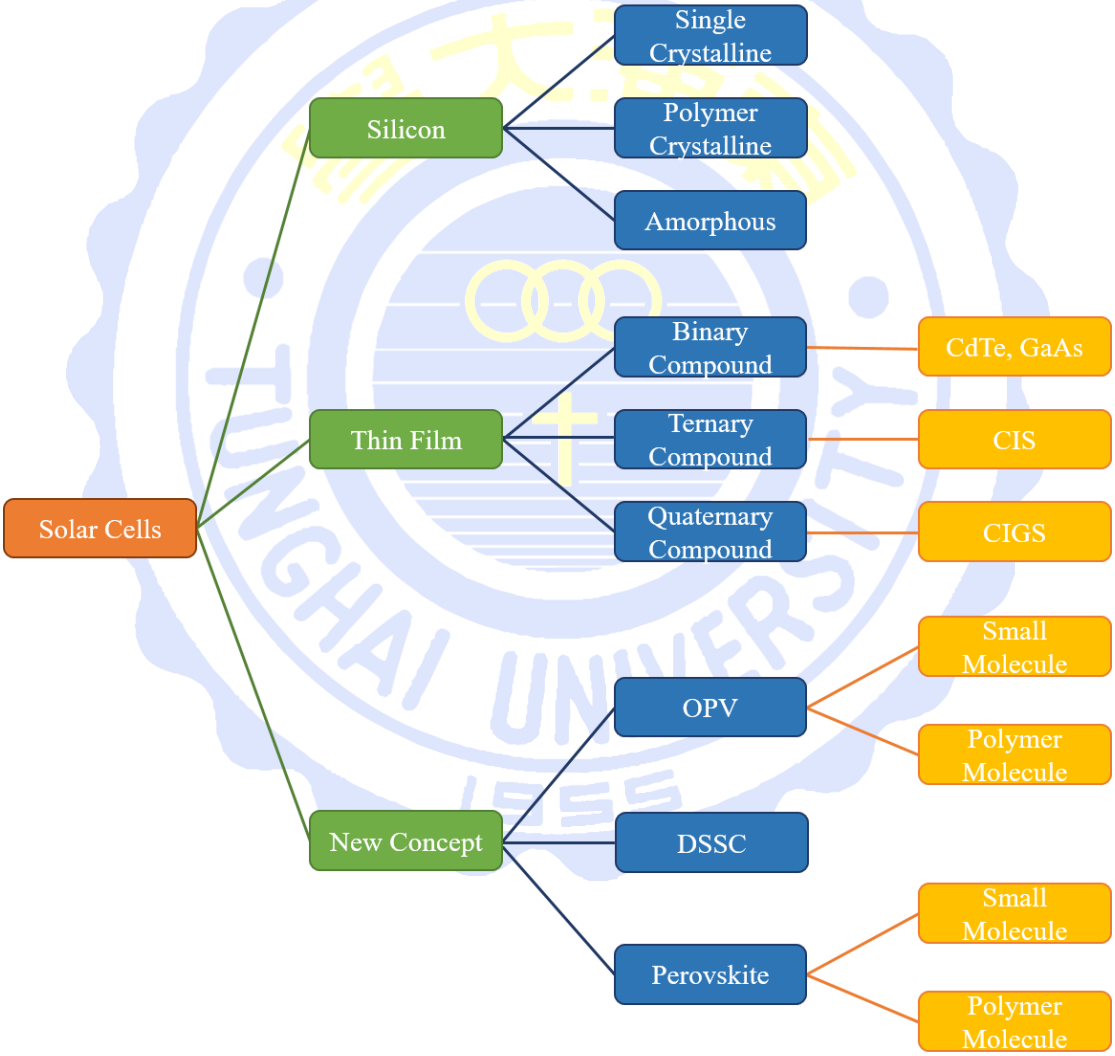

Figure 3. Different types of solar cells

1-3-1 Silicon-Based Solar Cells

Most of the silicon on Earth exists in the form of compounds. It is an extremely rich element, second only to the oxygen. High purity silicon can apply to solar cells, however it is hard to refine, which results in high production cost, and indirectly hinders further promotion of solar cells. Generally, silicon-based solar cells can be divided into three categories: single crystalline, polymer crystalline and amorphous crystalline. The difference between these three kinds of silicon-based solar cells is their different arrangement (Figure 4). [4]

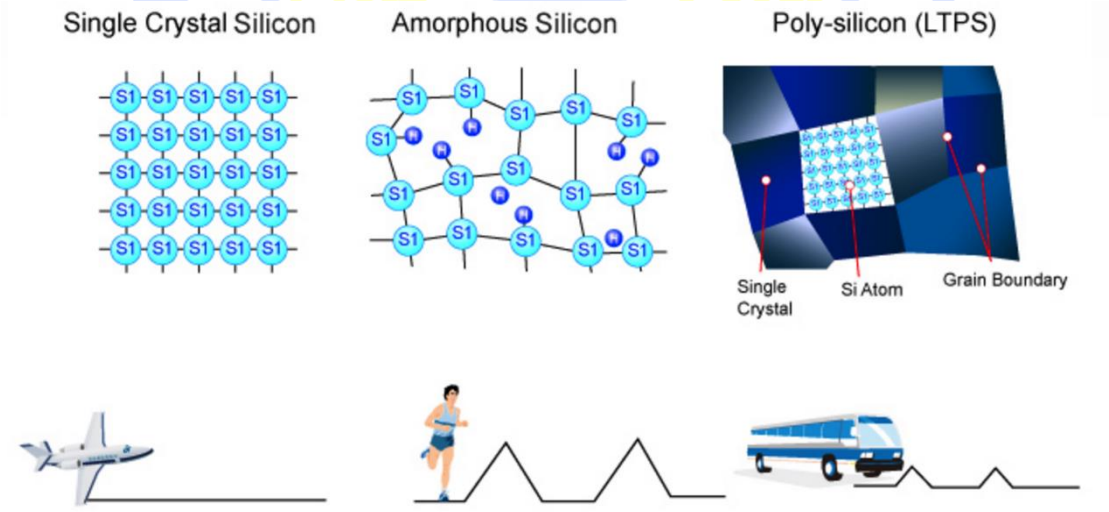

Figure 4. Arrangement of different types of solar cells [4]

1-3-1-1 Single Crystalline Silicon Solar Cells

Single crystalline silicon solar cells are manufactured with 99.999% pure silicon, according to the periodic arrangement. Its high efficiency and good stability make it the most widely used solar cell. It is the most efficient silicon solar cell, and indication of its high efficiency was published in 1999 by Dr. Jianhua Zhao from the University of New South Wales, Australia, who showed it to have an efficiency of 25% for a 4 cm^2 PERL silicon battery, [5] and which currently is excepted to break 28%. [6]

1-3-1-2 Polymer Crystalline Silicon Solar Cells

Since polymer crystalline is composed of different crystal orientations, there is more than one stacking method. Because of its simple processing, its production cost is low and it can be prepared for production using large-size square silicon ingots. Although its efficiency is lower than single crystalline, production of this cell continues to increase yearly. The highest efficiency polymer crystalline silicon solar cell currently available is FhG-ISE, with an efficiency rating of 20.4%. The research on this was conducted and published by Fraunhofer-Gesellschaft zur Förderung der angewandten Forschung e.V. in 2004. [7]

1-3-1-3 Amorphous Silicon Solar Cells

α-Si for short. The arrangement of atoms is periodic only in the range of several atoms or molecules, and in some materials, there is no periodic atomic arrangement. The type of cell is manufactured by a plasma chemical vapor deposition method, and an amorphous silicon film with a thickness of about one micron will grow on the substrate. The absorption of amorphous silicon is 500 times greater than that of crystalline silicon, so the photon of energy can be absorbed effectively as a long, thin layer. It also uses less expensive glasses, and ceramic or metal substrate instead of costly crystalline silicon substrate. This not only saves material costs, it can also create a large area of solar cells. In addition, its production speed is relatively fast, so it's easy to apply to consumer electronics products. But it only has 13% photoelectric conversion efficiency, which is lower than crystalline silicon solar cells, due to its recombination rate of electrons and holes. It is also not as stable as crystalline silicon solar cells, which leads to them having shorter lifetimes. Fortunately, a new generation of amorphous silicon multi-faceted solar cells has been able to significantly improve the stability and

lifetime of pure amorphous silicon solar cell (Figure 5).

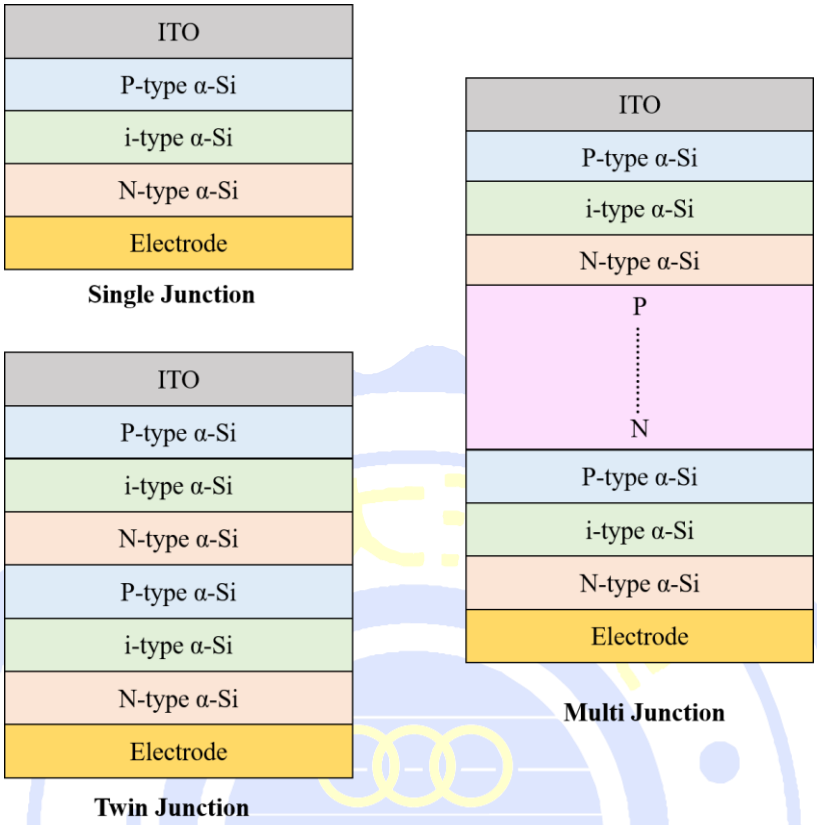

Figure 5. Arrangement of different types of solar cells

1-3-2 Thin Film Solar Cells

This kind of solar cells is mainly made of Ⅲ-Ⅴ groups or Ⅱ-Ⅵ groups elements, such as CdTe, GaAs, $CuInSe_2$(CIS) and $CuInGaSe_2$(CIGS). Compared with silicon, these compound semiconductors are usually direct-bandgap, can directly absorb photon energy, and have a higher absorption coefficient, so these solar cells are thinner than others, in order to reduce the chance of electronic recombination, which then results in higher efficiency. Single junction module – GaAs has the best efficiency of 28.4%, [8] even higher than single crystalline silicon solar cells. And the efficiency of tandem solar cells had already exceeded 43% (Figure 6). [9] However, Cadmium (Cd) creates pollution, and selenium (Se), indium (In), tellurium (Te) are rare metals, which limit

large-scale production of this type of solar cell.

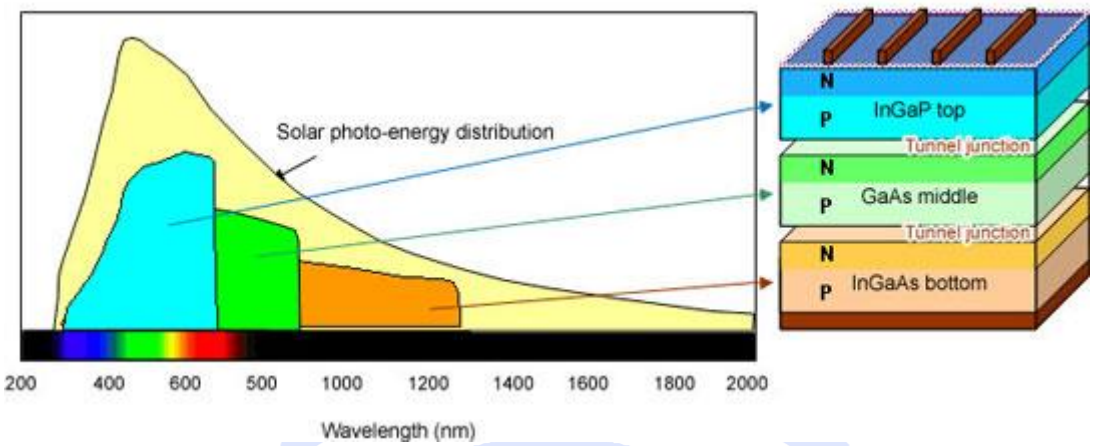

Figure 6. The tandem solar cells with the highest efficiency [10]

1-3-3 New Concept Solar Cells

These are solar cells based on using organic-inorganic material as the absorbing layer, and then transferring photons to electrons. These kinds of solar cells can enhance efficiency by tuning the structure and band gap of organic material to attain a broader absorbing range. Compared to the previous two generations of solar cells, they have a simpler fabrication method, and can be produced via 3D printing so as to quickly produce large-scale laying, which can form the film through deposition or spin-coating. Besides this, it is also easy to design and synthesize organic molecule structure with a high extinction coefficient. Additionally, its transparency and flexibility not only meets the architect's functional and aesthetic needs, but also allows it to absorb the light from any angle, even if it's weak light. Furthermore, the most important point is that it can get the comparable efficiency with single crystalline silicon solar cell as long as a thin layer, only 10 mg / cm^2, one-tenth of the traditional single crystalline silicon solar cell, it is relatively light and thin.

The new concept solar cells still have many disadvantages and haven't yet replaced earlier solar cell models. Silicon-based solar cells have the advantage on large power

plants and roof solar cells with the efficiency of 17~18%, but the new concept solar cells have superiority in in-depth families, glass curtain and art landscape design.

This generation can generally be divided into three different kinds of solar cells: Organic Photovoltaic (OPV), Dye-Sensitized Solar Cells (DSSCs) and Perovskite Solar Cells (PSCs).

1-3-3-1 Organic Photovoltaic (OPV)

Organic photovoltaic can subdivided into three types: Organic small molecule solar cells, organic-inorganic nanocomposite solar cells and organic polymer/C_{60} nanocomposite solar cell.

1-3-3-1-1 Organic small molecule solar cells

It has a facile synthetic route and can tune bandgap by designing or modifying the structure, only to achieve good charge separation. The most common structures are: the structure of chlorophyll, porphyrin, the derivative of perylene, (PTC), benzothiadiazole (BTD), Cu-phthalocyanine (CuPc), Diketopyrrolopyrroles (DPP), Borondipyrromethane (BODIPY) etc.. [11~13] Their absorbing range is located at visible region, and they have good chemical stability, as well as being good electric generating material.

1-3-3-1-2 Organic-inorganic nanocomposite solar cells

The common organic polymer such as: Poly(3-hexylthiophene) (P3HT), Poly(1-methoxy-4-(2-ethylhexylloxy)-*p*-phenylenevinylene) (MEH-PPV), Poly(2-methoxy-5-(3,7-dimethyloctyloxy)-1,4-phenylene-vinylene) (MDMO-PPV) etc. And the common N-type material, e.g., [6,6]-phenyl-C61-butyric acid methyl ester (PCBM), Titanium

dioxide (TiO_2) (Figure 7). TiO_2 is a good N-type semiconductor because of its well-adjusted chemical stability and electron conductivity, and as its energy level is about 3.2 eV, it can be used to modify the approach to excellent electron-hole separation. Therefore, some scientists use MEH-PPV as a hole transporting layer and TiO_2 as an electron transporting layer, then add $(CH_3)_3SiCl$ into the device bonding with -OH of TiO_2, which enhances the compatibility, and then changes the properties of device. [14]

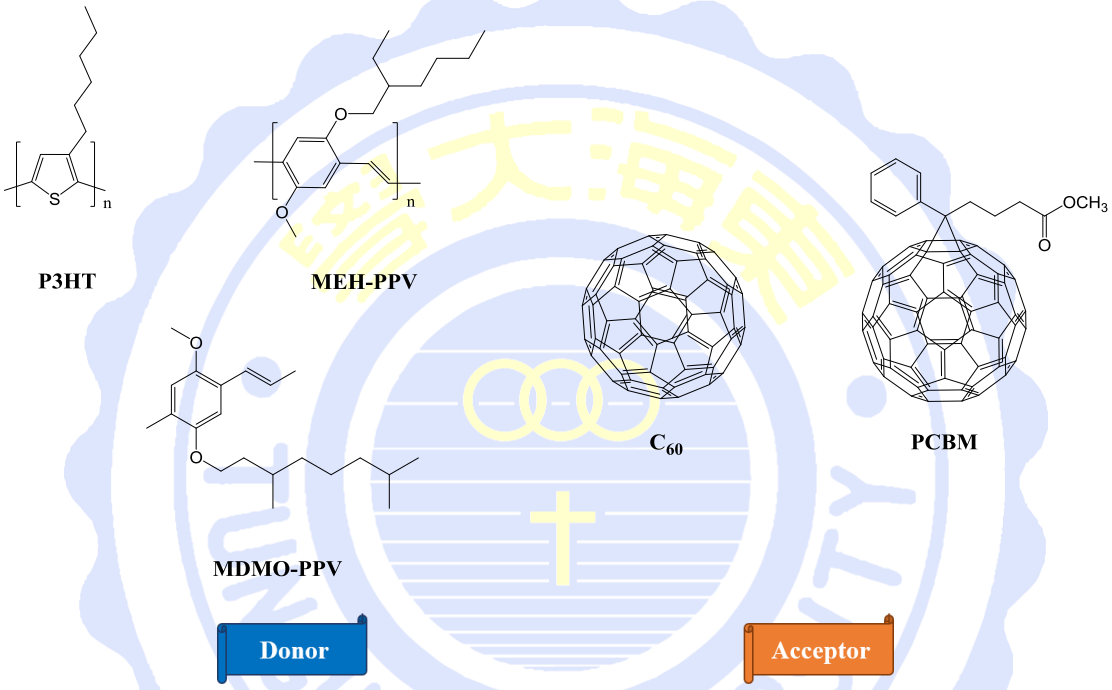

Figure 7. Donor and acceptor of organic-inorganic nanocomposite solar cells

1-3-3-1-3 Organic polymer/C_{60} nanocomposite solar cells

Conductive polymer is a polymer with chemical and physical properties, as well as semiconductor photoelectric properties, and is thus called "synthetic metal". Good conductive polymer can usually be dissolved in organic solvents and can be evaporated under vacuum. Conjugated polymer extends the conjugated double bonds, which means delocalized electron won't be tied by atoms, and can move within the polymer chains. After doping, it will form a pair of electron-hole and make electrons move within the

chain. Common conductive polymers include Poly-*p*-Phenylene Vinylene (PPV), Polythiophene (PT), Polypyrrole (PPy). But if we only used organic polymer to manufacture solar cells, the efficiency will be unfavorable due to the poor electron mobility, which will cause fast recombination after electron-hole separating. [15] Hence, we need to introduce a high electron transfer material, a derivative of C_{60}, [16] as the N-type conductor, when absorbing the sun light, electron was excited from the organic polymer P-type conductor to the lower LUMO of C_{60} then inject to cathode, and the

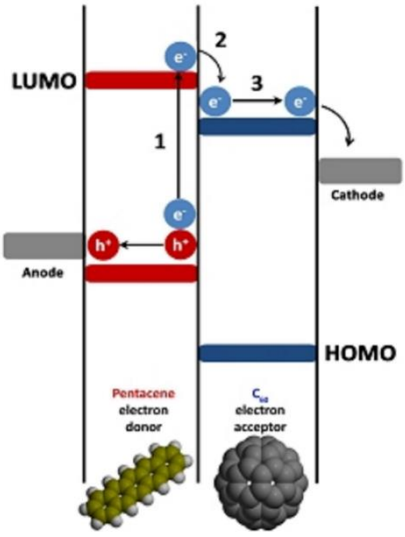

hole inject to anode, electron-hole separate and then generate current (Figure 8). [17]

Figure 8. The illustration of organic polymer/C_{60} nanocomposite solar cells [17]

1-3-3-2 Dye-Sensitized Solar Cells (DSSCs)

Dye-sensitized solar cell is a low-cost solar cell, based on a semiconductor formed between a photo-sensitized anode and electrolyte. It is a kind of photoelectrochemical system. The earliest conception of this type of solar cell was proposed by H. Tsubomura et al. in 1976. They used porous zinc oxide (ZnO) as the working electrode, but the photoelectric conversion efficiency was not high enough, so it was not taken seriously. [18] Until the Swiss scientist, Michael Grätzel et al. published the new type modern

version of a dye solar cell in 1991, they used nanoscale titanium dioxide (TiO_2) as the working electrode, and fabricated this with ruthenium metal derivatives to produce a photoelectric conversion efficiency 7% of the solar cells. [19] This solar cell mainly uses nano-titanium dioxide to adsorb the dye which can be excited by absorbing visible light to gain electrons. It is characterized by cheaper materials and simple production, and has good photoelectric conversion efficiency even under dim lighting. Subsequently, dye-sensitized solar cells have begun to attract the world's attention, and is commonly known as Grätzel Cell.

Dye sensitizer has a broad absorbing range within the visible region as well as higher electron conductivity, then attaching the group with good adsorptive property like -COOH, $-SO_3H$, $-PO_2H_2$ at the tail to make the dye embedded in TiO_2. And the excited state of dye has to be higher than the conduction band of TiO_2 to insure the electron injecting. The famous dyes are **N719**, **N_3** and **Black dye** which are published by Prof. Michael Grätzel (Figure 9), among them, **N719** was used to be the standard afterward. **ADEKA-1** and **LEG4**, the best efficiency of dye-sensitized solar cell, which were published by Toru Yano from ADEKA company and Minoru Hanaya from Gunmma University, co-adsorb on TiO_2 with the Co^{2+}/Co^{3+} electrolyte and the modification of electrode, gained the photoelectric conversion efficiency of 14.7% (Figure 10). [20]

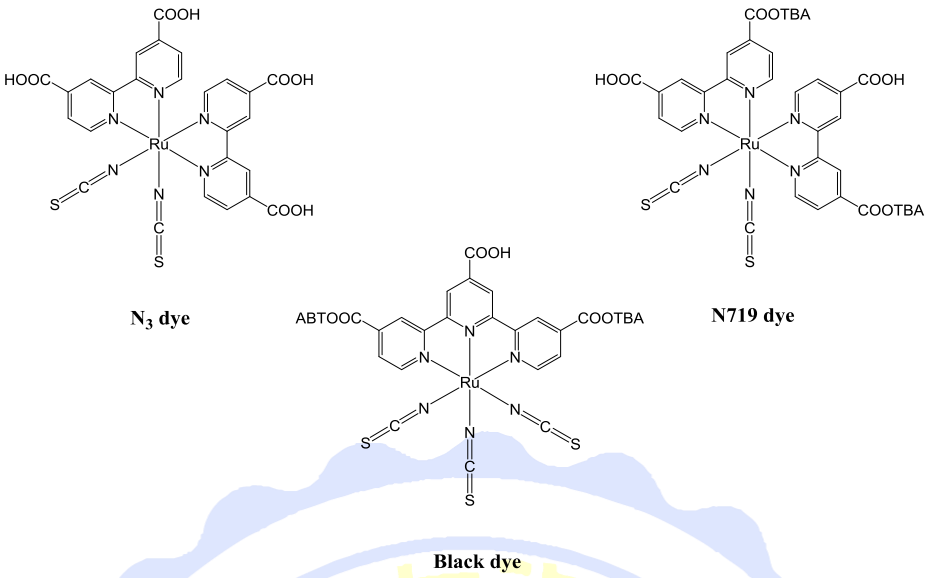

Figure 9. **N719**, **N3** and **Black dye**

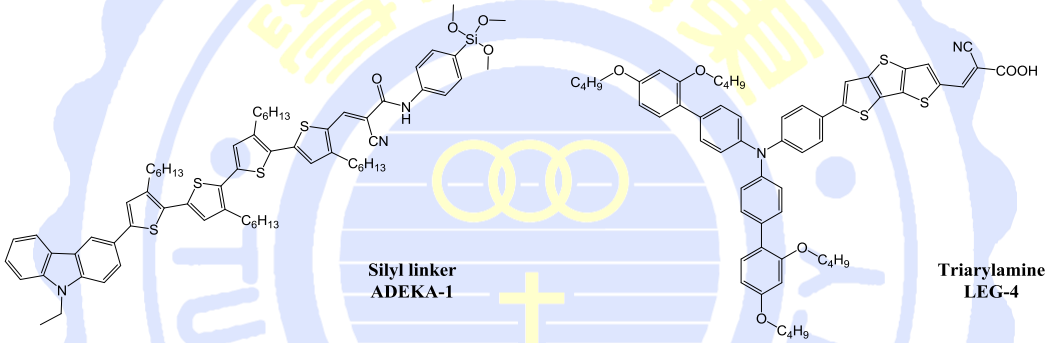

Figure 10. **ADEKA-1** and **LEG4** dyes

1-3-3-3 Perovskite Solar Cells (PSCs)

Organic-inorganic perovskite solar cells have attracted significant attention in the photovoltaics owing to their inexpensive precursors, simple fabrication methods and remarkably high power conversion efficiency (PCE). They have even exceeded commercialized polycrystalline silicon solar cells. [21] Perovskite is a mineral composed of calcium and titanium metal oxide ore discovered by German mineralogist Gustav Rose in 1839. [22] Its molecular formula is $CaTiO_3$, and afterwards, if the structure's chemical formula is like ABX_3, we call it "perovskite" (Figure 11). It possesses a unique combination of intrinsic properties, such as an appropriate direct band gap, a low

exciton binding energy, strong and broad absorption, ambipolar charge transport, a long carrier diffusion length and lifetime. [23-26] The most common perovskite is Methylammonium lead iodide ($MAPbI_3$).

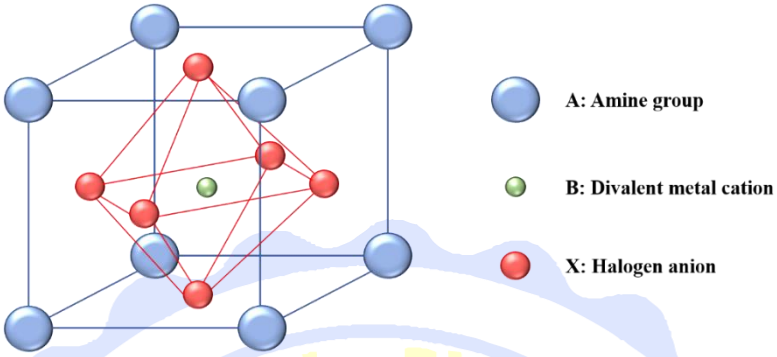

Figure 11. The structure of perovskite

In 2009, Miyasaka and coworkers first attempt to employ $MAPbI_3$ as a sensitizer in liquid-based dye-sensitized solar cells. As a result of the hydrolysis of halide in perovskite with liquid electrolyte, the stability of the device was relatively lower, and finally reached a power conversion efficiency of 3.8%. [27] It was only in 2012, Prof. Michael Grätzel introduced the solid hole-transporting material 2,2',7,7'-tetrakis(N,N-di-p-methoxyphenyl-amine)-9,9'-spirobifluorene (**Spiro-OMeTAD**) (Figure 12) to replace the liquid electrolyte, which led to a promising power conversion efficiency of 9.7%. [28]

Along with the development of processing techniques, device architectures and novel materials, the power conversion efficiency of perovskite-based solar cell has dramatically increased from the initial 3.8% to a recently certified 22.1% within five years (Figure 13). [29] It's obviously that tremendous progress has been achieved in the field of perovskite solar cells.

In having attained such impressive progress in respect to power conversion efficiency, there are concerns about perovskite solar cell's stability upon contact with moisture. [30] Nowadays, scientists are working hard towards overcoming this disadvantage of perovskite.

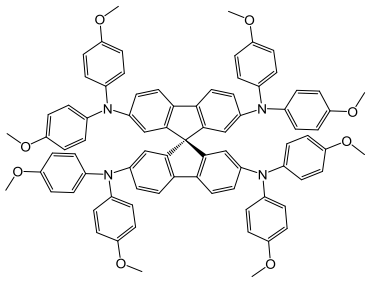

Spiro-OMeTAD

Figure 12. **Spiro-OMeTAD**

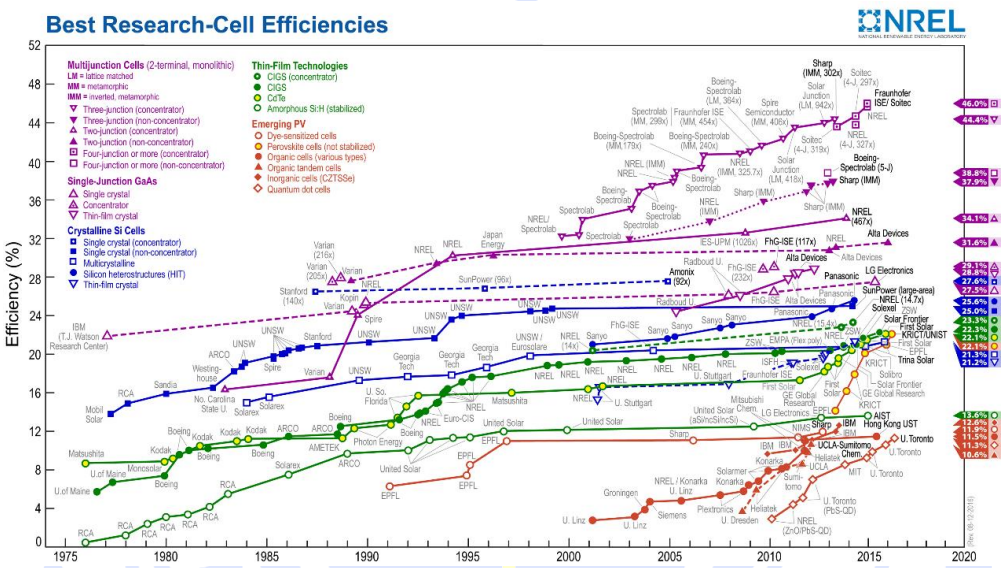

Figure 13. Best Research-Cell Efficiencies [31]

Chapter 2 Theoretical Background and Literature Review

2-1 Configuration of Perovskite Solar Cells

The device of perovskite solar cells was made by a series of spin-coating. First, the etched FTO glass was covered with titanium dioxide (TiO_2) by spin-coating, TiO_2 is not expensive, non-toxic, stable performance, broad band gap, and it also has high index of refraction, light scattering power due to its porosity. On top of it, the perovskite precursor solution was spin-coated as the light sensitizer, after annealing, spin-coated the hole-transporting material (HTM) precursor solution as the solid electrolyte. Finally, the gold electrodes were deposited by thermal evaporation. The whole device is showed at Figure 14:

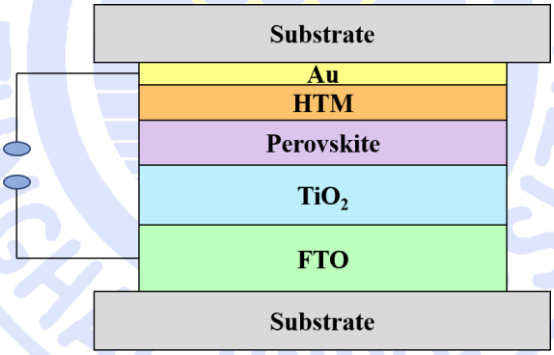

Figure 14. Configuration of Perovskite Solar Cells

2-2 Fabrication of Device

A、Solution preparation

a、TiO_2 precursor solution:

Mixing 146 μL titanium isopropoxide (TTIP: 2.25 mmol), 1 mL isopropyl alcohol (IPA) and 1 mL 0.046 M HCl (diluted with IPA) in a sample vial, and stirring at room temperature.

b、Perovskite precursor solution:

A mixture of 0.576 g lead(II) iodide (PbI_2) and 0.2 g methylammonium iodide (MAI) was dissolved with *N*,*N*-dimethylformamide (DMF) and stirring at 60 ^oC for 12 hours inside the glove box.

c、Hole-transporting material precursor solution:

Hole-transporting material (HTM, 80 mg) was dissolved with a solution contain 1 mL chlorobenzene (CB), 17.5 μL lithium bis(trifluoromethyanesulfonyl)imide (Li-TFSI, 520 mg, 1.8 M, Acetonitrile) and 28.5 μL 4-*tert*-butylpyridine (*t*BP) and stirring at room temperature inside the glove box.

B、Washing FTO glass

Conductive FTO glass (1.9 cm x 1.9 cm) was sequentially cleaned by sonication in neutral detergent, deionized water, acetone and isopropyl alcohol (IPA) for 15 min, respectively. After rinsing with deionized water, the substrates were further cleaned with ultraviolet ozone treatment for 20 min.

C、TiO_2 film formation

70 μL TiO_2 precursor solution was deposited by spin-coating for 60 s at 2000 rpm. After the spin-coating, the substrates were immediately dried at 180 ^oC for 5min and then left at 550 ^oC for 20 min to sinter film and then allowed to cool down to room temperature.

D、Perovskite film formation

80 μL perovskite precursor solution was spin-coated in a two-step procedure at 5000 rpm for 8 s and 22 s, respectively. During the second step, 200 μL chlorobenzene (CB) was poured on the spinning substrate. The substrates were then annealed at 100^oC for 10 min in a nitrogen atmosphere glove box.

E、 Hole transporting material film formation

After the perovskite annealing, the substrates were cooled down for a few minutes and the 60 μL hole-transporting material precursor solution (65 mM in chlorobenzene) was spin-coated at 2000 rpm for 30 s.

F、 Top electrode formation

Finally, 100 nm of gold top electrode was thermally evaporated under high vacuum.

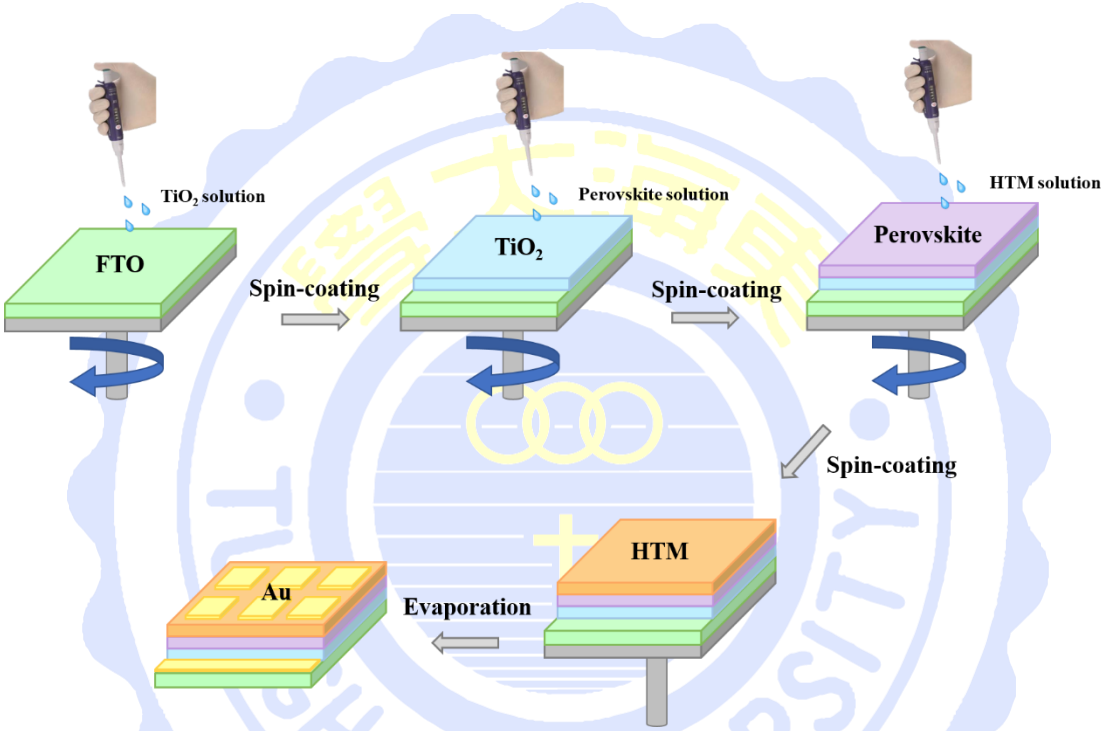

Figure 15. Fabrication of device

2-3 Working Principle of Perovskite Solar Cells

The mainly working process is: (A) Perovskite layer absorb the sun light to produce electrons, then electrons will bump to the excited state; (B) Then inject to TiO_2 conduction band and diffuse to FTO glass; (C) and then import to the Aurum cathode via the outer circuit; (D) Finally, electrons will reduce to the HOMO of perovskite layer and become the loop. There are three routes that we are unexpectable to see:

(1) The disproportionation of perovskite: Electrons will self-combine at perovskite.

(2) Charge recombination: When electrons inject to TiO_2 conduction band, it might recombine with the electron holes at the HOMO of perovskite.

(3) Dark current: When electrons inject to TiO_2 conduction band, it might recombine with the electron holes at the hole-transporting material.

These three routes will block the loop and influence the efficiency of device (Figure 16). The speeds of process (A), (B) and (D) are 10^{-15} s, 10^{-10}~10^{-12} s and 10^{-8} s, respectively. But the speed of electrons diffusing is not fast, so we have to reduce the diffusing distance or increase the diffusing rate to avoid the unfavorable routes.

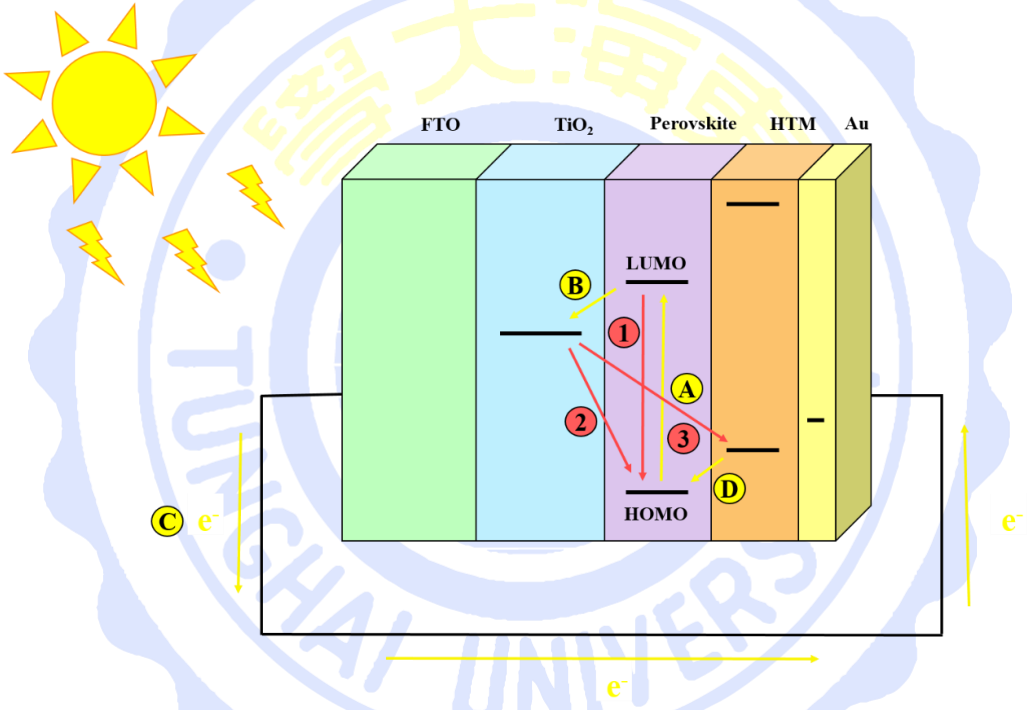

Figure 16. Working principle of Perovskite Solar Cells

2-4 Mainly Parameters of Solar Cells

Generally, the electrochemical properties of organic solar cells are demonstrated by short circuit current (J_{sc}), open circuit voltage (V_{oc}), fill factor (FF), power conversion efficiency (PCE), monochromatic incident photo-to-electron conversion efficiency (IPCE), series resistance (R_s) and shunt resistance (R_{sh}). These parameters

are not only affected by the material of different layers, the process of device manufacturing is another factor.

2-4-1 Short Circuit current (J_{sc})

When solar cells in the no-load condition, the current output when the external current is short circuit, then the voltage is 0. In the ideal state, the short circuit current of the solar cell is equal to the current generated when the light is generated.

2-4-2 Open Circuit Voltage (V_{oc})

Solar cell in the case of an infinite load, the voltage we have measured when the external current is open circuit, then the output current is 0.

2-4-3 Fill Factor (FF)

The ratio of solar cells' ideal short circuit current and open circuit voltage performance and the practical application. The output power of any one operating point is equal to the current density and voltage product corresponding to the point. FF is a value without a unit, the closer to 1 the value is, the better performance is (Figure 17).

$$\mathrm{FF} = \frac{J_{\mathrm{MP}} \times V_{\mathrm{MP}}}{J_{\mathrm{sc}} \times V_{\mathrm{oc}}}$$

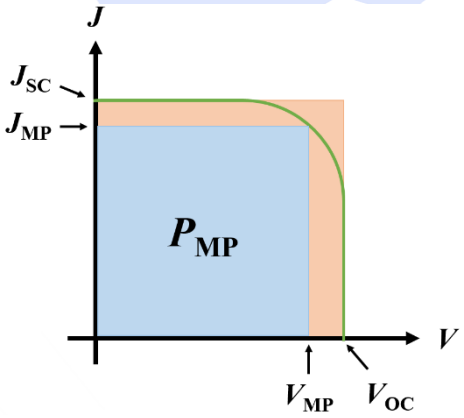

Figure 17. Definition of FF

2-4-4 Power Conversion Efficiency (PCE)

The power conversion efficiency of the solar cell can be defined as the ratio of the maximum output power of the solar cell to the incident optical power, which is the most capable representation of the solar cell.

$$\mathrm{PCE} = \frac{(J_{sc} \times V_{oc})_{max} \times FF}{\mathrm{P_{light}}} \times 100\%$$

2-4-5 Monochromatic Incident Photo-to-Eectron Conversion Efficiency (IPCE)

It is the efficiency of photon convert to electron in the unit area, it can be defined as:

$$\mathrm{IPCE} = \frac{1.24 \times 10^3 \times \text{photocurrent density}(\mu\mathrm{A/cm^2})}{\lambda(\mathrm{nm}) \times \mathrm{J(W/m^2)}}$$

2-4-6 Series Resistance (R_s)

In the physical meaning, series resistance is the sum of resistance of interface between every layers of device. Generally, series resistance is less than 10 Ω, if the value is too large, it means that there is some blemish on the interface between each material, it will open circuit and then effect the efficiency of device. The way to estimate the series resistance is drawing a tangent at the point of current density is zero in *J-V* curve, get the slope, and the reciprocal of the slope is series resistance.

$$R_s = \left(\frac{\mathrm{d}I}{\mathrm{d}V}\right)^{-1} \quad V = V_{oc}$$

2-4-7 Shunt Resistance (R_{sh})

In the physical meaning, shunt resistance is value of leakage current due to the defect of device's structure. When measuring the electrochemical properties of device, the J_{sc} will be over-estimated. Thus, the shunt resistance of a good device has to larger than 10000 Ω to inhibit the leakage current. The way to estimate the shunt resistance is drawing a tangent at the point of open circuit voltage is zero in *J-V* curve, get the slope, and the reciprocal of the slope is shunt resistance.

$$R_{sh} = \left(\frac{dI}{dV}\right)^{-1} \quad V = 0$$

2-5 Air Mass

The solar spectrum will be affected by the location, the atmospheric environment, the angle of exposure, the distance between the sun and the earth and the activity of the sun's surface. Hence, scientist had defined a set of standard to represent the sunlight went through the different thickness of several atmospheres (Figure 18).

A、AM0 (In space, not through the atmosphere) ~1353 W/m^2

B、AM1 (sec θ =1→ θ ~0^o) ~1000 W/m^2

C、AM1.5 (sec θ =1.5→ θ ~48^o) ~936.8 W/m^2

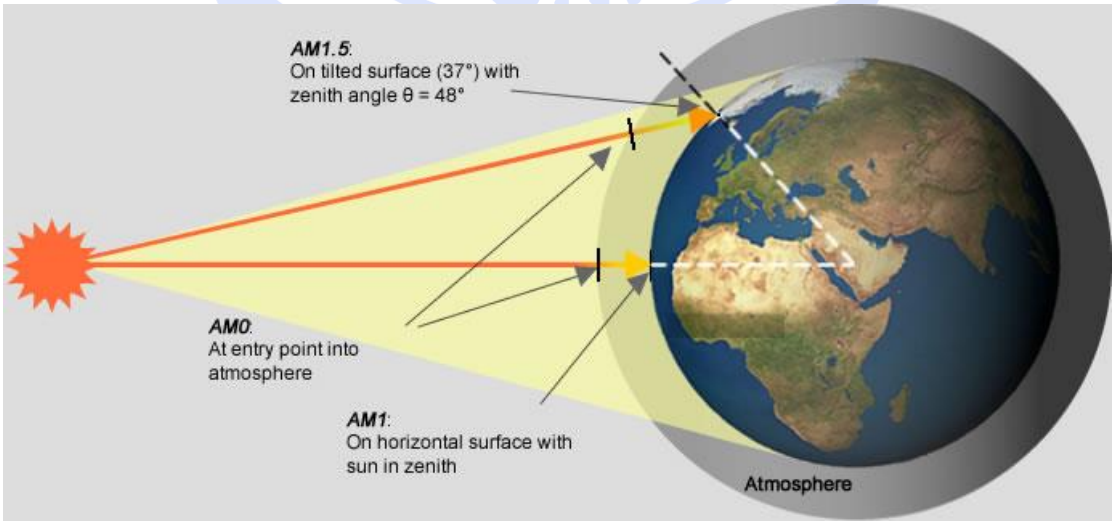

Figure 18. Illustration of Air Mass [32]

2-6 Literature Review

2-6-1 FTO Glass (Conductive Layer)

In optoelectronic industry, the choice of conductive material will decide the efficiency of a device. A good quality of conductive material shall have the following qualifications: good optical transmission in visible region (transmittance should at least over 80%), high conductive (resistivity should lower than 1×10^{-5} Ω・m), and high concentration of carrier (10^{20} n・cm^{-3}).

Indium tin oxide (ITO) is one of the most widely used transparent conducting oxides in optoelectronic market due to its optical transparency, electrical conductivity and large bandgap of around 4 eV. However, indium is the rare metal leading to rising prices, to overcome this condition, scientists had figured out some substitute such as carbon nanotube, PEDOT, PEDOT:PSS and some compound-doped oxide. Above all, Fluorine-doped tin oxide (FTO) had been the most prosperous material with the high transparency of about 85% and low resistivity of 10^{-4} Ω・m.

In DSSCs and PSCs, FTO glass was adopted instead of ITO glass, not only because of the price. During the fabrication of devices, high temperature is necessary, but the face resistance of ITO will increase in doubled fold, and FTO doesn't has this problem.

2-6-2 TiO_2 (Optical Scattering Layer)

Titanium is one of the richest element on the Earth, and titanium dioxide (TiO_2) is the most common and stable compound. It has a wide range of applications, from paint to sunscreen to solar cells. Generally, it is soured from ilmenite, rutile and anatase, but only rutile and ilmenite have economic importance, in which solar cells that is rutile.

TiO_2 has an extremely high refractive index, there are many small particles orientated in different directions, a high refractive index will lead to the scattering of

light as not much light passes through, then the lights will be locked in the devices.

2-6-3 Perovskite (Optical Sensitizer)

Compare to the indirect bandgap material like crystal silicon, perovskite is a direct bandgap material, it is means that it has strong light absorbing ability. To achieve the saturation absorption of the incident light, the silicon wafer must reach more than 150 microns, while the perovskite only need 0.2 microns, nearly one a thousandth thickness than silicon. Therefore, the consumption of active materials in perovskite solar cells is much smaller than the crystalline silicon solar cells.

Besides, perovskite has a high carrier mobility and is almost completely balanced. The high carrier mobility means that the charge generated by the light can be moved to the electrode in the fast rate. The mobility balanced means the mobility of electrons and holes is substantially the same. By contrast, the carrier mobility of crystalline silicon is unbalanced, its electron mobility is much greater than hole mobility, with the consequence that when the incident light has a high intensity, the current output will be saturated easily, and limit the photoelectric conversion efficiency.

Most important of all, the carrier recombination in perovskite crystals in almost entirely a radiant complex, it suggests that when the electrons and holes are recombined, a new photon is released, and will reabsorbed by the nearby perovskite crystals. Hence, the utilization efficiency of the incident photon is extremely high. On the contrary, the carrier recombination in crystalline silicon is almost completely nonradiative, when the electrons and holes are recombined, the energy they carry will be converted into heat and can’t be reused. Accordingly, the theoretical efficiency of perovskite solar cells is significantly higher than crystalline silicon solar cells, and have the potential to achieve as high as GaAs solar cells, or even break through 29%. [33]

The most highlighted perovskites are those based on $MAPbI_3$, like $FAPbI_3$, $MAPbBr_3$, $MAPbI_{(3-x)}Cl_x$ and so forth. However, $MAPbI_3$-based perovskites raise some concerns about degradation and thermal stability upon contact with moisture. Larger cations such as formamidinium (FA) instead of methylammonium (MA) lead to an enhancement of the light-harvesting ability. Still, FAPbI3 is sensitive to solvents and humidity and is also suffered from structural instability. To overcome them, compositionally engineered perovskites such as $(FAPbI_3)_x(MAPbBr_3)_{(1-x)}$ [34] [35] were introduced. The MA cation acts as "stabilizer" of perovskite phase and, simultaneously, forms crystallites, which leads to significantly improved PCE values. [36]

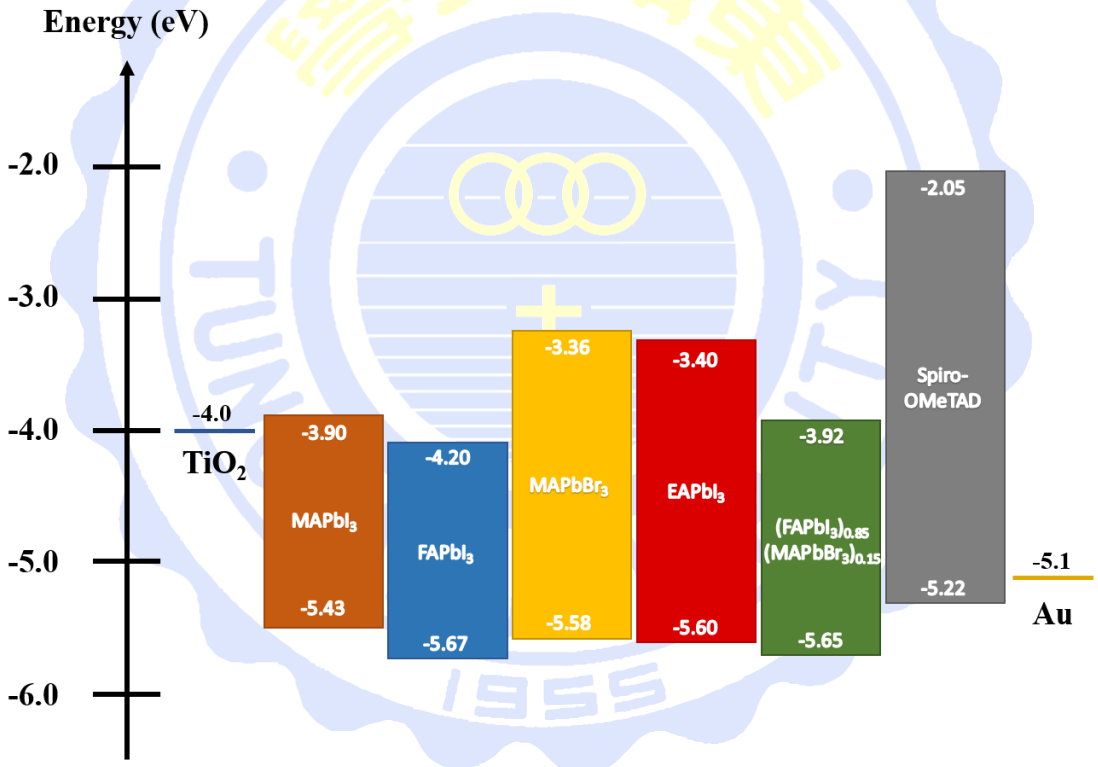

Figure 19. Energy Level of different kinds of perovskites [37] [38]

2-6-4 HTMs (Solid Electrolyte)

HTM is to collect and transfer the holes which are injected from perovskite layer, and achieve effective electron-hole separation. An ideal HTMs should meet the following requirements: good hole mobility, stability, dissolving ability, film formation

and matching HOMO level to ensure efficient injection and transport of holes. HTMs applied in perovskite solar cells are mainly divided into two types: inorganic and organic HTMs, and organic HTMs are subdivided into two types: polymers and small molecules.

2-6-4-1 Inorganic HTMs

Some inorganic HTMs like CuI, [39] its electrons will recombine with holes easily, resulting the low J_{sc} value, but the conductivity is better than most of the organic HTMs and lead to the higher FF. After that, NiO, [40]~ [42] CuSCN, [43]~ [48] Cu-doped NiO [49] and Cu_2O, [50] quaternary compound LiMgNiO [51] etc. are also used in perovskite solar cells. Furthermore, some quantum dots such as PbS, [52] $CuInS_2$ [53] were found to have a function as the HTMs applied in perovskite solar cells, providing a new direction of research and development. Although inorganic-based HTMs have lower cost, the material range of choice is narrow, limiting their application.

2-6-4-2 Organic HTMs

Comparing to inorganic HTMs, organic HTMs are more flexible attributed to their variety configuration, especially in small molecules HTMs are easier to modify and purify. By designing the structures, energy levels and surface properties can be adjusted to reach better efficiency. Therefore, the performance of the devices is generally excellent and the research of organic HTMs is relatively more extensive.

2-6-4-2-1 Polymeric HTMs

The structures of polymeric HTMs mainly containing two units, aniline and thiophene. The former is aniline, carbazole or fluorene units of the polymer, they have

higher hole mobility and film formation, The most widely used aniline-containing polymeric HTMs applied in perovskite is **PTAA**, the device of **PTAA**-based HTM has the lower Rs and the highest V_{oc} and FF. Recently, the Seok group got the PCE of over 20% by optimizing the perovskite layer with **PTAA** as the HTM. [54] [55] The latter is benzodithiophene or diketopyrrolopyrrole (DPP) units of the polymer, they have stronger light absorbing ability to complement perovskite, it can also introduce carbon nanotubes or graphene to improve its hole mobility, The most common thiophene-containing polymer HTMs applied in perovskite solar cells are **P3HT** [56]~ [61] and **PEDOT:PSS**. [62]~ [66]

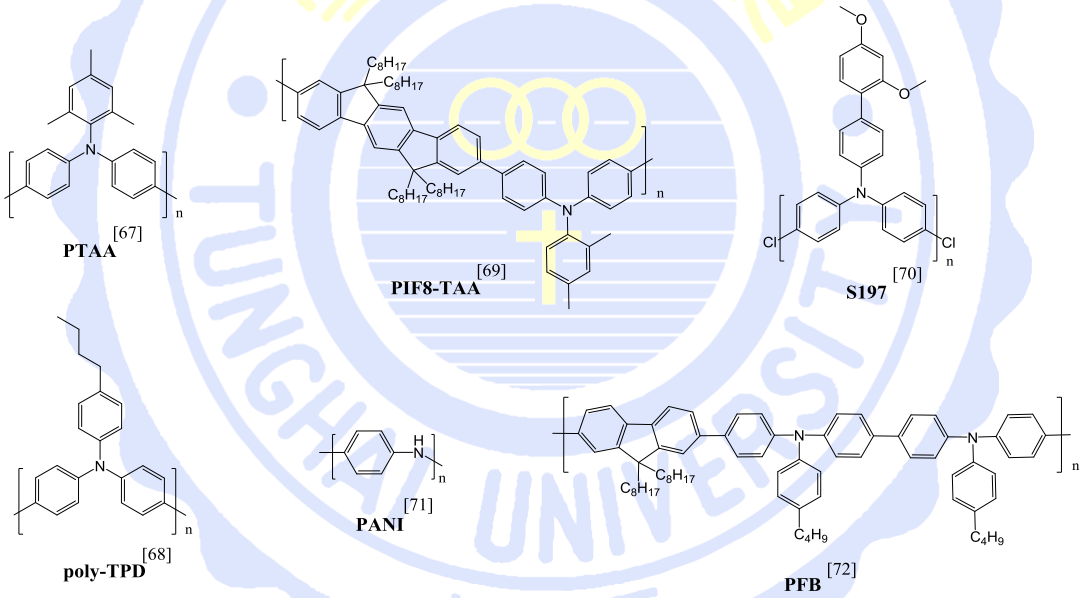

Figure 20. Polymeric HTMs with aniline moiety [67]~[72]

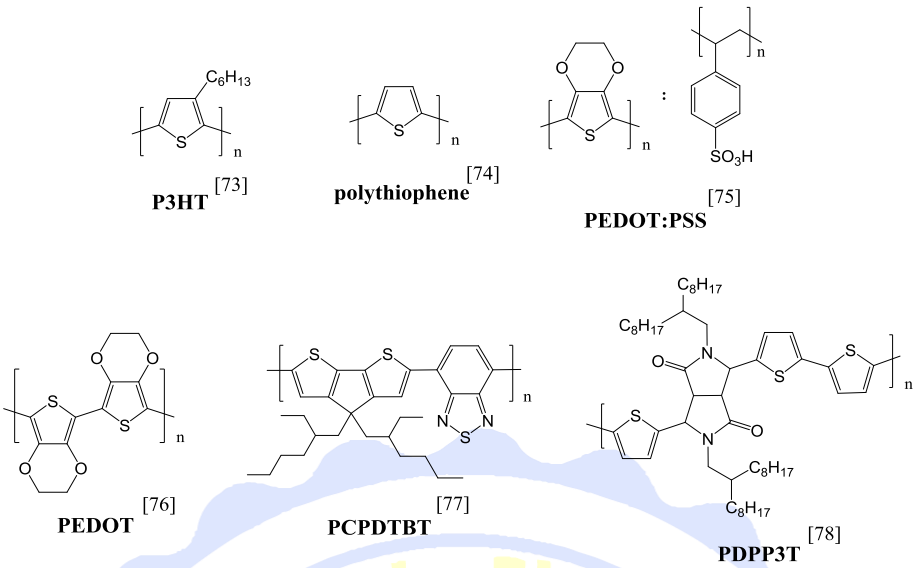

Figure 21. Polymer HTMs with aniline moiety [73]~[78]

2-6-4-2-2 Small Molecule HTMs

Generally, small molecule HTMs containing triphenylamine (TPA), thiophene and phthalocyanine. Above all, TPA-based HTMs is the most common material applied in perovskite solar cells since the electrophilic nitrogen atom in it can attracts the electrons on the aromatic rings by inductive effect. Besides, the lone pair of nitrogen can supply to aromatic ring, and conjugated effect is greater than inductive effect lead to the widely distributed of electron cloud, makes it easy to lose electrons and form the vacancies with positive charges and transfer the holes easily. After modifying, the solubility, film-forming property and light stability can be improved to meet the requirements of HTMs in perovskite solar cells.

The most widely used TPA-based HTM is **spiro-OMeTAD**. However, the challenging synthetic route, low yield and costly purification render it a relatively expensive material, and hinder its further commercial application. Moreover, its relatively low intrinsic hole mobility makes it necessary to be doped with bis(trifluoromethane)sulfonimide lithium salt (Li-TFSI), 4-tert-butylpyridine (*t*BP) and

Co(III)-based oxidizing agent (**FK209**). [79] [80] Since hygroscopic nature of lithium salt makes the HTL highly hydrophilic, influencing the stability of the entire device, [81] [82] the exploration of novel HTMs with low cost, good stability and high efficiency is urgently needed. According to the overall structure of the TPA-based HTMs can further divided into spiro-type, star-shaped and linear-shaped.

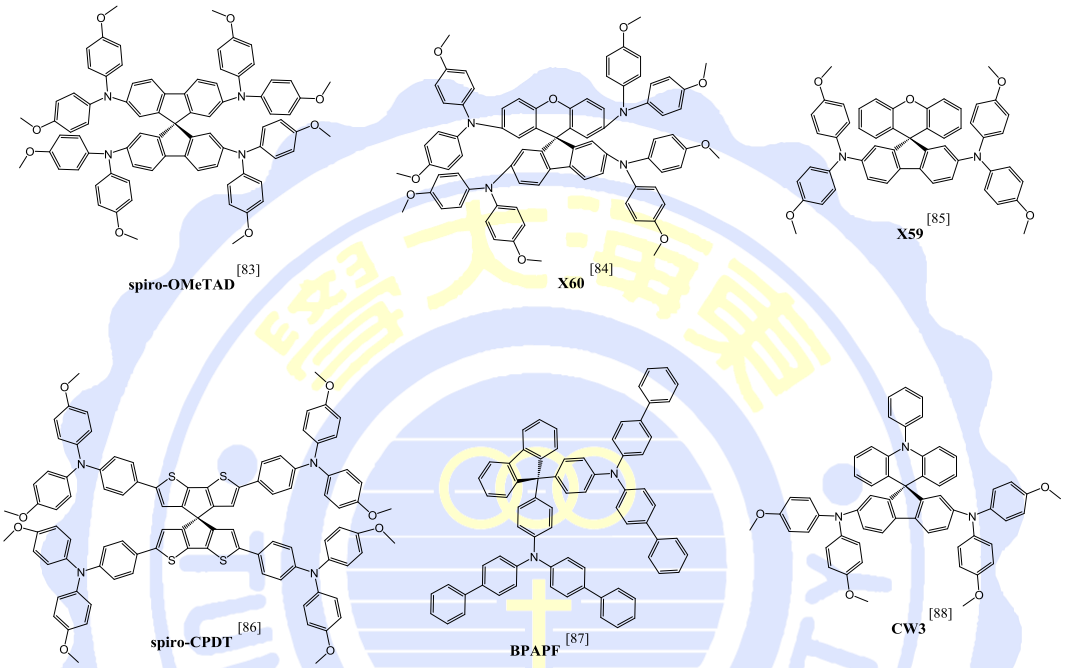

Figure 22. Spiro-type HTMs with triphenylamine moiety [83]~[88]

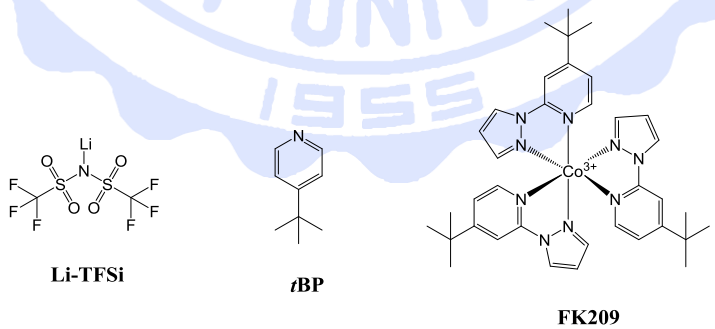

Figure 23. Molecular structures of additives in HTMs

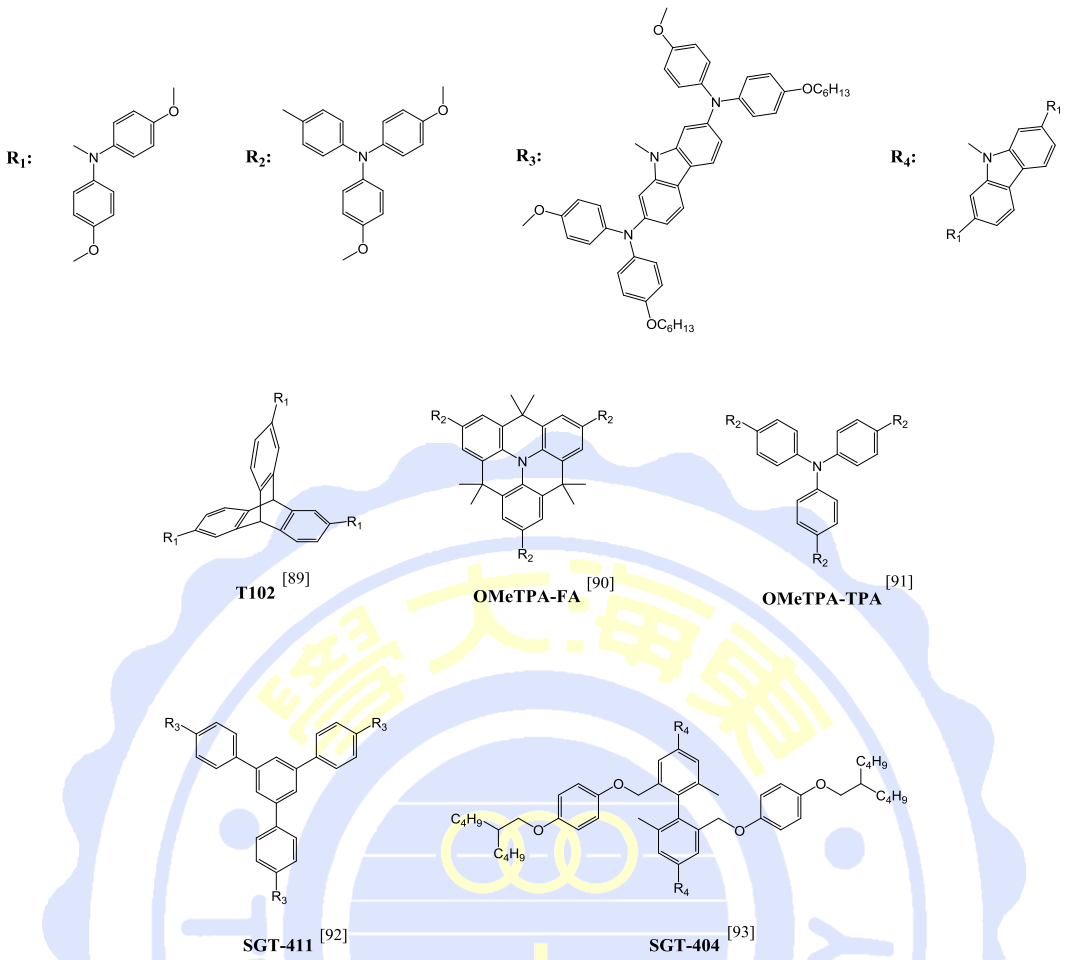

Figure 24. Star-shaped HTMs with triphenylamine moiety [89]~[93]

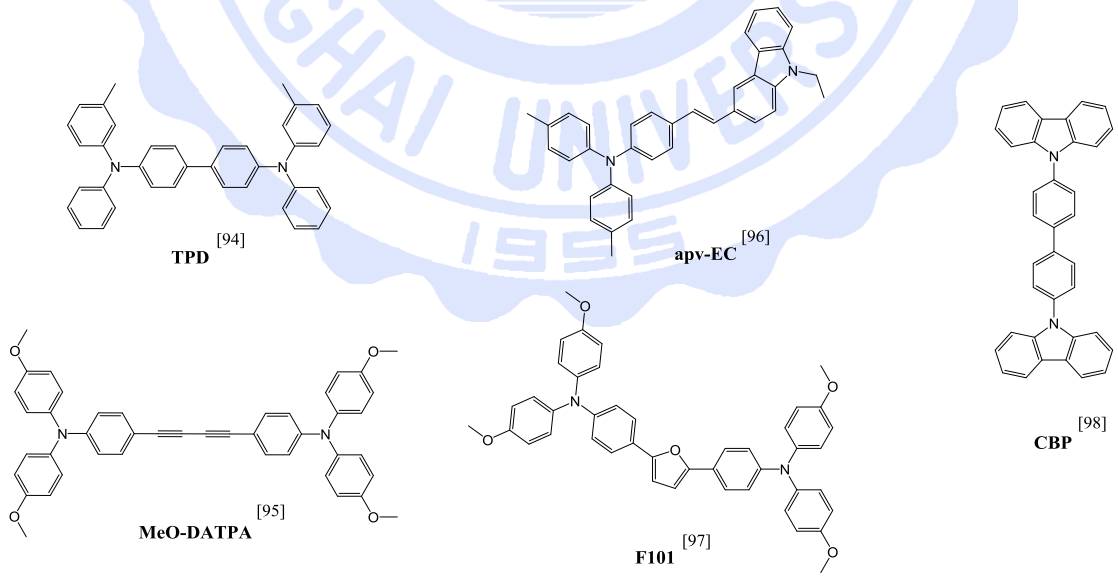

Figure 25. Linear-shaped HTMs with triphenylamine moiety [94]~[98]

As a result of the non-planar structure of TPA, the intermolecular interaction distance is longer, which makes the hole mobility lower. In order to enhance the hole mobility, thiophene had introduced to increase the conjugation of the molecule. The synthesis of donor-acceptor (D-A), A-D-A or D-A-D types small molecules with thiophene as a bridge and introduce different electron donors and electron withdrawing groups is also worth to research.

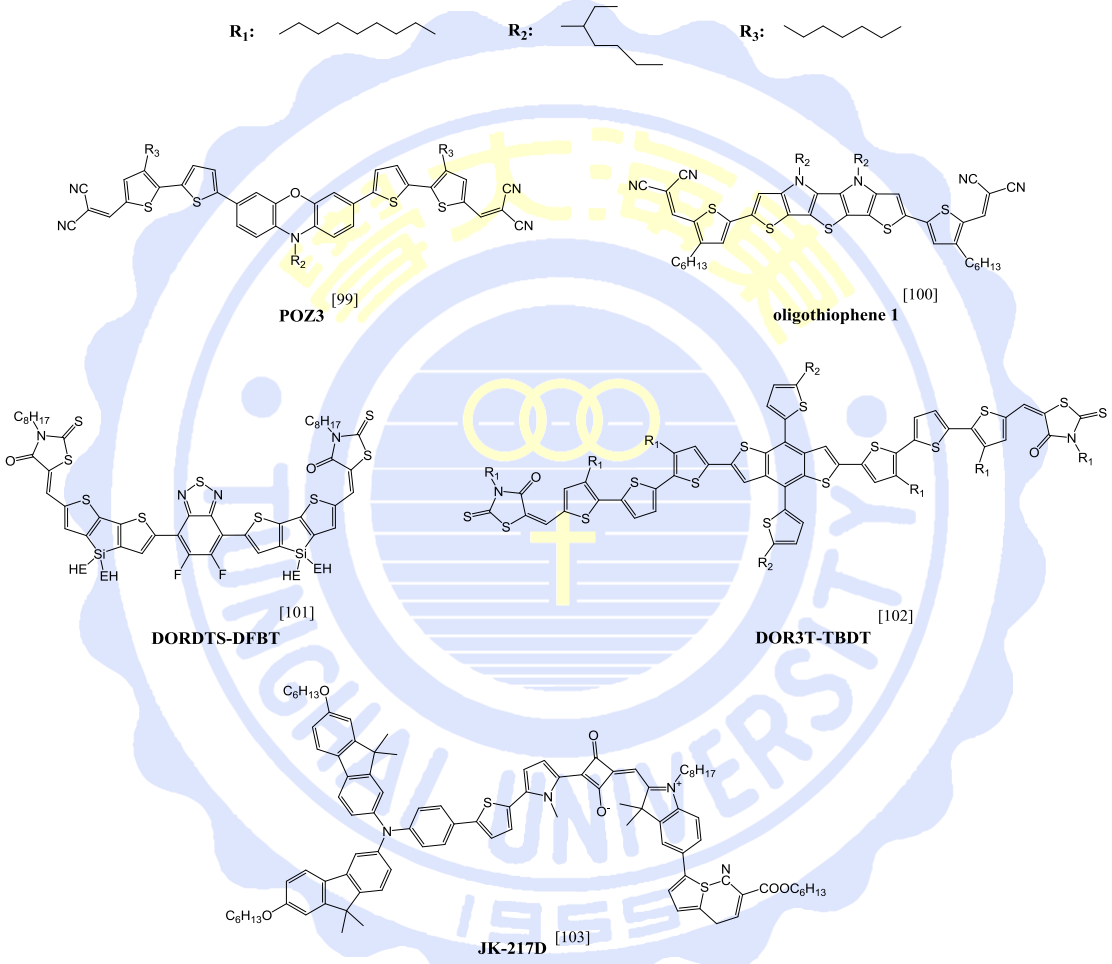

Figure 26. Small molecule HTMs with thiophene moiety [99]~[103]

Phthalocyanine compounds have been used in organic light-emitting diodes (OLEDs) and organic photovoltaic (OPV) as p-type semiconductor, scientists also applied to the perovskite solar cells. Though the FF and PCE are lower than other structures, the relatively low cost still makes it a potential structure to develop.

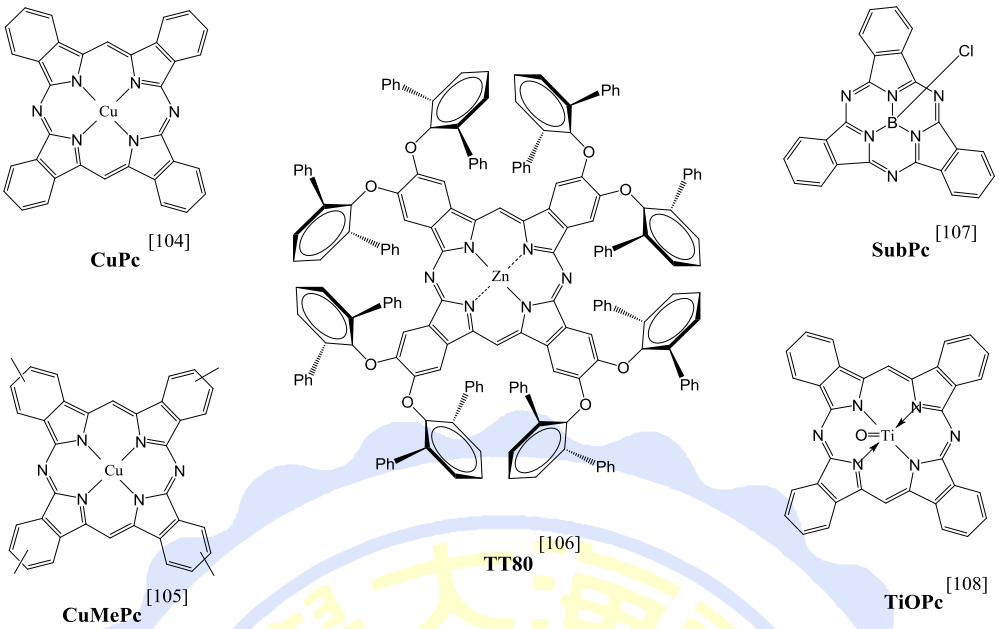

Figure 27. Phthalocyanine HTMs [104]~[108]

Except for the structures mentioned above, scientists also introduce other structures as HTMs, with most molecules appear linear and star-shaped. These small molecules do not contain the thiophene and TPA structures common in HTMs. The structures are relatively simple and its HOMO energy level is also suitable for perovskite solar cells and achieve good PCE.

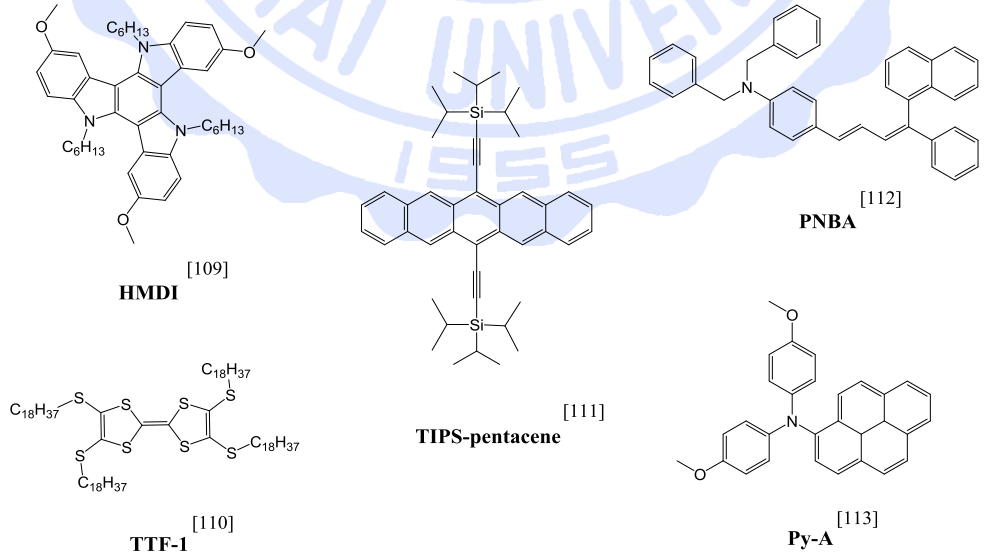

Figure 28. Other types molecular HTMs [109]~[113]

In general, organic HTMs have weaker conductivity than inorganic HTMs. Although the conductivity can enhance by adding additives, the stability is relative decline due to the hygroscopic nature of additives. In order to solve this problem, dopant-free HTMs were synthesized, and they all have one feature in common, planar-core. Planar-core can be considered as a two-dimensional π -system, which provides a large aromatic surface to overlap with each other favor to increase intermolecular charge transfer then enhance the conductivity of devices.

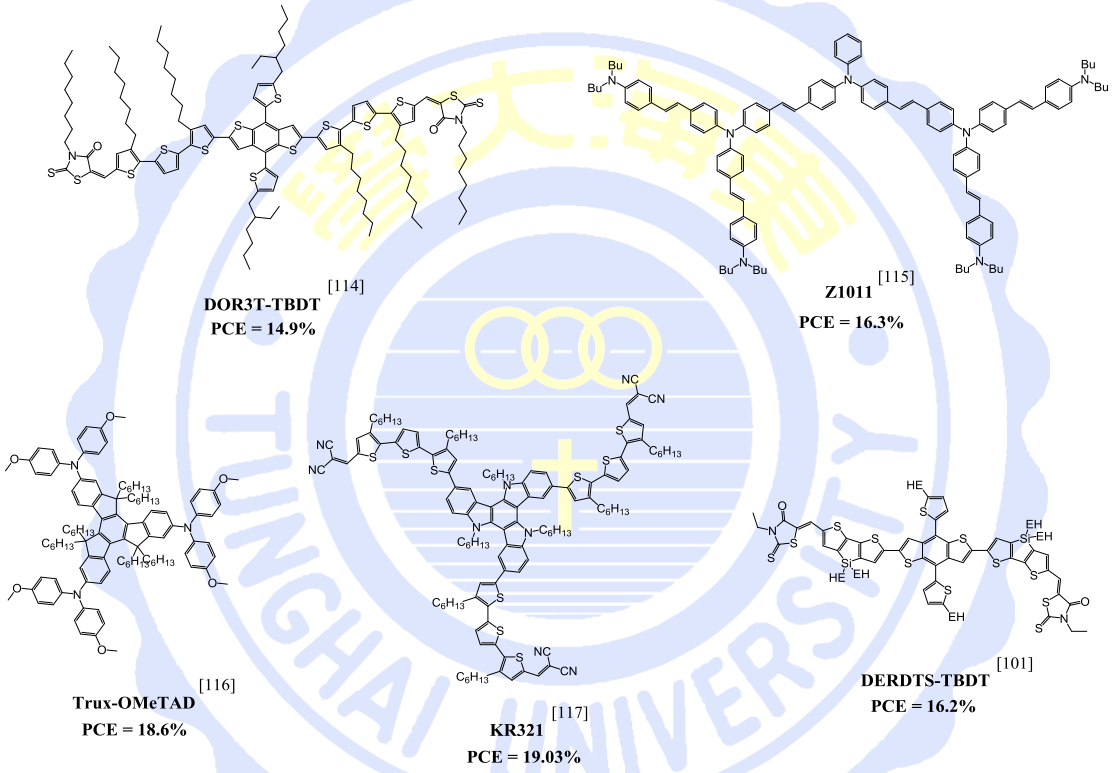

Figure 299. HTMs without additives [114]~[117] [101]

2-6-5 Au (Reducing Agent)

Aurum is widely applied in electrical devices as a connector by virtue of its highly conductive to electricity, the concentration of free electrons in aurum is 5.9×10^{22} cm^{-3}. Though silver and copper are more conductive, aurum has the advantage of corrosion resistance, besides, ductility and the lack of toxicity also lead to its widespread industrial use in the electronic era as a thin-layer coating on electrical connectors.

Chapter 3 Synthetic Strategy and Properties Discussion

3-1 Motivation

The molecular structure of the hole transporting material (HTM) plays an important role in hole extraction in a perovskite solar cells (PSCs). By modifying the structure, it has a significant influence on the molecular planarity, energy level and charge transport properties. So far, the most widely used and efficient HTM employed for PSCs is **spiro-OMeTAD**, with the cruciform shape core and four arms, which yields a maximum power conversion efficiency (PCE) close to 20%. [118] [119] In a like manner, a large number of cruciform-shaped based materials have been reported reaching an efficiency of 16~18%, [120] ~ [122] and some of them even over 19%. [123] [124] Based on this concept, **Yih-3~5** were synthesized.

Dibenzo[g,p]chrysene is a promising structure in organic photoelectric materials and was applied in liquid crystal because of its good quantum yield, small stoke-shift and long excited-state lifetime. [125] [126] It is in the shape of twisted due to the steric effect of hydrogen atom in fjord area (Figure 30). [127] [128] In 2014, Eiichi Nakamura had synthesized a series of dibenzo[g,p]chrysene derivatives with the substituted in para position. The X-ray suggested the brickwork packing structure because of the twist-shaped core, and lead to ambipolar charge carrier transport properties and higher hole mobility (Figure 31). [129] On the above basis, dibenzo[g,p]chrysene was chosen as one of our cores.

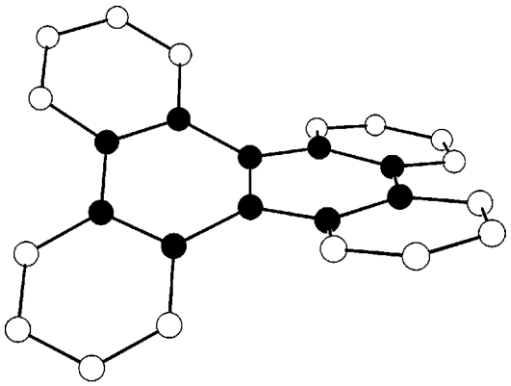

Figure 30. Twist-shaped of dibenzo[g,p]chrysene [128]

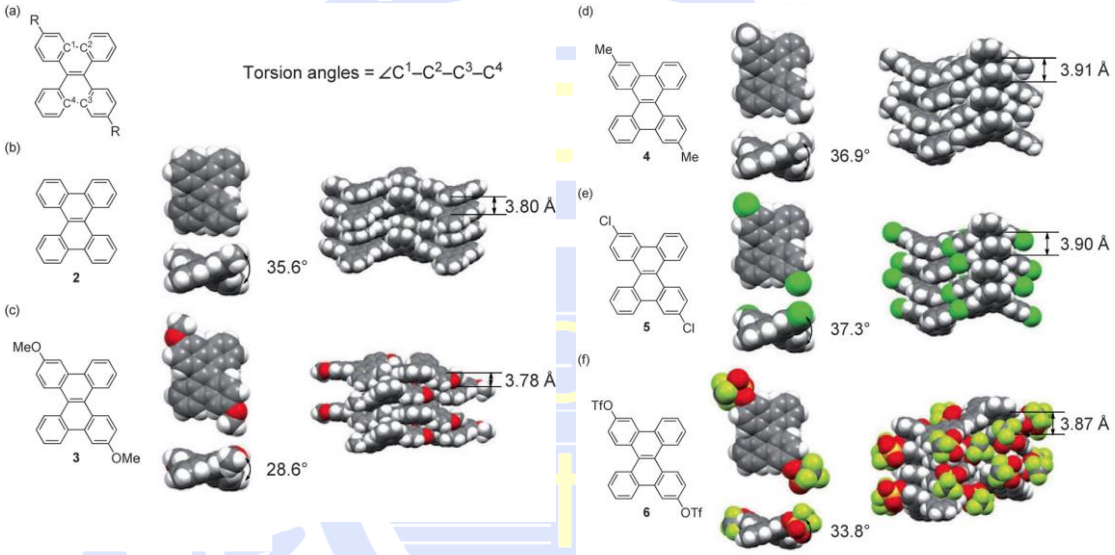

Figure 31. Molecular and packing structures of dibenzo[g,p]chrysene derivatives [129]

When synthesized dibenzo[g,p]chrysene, the intermediate product, 10'-H-spiro[fluorene-9,9'-phenanthren]-10'-one, was found and the X-ray indicated that the structure of it is in cruciform-shaped. Hence, it had adopted to be one of our cores and **Yih-6** and **Yih-7**were synthesized.

In contrast to cruciform-shaped core, the planar core is springing up in recent years, due to strong intermolecular interaction, the molecules have a great potential to show high charge carrier mobility. Some of them even can reach an efficiency close to 19% without adding additives. [130] [131] Based on this concept, **Yih-1** and **Yih-2** were synthesized.

Besides the common four-armed materials, two-armed and three-armed materials also became a remarkable direction in synthesizing HTMs. To date, there are many examples applied in PSCs had gotten a good efficiency and even over 20%. [132] In this work, **Yih-1**, **Yih-2** and **Yih-6** were synthesized in two-armed materials.

To the efficiency of solar cells, open circuit voltage (V_{oc}) and short circuit current (J_{sc}) are important factors, the larger V_{oc} and J_{sc} are, the higher efficiency it will be. In order to improve the V_{oc} and J_{sc}, electron withdrawing cores were introduced in **Yih-1**, **Yih-2**, **Yih-6** and **Yih-7**. Electron withdrawing core can not only lower the HOMO of materials but also help the transmission of current, and then enhance the values of V_{oc} and J_{sc}.

All the cores of HTMs were functionalized with electron-donating bis(4-methoxyphenyl)aniline, bis(4-methoxyphenyl)amine groups, in addition, we introduced 10-(4-(hexyloxy)phenyl)-10H-phenothiazine groups which has stronger electron-donating property as another donor, and investigated the relationship between the molecular structure and photovoltaic properties (Figure 32).

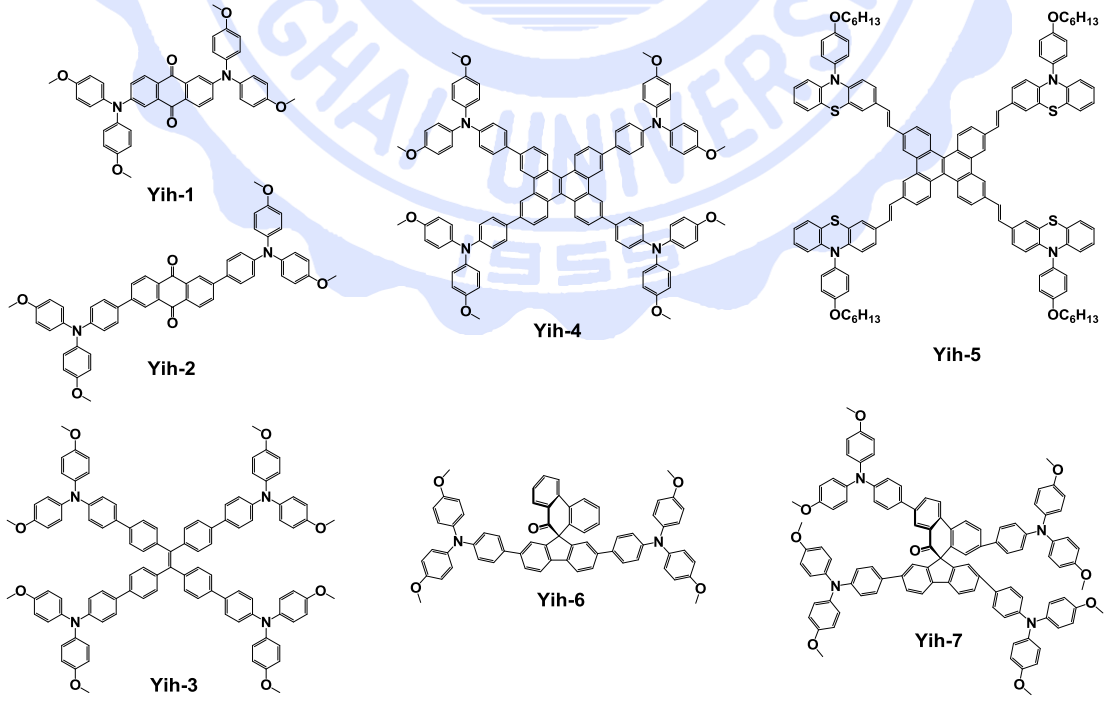

Figure 32. **Yih-** series HTMs structures

3-2 Synthetic Routes

Synthetic route 1:

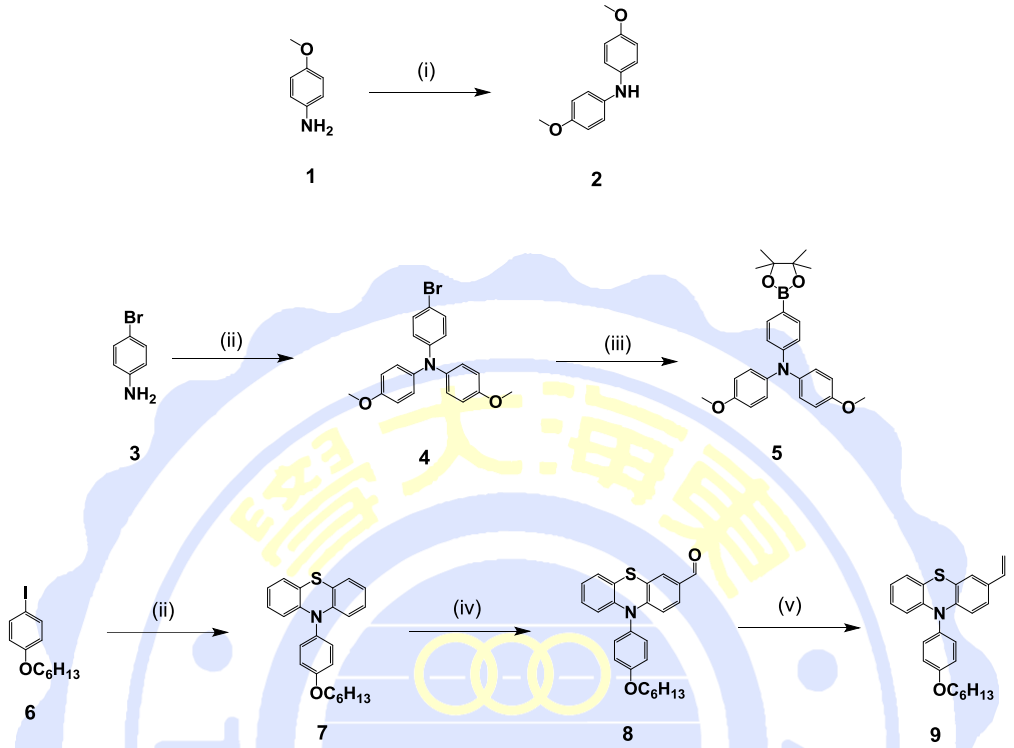

Reagents and conditions: (i) $Pd_2(dba)_3$, NaO^tBu, Tri-*tert*-butylphosphine, Toluene, 120 ℃; (ii) 1,10-phenanthroline, KOH, CuCl, Toluene, 120 ℃; (iii) *n*-BuLi, 2-Isopropoxy-4,4,5,5-tetramethyl-1,3,2-dioxabrolane, THF, -78℃; (iv) $POCl_3$, DMF, 0ºC, 45ºC; (v) *n*-BuLi, CH_3PPh_3I, THF, 0℃

Part one is the synthetic routes of my different donors, compound **2**, **5** and **9**. Compound **2** was synthesized via Buchwald-Hartwig amination; compound **5** was synthesized via Ullmann condensation and boronation; compound **9** was prepared from compound **6**, went through Ullmann condensation, Vilsmeier-Haack formylation and Wittig reaction to afford compound **9**.

Synthetic route 2:

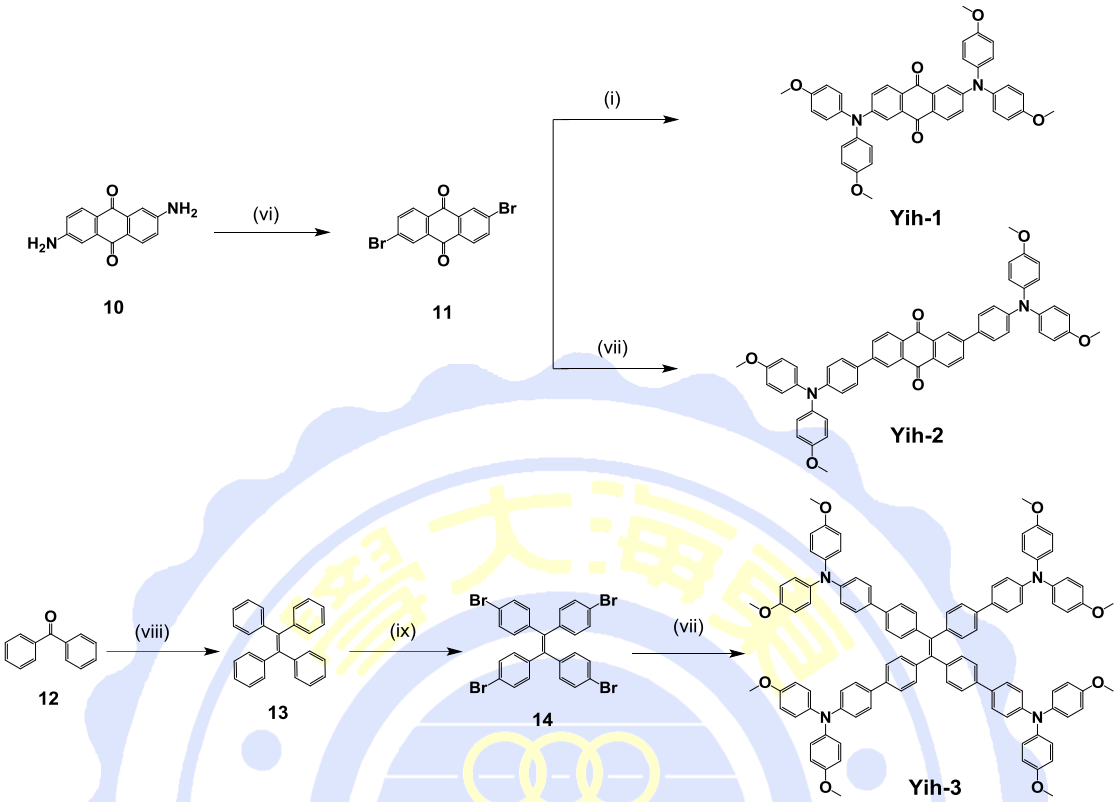

Reagents and conditions: (i) $Pd_2(dba)_3$, NaO^{t}Bu, Tri-*tert*-butylphosphine, Toluene, 120 ℃; (vi) $CuBr_2$, *t*-BuONO, 90℃; (vii) $Pd(pph_3)_4$, Aliquat@336, 2M K_2CO_3, THF, 90 ℃; (viii) Zn, pyridine, $TiCl_4$, THF, 0℃, 90℃; (ix) Br_2, I_2, $CHCl_3$, R.T

Part two is the synthetic routes of my final materials. First, 2,6-diaminoanthracene-9,10-dione went through the reduction reaction to get compound **11**, the core of **Yih-1~2**, and then went through Buchwald-Hartwig amination and Suzuki coupling with compound **2** and **5**, respectively to get **Yih-1** and **Yih-2**. Next, **Yih-3** was synthesized via McMurry reaction and bromination, finally, Suzuki coupling was carried on with compound **5** to get **Yih-3**.

Synthetic route 3:

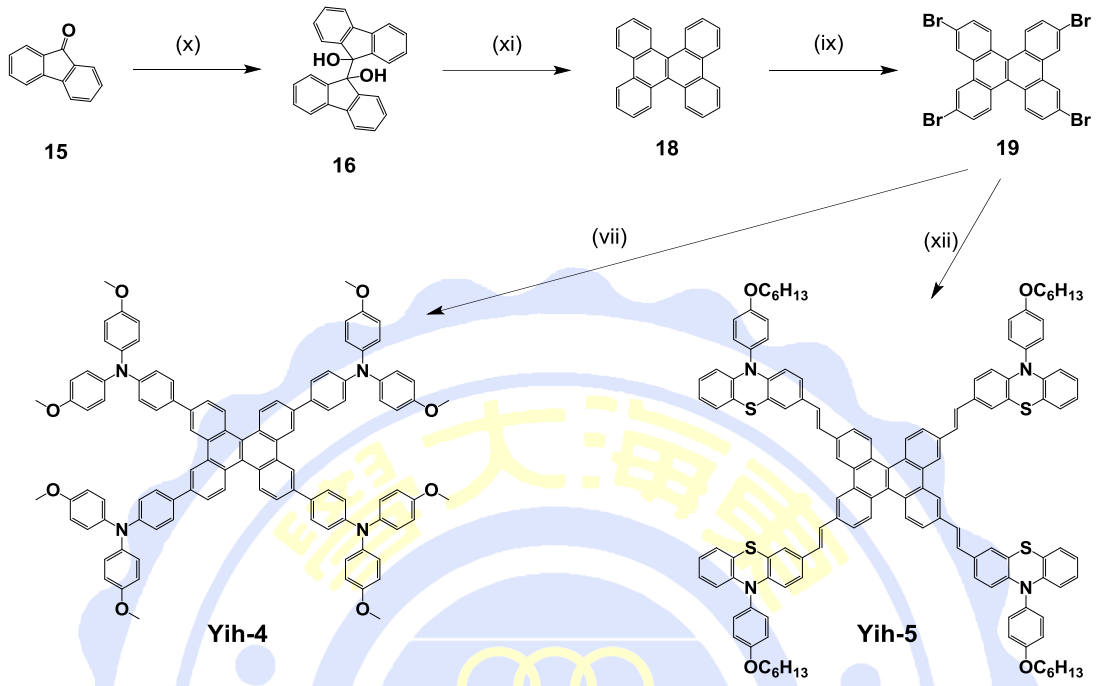

Reagents and conditions: (vii) $Pd(PPh_3)_4$, Aliquat@336, 2M K_2CO_3, THF 90 ℃; (ix) Br_2, I_2, $CHCl_3$, R.T.; (x) Zn, $ZnCl_2$, THF/H_2O, R.T.; (xi) CF_3SO_3H, DCM/Toluene, 0℃; (xii) $Pd(OAc)_2$, K_2CO_3, TBAB, DMF, 160 ℃

The core of **Yih-4~5** was prepared from benzophenone, went through Pinacol coupling, Pinacol rearrangement and bromination, finally, went through Suzuki coupling and Heck reaction with compound **5** and **9**, respectively to afford **Yih-4** and **Yih-5**.

Synthetic route 4:

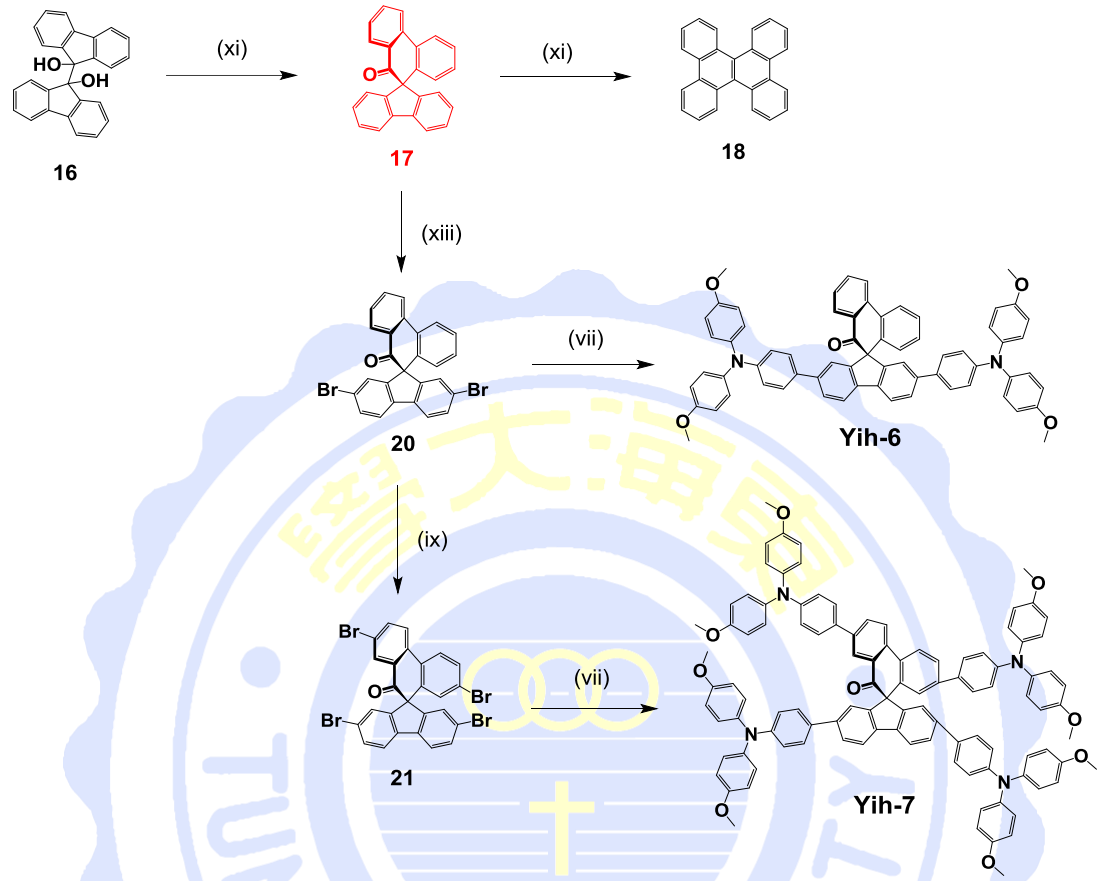

Reagents and conditions: (vii) $Pd(PPh_3)_4$, Aliquat@336, 2M K_2CO_3, THF 90 ℃; (ix) Br_2, I_2, $CHCl_3$, R.T.; (xi) CF_3SO_3H, DCM/Toluene, 0℃; (xiii) Br_2, I_2, dichloromethane, R.T.

When going through Pinacol rearrangement reaction, the intermedium product, compound **17**, is occurred. Using different equivalent of bromine and solvent to yield compound **20** and **21**, and then went through Suzuki coupling with compound **5** produced **Yih-6** and **Yih-7**.

3-3 X-Ray Single Crystal Analysis

Compound **20**, 10′H-spiro[fluorene -9,9′- phenanthren]-10′-one, crystallizes with two independent molecules in the asymmetric unit (Figure 33). In the left molecule, the mean plane of the fluorene unit (r.m.s. deviation = 0.02 Å) is inclined to the mean plane of the phenanthrene unit (r.m.s. deviation = 0.096 Å) by 82.38 (5)°. In the right molecule, the corresponding angle is 80.25 (5)° (r.m.s. deviation are 0.02 and 0.123 Å, respectively), indicating that the conformation of the two molecules is very similar.

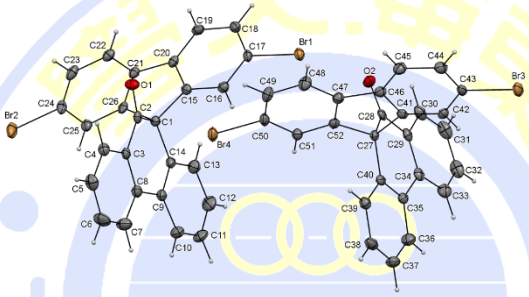

Figure 33. The molecular structure of two independent molecules of compound **20** with the atom labelling.

In the crystal, each molecule forming a centrosymmetric four-molecule unit. These unit are linked by C-H···π interactions, forming ribbons along the b axis direction (Figure 34-a). The ribbons are linked by C-Br···π interactions, forming layers parallel to *ab* plane (Figure 34-b).

(a) **(b)**

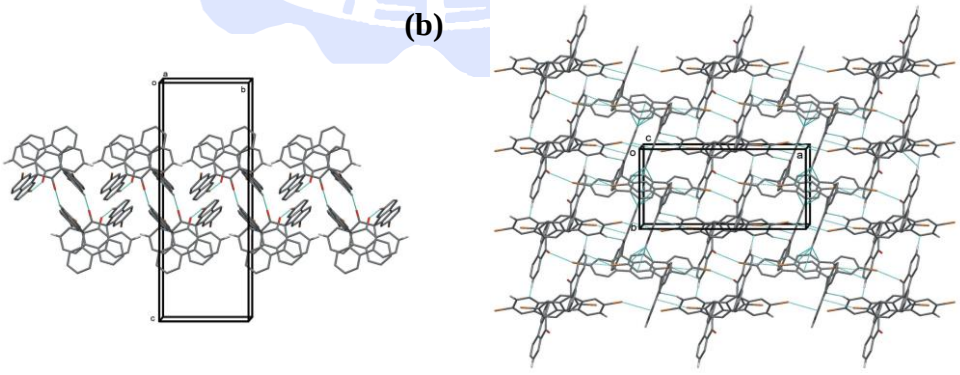

Figure 34. (a) A view along the *a* axis of the ribbons. (b) A view along the *c* axis of crystal packing of the compound **20**

Published source: *IUCrData*, 2017, **2**, x170301

3-4 Theoretical Calculation

The structures of the **Yih-** series materials were optimized using the B3LYP/6-31G* hybrid functional. For the excited states, time-dependent density functional theory with the B3LYP functional was used. All analyses were performed using Q-Chem 3.0 software. The frontier orbital plots of the highest (HOMO) and lowest (LUMO) occupied molecular orbitals were drawn using GaussView 04.

Figure 35 displays the optimized structures of the **Yih-** series HTMs. For **Yih-1~2**, the anthracene-9,10-dione core preserve its planar structures, and in principle, can give rise to stacking aggregation in the solid state, could favor to transport charges. For **Yih-3**, the dihedral angles formed by two phenyl rings at the same side in the 1,1,2,2-tetraphenylethene core is about 46~48º. For **Yih-4**, the dibenzo[g,p]chrysene cores exhibits twisted shape with the dihedral angle of 25º. And for **Yih-6** and **Yih-7**, the mean plane of the phenanthrene unit is twisted with respect to the mean plane of the fluorene unit by 80~82.5º can be determined from the X-ray single crystal analysis, almost perpendicular to each other.

The dihedral angles formed by the phenyl rings connecting the peripheral bis(4-methoxyphenyl)aniline and anthracene-9,10-dione core are around 23~25º. The dihedral angles formed by bis(4-methoxyphenyl)amine and anthracene-9,10-dione, 10'H-spiro[fluorene-9,9'-phenanthren]-10'-one cores are about 31~38º.

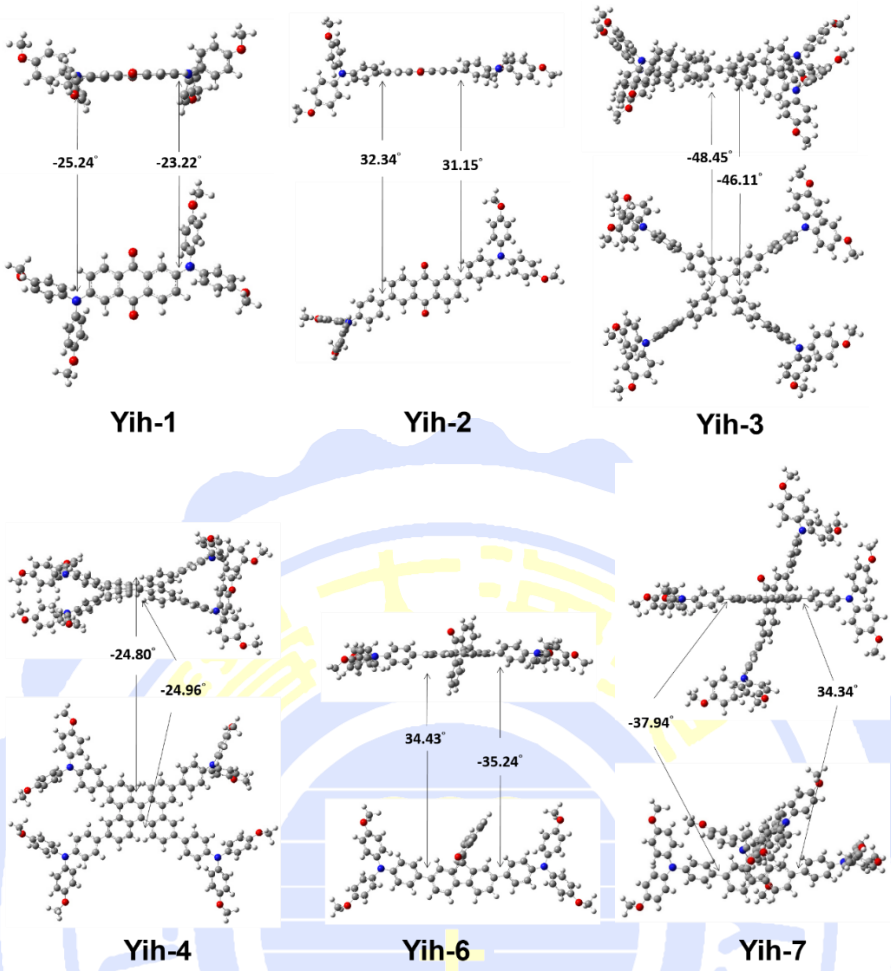

Figure 35. Optimized structure of **Yih-** series HTMs estimated by time-dependent DFT/B3LYP (6-31G* basis set)

Figure 36 depicts the topology and energy of the frontier molecular orbitals participating in the electronic transitions to the lowest-energy singlet excited states. Investigating the charge distribution and the molecular structure of the HTMs in different oxidation states. All of the HOMOs of **Yih-** series HTMs and **spiro-OMeTAD** are found to delocalize over the whole molecule, while the LUMOs are mainly located on the cores, and exhibit the great charge separation.

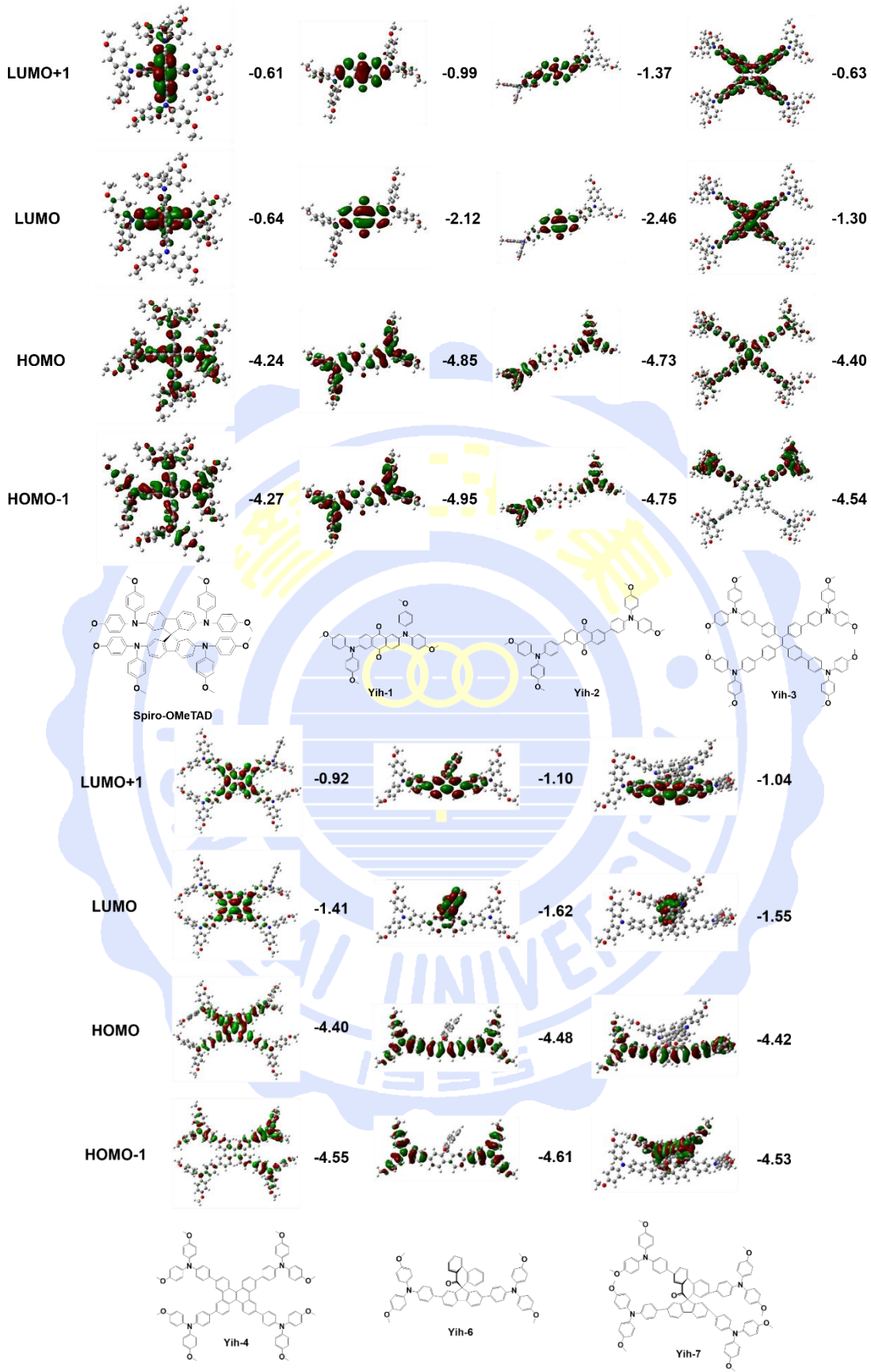

Figure 36. Computed HOMO and LUMO orbitals of **spiro-OMeTAD** and **Yih-** series HTMs

Table 1 collects the vertical excitation energies (λ_{cal}), oscillator strengths (*f*) and electronic descriptions in terms of one-electron molecular orbital excitations calculated for the most first three singlet→singlet ($S_0 \rightarrow S_n$) transitions of **spiro-OMeTAD** and **Yih-** series HTMs. S1 is the state of HOMO to LUMO, the trend of it can be consistent with UV-vis absorption spectra, the lower the energy is, the more red-shift it will be.

Table 1. Calculated Low-Lying Transition for **spiro-OMeTAD** and **Yih-** series HTMs

Dye	State	Excitation[a]	λ_{cal} (eV, nm)	f [b] B3LYP/6-31G*
Spiro-OMeTAD	S1	50.76% H→L	**3.13(395)**	**0.5877**
	S2	59.75% H→L+1	**3.16(392)**	**0.8018**
	S3	53.64% H-1→L	**3.18 (390)**	**0.1524**
Yih-1	S1	98.60% H→L	**2.32(532)**	**0.0004**
	S2	98.36% H-1→L	**2.44(507)**	**0.3596**
	S3	88.00% H-3→L	**3.00(412)**	**0.0007**
Yih-2	S1	74.08% H-1→L	**1.97(627)**	**0.3068**
	S2	73.96% H→L	**1.98(623)**	**0.0450**
	S3	96.74% H→L+1	**2.99(414)**	**0.7157**
Yih-3	S1	97.10% H→L	**2.76(448)**	**0.8432**
	S2	91.08% H-1→L	**2.93(423)**	**0.1310**
	S3	85.10% H-2→L	**2.95(421)**	**0.5922**
Yih-4	S1	96.86% H→L	**2.69(461)**	**0.6005**
	S2	94.43% H-1→L	**2.82(439)**	**0.6953**
	S3	97.51% H-2→L	**2.86(433)**	**0.1058**
Yih-6	S1	96.21% H→L	**2.49(496)**	**0.0378**
	S2	97.61% H-1→L	**2.67(464)**	**0.0006**
	S3	96.60% H→L+1	**3.00(412)**	**1.4147**
Yih-7	S1	97.61% H→L	**2.51(494)**	**0.0231**
	S2	83.55% H-1→L	**2.64(469)**	**0.7065**
	S3	83.74% H-2→L	**2.68(462)**	**0.0267**

[a]H=HOMO, L=LUMO, H+1=HOMO+1, L+1=LUMO+1, and L+2=LUMO+2. [b]Oscillator strengths.

3-5 Optical Electrochemical and Thermal Properties of the Materials

Figure 37 shows the UV-Vis absorption spectra of **Yih-** series HTMs dissolved in CH_2Cl_2. In general, the absorption bands of the D-A-D type molecules were found in the visible region, due to their strong dipole, which could act as both light harvesting and hole transporting layers in perovskite solar cells. Besides, the maximum of the absorption bands increases with the addition of more aromatic substitutions. In terms of the point above, **Yih-2** (λ_{max} = 482 nm) is slightly red-shifted compared to **Yih-1** (λ_{max} = 459 nm), **Yih-5** (λ_{max} = 431 nm) to **Yih-4** (λ_{max} = 385 nm) to **Yih-3** (λ_{max} = 339 nm), and **Yih-6** (λ_{max} = 382) to **Yih-7** (λ_{max} = 377 nm). It completely corresponds to the theoretical calculation. The optical bandgap (E_g) is estimated from the tangent of the absorption band, the wavelengths for **Yih-** series HTMs are 560, 590, 385, 465, 515, 435 and 455 nm, which corresponds to E_g of 2.21, 2.10, 3.22, 2.67, 2.41, 2.85 and 2.73 eV, respectively. It known that reducing the bandgap of a semiconductor can increase the carrier concentration, then enhance the intrinsic electrical conductivity. **Yih-1** and **Yih-2** show lower bandgap than that of other HTMs, especially for **Yih-2** with more aromatic substitution. Therefore, relatively high intrinsic electrical conductivity is anticipated. **Yih-5** with stronger donor, 10-(4-(hexyloxy)phenyl)-10H-phenothiazine, was red-shifted compare to **Yih-3** and **4**, resulting in the lower bandgap. And the four-armed **Yih-7** has lower bandgap compare to the two-armed **Yih-6** was attributed to the stronger electron-donating ability.

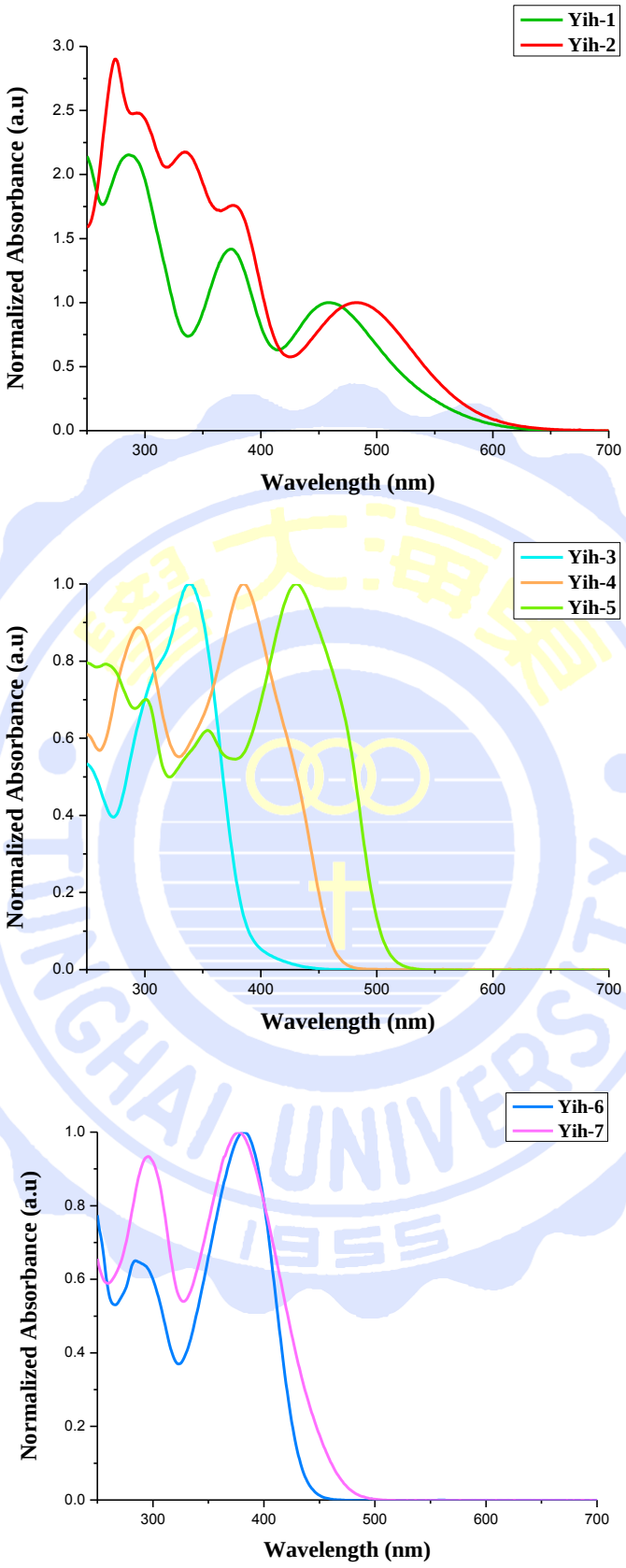

Figure 37. UV-vis absorption spectra of **Yih-** series HTMs normalized at the peak value (top) in CH_2Cl_2

The experimental oxidation potential, corresponding to the HOMO energy levels of **spiro-OMeTAD** and **Yih-** series HTMs were estimated from cyclic voltammogram, using a conventional three-electrode configuration, showing in Figure 38 and the values are presented in Table 2. The HOMO levels of all the **Yih-** series HTMs calculated from CV are -5.25, -5.07, -5.02, -5.03, -4.97, -5.03 and -5.04 eV, respectively. All of the **Yih-** series HTMs showed the lower HOMO level than that of **spiro-OMeTAD** (-4.96 eV). Therefore, relatively high open circuit voltage (V_{oc}) values are anticipated, especially for **Yih-1** exhibit the lowest HOMO level. The relative energy level diagram of **Yih-** series is shown in Figure 39.

Table 2. Optical and electrochemical properties of **Yih-** series HTMs

ID	λ_{abs} (nm)[a]	$E_{s+/s}$ (eV)[b]	E_g[c]	$E_{s+/s*}$ (eV)[d]	$E_{s+/s}$ (eV)[e]	$E_{s+/s*}$(eV)[e]
Spiro-OMeTAD	415	-4.96	2.99	-1.97	-4.24	-0.64
Yih-1	459	-5.25	2.21	-3.04	-4.85	-2.12
Yih-2	482	-5.07	2.10	-2.97	-4.73	-2.46
Yih-3	339	-5.02	3.22	-1.80	-4.40	-1.30
Yih-4	385	-5.03	2.67	-2.36	-4.40	-1.41
Yih-5	431	-4.97	2.41	-2.56		
Yih-6	382	-5.33	2.85	-2.48	-4.48	-1.62
Yih-7	377	-5.02	2.73	-2.29	-4.42	-1.55

[a]Measured in CH_2Cl_2 solution. [b]Oxidation potentials of HTMs (10^{-3} M) were measured in CH_2Cl_2 solution containing 0.1 M $(n\text{-}C_4H_9)_4NPF_6$ with scan rate of 100 $mV{\cdot}s^{-1}$, using glassy carbon working electrode, Pt reference electrode, and Pt counter electrode with Fc/Fc+ as an internal standard. [c]Estimated from the tangent of the normalized absorbance spectra. [d]Calculated from $E_{s+/s*} = E_{s+/s} + E_g$. [e]Ground- and excited-state TD-DFT calculations were done at B3LYP/6-31G*.

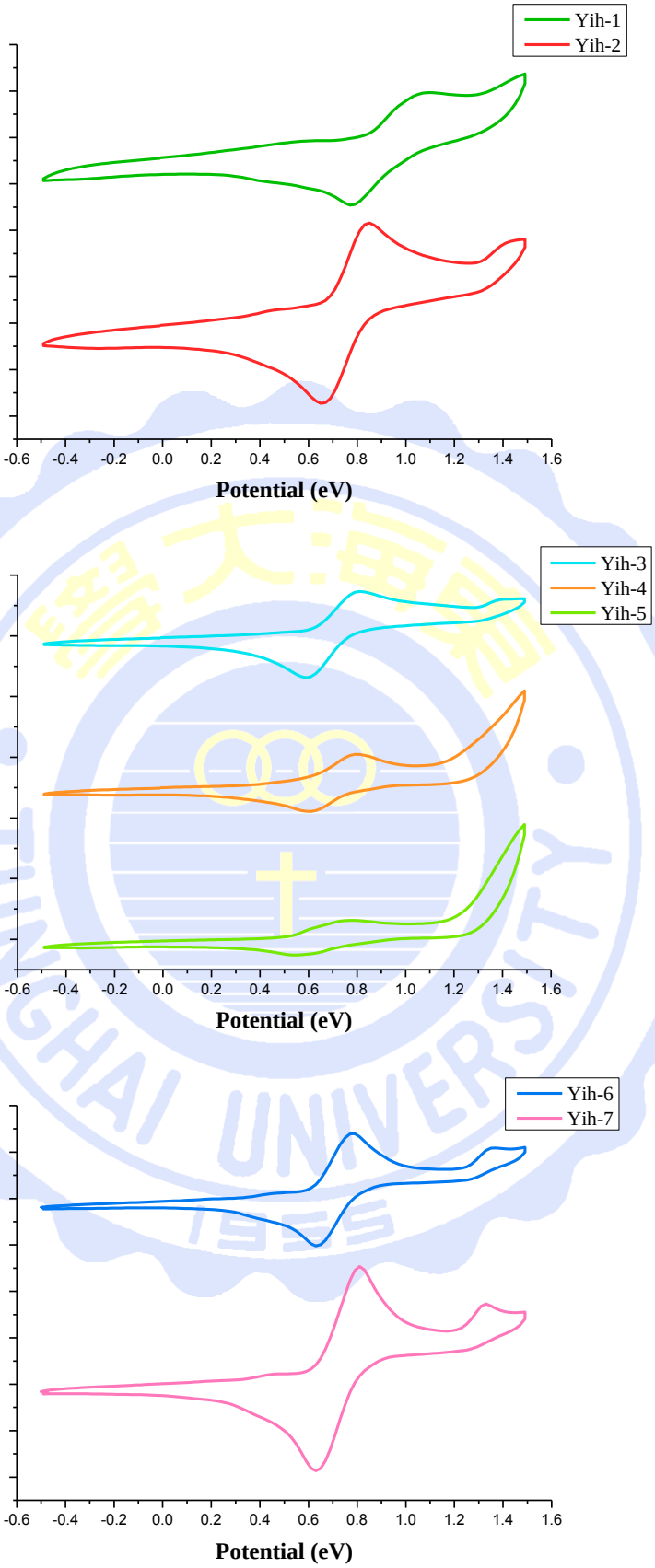

Figure 38. Cyclic voltammograms of **Yih-** series HTMs

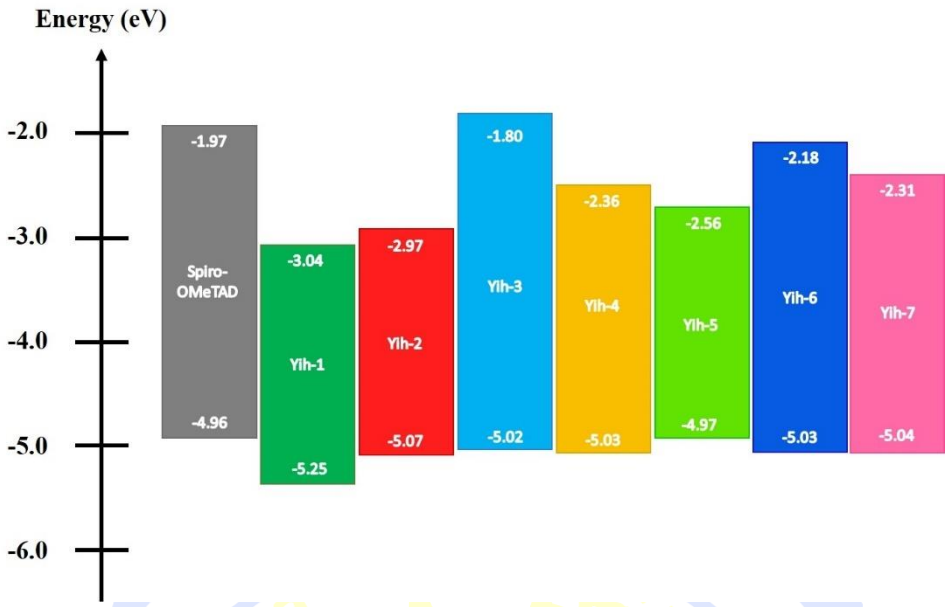

Figure 39. Energy level diagram of **spiro-OMeTAD** and **Yih-** series in CH_2Cl_2

The thermal properties of the compounds are investigated by thermogravimetric analysis (TGA). As demonstrated in Figure 40, the results show that **Yih-3~7** exhibit more than 300ºC of decomposition temperature (5% weight loss). **Yih-4** (395.2 ºC) and **Yih-6** (367.9 ºC) have superior thermal stability than **spiro-OMeTAD** (357.9 ºC), and a high thermal stability is beneficial to the long-term durability of perovskite solar cells. However, **Yih-1** and **Yih-2** show the relatively weak thermal stability than other, might due to their smaller molecular weight. The values are presented in Table 3.

Table 3. Thermal decomposition temperature (T_d) of **spiro-OMeTAD** and **Yih-** series HTMs

ID	T_d (ºC)	ID	T_d (ºC)
Spiro-OMeTAD	357.9	**Yih-4**	395.2
Yih-1	208.8	**Yih-5**	335.7
Yih-2	265.1	**Yih-6**	367.9
Yih-3	350.9	**Yih-7**	346.7

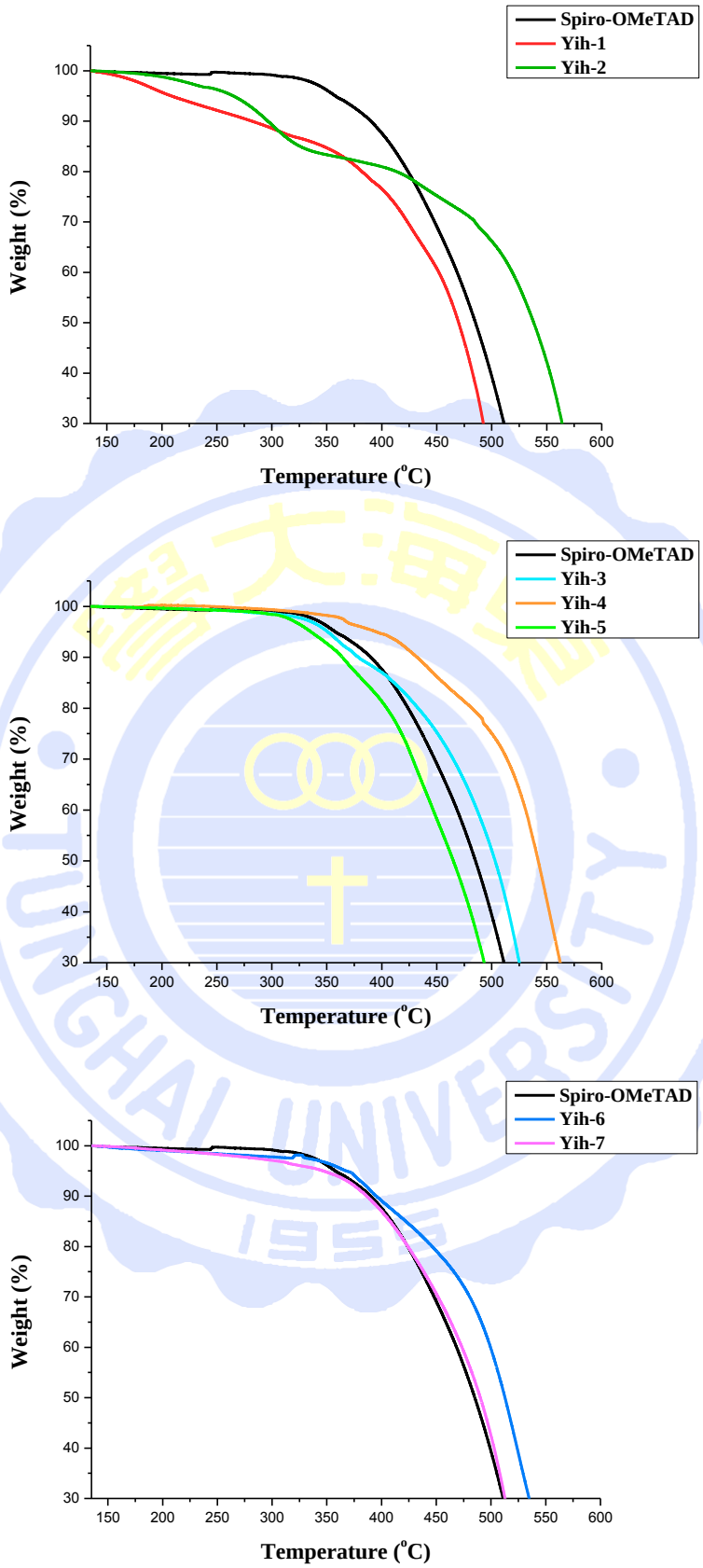

Figure 40. Thermogravimetric analysis of **Yih-** series HTMs in comparison with **spiro-OMeTAD**

3-6 Conclusions

In summary, we reported seven small-molecular hole transporting materials with electron withdrawing moiety by a rapid and efficient synthesis. Electron withdrawing core can not only lower the bandgap, which could make materials act as both light harvesting and hole transporting layer in perovskite solar cells, and expect to increase charge carrier transport, then enhance short circuit current, but also lower the HOMO levels and expect to enhance open circuit voltage. **Yih-1** and **2** with the planar core are expected to show face-on organization leading to vertical charge carrier transport without any additives. **Yih-4** and **6** showed stronger thermal stability than **spiro-OMeTAD**, expecting to show the good the long-term durability of perovskite solar cells.

The future work is to prove the assertions above by measuring the devices based on **Yih-** series HTMs.

Chapter 4 Experimental Section

4-1 Chemical and Analytical Measurement

A、Nuclear Magnetic Resonance spectrum (NMR):

Model: Bruker spectrometers (AV 300/AV 400/AVIII HD 400/AV 500 MHz). The unit of chemical shift (δ) is ppm, the unit of coupling constant (J) is Hz. Solvent are $CDCl_3$ (^1H δ = 7.26 ppm; ^{13}C δ = 77.0 ppm) and CD_3SOCD_3 (^1H δ = 2.5 ppm; ^{13}C δ = 39.52 ppm). Signal splitting: s is singlet, d is doublet, t is triplet, m is multiplet, dd is double doublet.

B、Ultraviolet & Visible spectrophotometer (UV/Vis):

Model: Shimadzu UV-1800 spectrophotometer. Solvent is use the spectral dedicated solvent, the size of sample cell is 1 cm in length and width, 5 cm in height, made of quartz. The range of absorbing is between 250~700 nm.

C、Cyclic voltameter (CV):

Model: CHI610. Using three-electrode setup, consisted of glassy carbon working electrode, auxiliary electrode and reference electrode (Pt). Working electrode is polished by 0.05 μ Al_2O_3, using $Ag/AgNO_3$ as auxiliary electrode and 0.1 M tetrabutylammoniumhexafluorophosphate ($TBAPF_6$) as the electrolyte. Concentration of sample is 10^{-3} M, anhydrous DCM as solvent, measuring oxidation-reduction potential at room temperature. Using ferrocene as the internal correction agent.

D、Mass spectrometer:

Model: JMS-700 double focusing mass spectrometer (JEOL, Tokyo, Japan). Compound are dissociated in FAB^+ and EI ways. This part is measured by Dr. Tseng, Mei-Chun in the mass spectrometry service center of institute of chemistry, Academia Sinica.

E、 Thermogravimetric Analyzer (TGA):

Model: TG/DTA 6200. Return to zero then weigh the sample 2~5 mg under nitrogen, the temperature raising 5 ^{o}C per minute to 600^{o}C then maintain for 20 minutes, observe the change of weight.

F、 X-ray data:

Computer programs: APEX2 and SAINT (Bruker, 2001), SHELXT (Sheldrick, 2015a), SHELXL2013 (Sheldrick, 2015b), Mercury (Macrae et al., 2008) and WinGX(Farrugia, 2012)

G、Column chromatography:

Using Kieselgel Si 60 (230~400 mesh) of silicon made by Merck, filling in the column in dry and wet ways.

H、*J-V* curve measuring instrument:

Model of xeono light source: Keithley 2636A. Model of AM1.5G solar simulator: Newport 91160A. Model of detector: Oriel reference solar cell (91150). Model of spectrometer: Oriel (74110).

I、 IPCE measuring instrument:

Model of monochromator: Newport 74100. Model of amplifier: Stanford Research Systems SR830.

J、 Chemical and Solvent:

All of them were bought at ACROS, Alfa, Sigma-Aldrich, Merck, Showa, Lancaster, TCI.

4-2 Synthesis

Compound 2

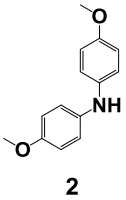

2

To a three-necked round bottom flask were added 4-methoxyaniline (10.0 g, 81.3 mmol) and 4-bromoanisole (16.7 g, 89.8 mmol), $Pd_2(dba)_3$ (1.86 g, 2.0 mmol), NaO^tBu (23.42 g, 243.7 mmol), Tri-*tert*-butylphosphine (20.3 mL, 0.1 M in toluene) and anhydrous toluene (60 mL) under nitrogen. The reaction was refluxed overnight and then cooled down to room temperature. The mixture was filtered by celatom then extracted with ethyl acetate. The organic layer was dried over anhydrous $MgSO_4$ and filtered. After removing the solvent, the crude product was purified by column chromatography on silica gel using CH_2Cl_2 : hexane (1 : 1) as an eluent, yielding a purple brown solid. Data: ^{1}H NMR (400 MHz, $CDCl_3$) : δ 6.95 (d, 4H, *J* = 8.8 Hz), 6.84 (d, 4H, *J* = 9.2 Hz), 5.32 (s, 1H), 3.80 (s, 6H). ^{13}C NMR (100 MHz, $CDCl_3$): 154.2, 137.9, 119.5, 114.7, 55.6.

Compound 4

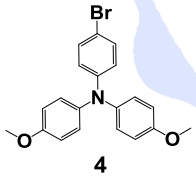

4

To a single-necked round bottom flask were added 4-bromoaniline (5.0 g, 58.5 mmol) and 4-iodoanisole (20.4 g, 174.3 mmol), 1,10-phenathroline (0.2 g, 2.2 mmol), KOH (13.0 g, 465.2 mmol), CuCl (0.1 g, 2.0 mmol) and toluene (150.0 mL) and put Dean-Stark on the neck to remove the water which is produce during the reaction. Refluxed overnight and then cooled down to room temperature. The mixture was filtered by celatom then extracted with ethyl acetate. The organic layer was dried over anhydrous $MgSO_4$ and filtered. After removing the solvent, the crude product was purified by column chromatography on silica gel using CH_2Cl_2 : hexane (1 : 5) as an eluent, yielding a white solid (95.3%). Data: ^{1}H NMR (500 MHz, $CDCl_3$) : δ 7.13 (d, 2H, *J* = 9.0 Hz), 6.93 (d, 4H, *J* = 9.0 Hz),

6.72 (d, 4H, *J* = 9.0 Hz), 6.70 (d, 2H, *J* = 8.5 Hz), 3.69 (s, 6H).

Compound 5

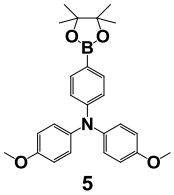

5

To a three-necked round bottom flask were added compound **4** (3.0 g, 7.8 mmol) in anhydrous THF (40.0 mL) under nitrogen at -78°C, then *n*-BuLi (4.7 mL, 2.5 M in hexane) was added drop-wise. After 30 min of stirring, 2-isopropoxy-4,4,5,5-tetramethyl-1,3,2-dioxaborolane (2.2 mL, 10.8 mmol) was added slowly to the reaction solution at -78°C. The temperature of the solution was warmed to room temperature and stirred overnight. Then, the reaction was quenched by cool water and extracted with ethyl acetate. The organic layer was dried over anhydrous $MgSO_4$ and filtered. After removing the solvent, the crude product was purified by column chromatography on silica gel using CH_2Cl_2 : hexane (1 : 1) as an eluent, yielding a yellow solid. Data: ^{1}H NMR (500 MHz, $CDCl_3$) : δ 7.60 (d, 2H, *J* = 8.5 Hz), 7.06 (d, 4H, *J* = 9.0 Hz), 6.86 (d, 4H, *J* = 8.5 Hz), 6.80 (d, 2H, *J* = 9.0 Hz), 3.80 (s, 6H), 1.32 (s, 12H). ^{13}C NMR (125 MHz, $CDCl_3$): 156.1, 151.3, 140.4, 135.7, 127.1, 118.6, 114.7, 83.4, 55.5, 24.8.

Compound 7

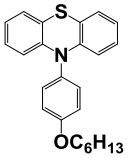

7

Compound **7** was synthesized following the procedure similar to that we used for compound **4**, except that compound **6** (17.2 g, 56.6 mmol) and phenothiazine (10.0 g, 50.2 mmol) was used in place of 4-bromoaniline and 4-iodoanisole. Yielding a yellow solid. Data: ^{1}H NMR (400 MHz, $CDCl_3$) : δ 7.28 (dd, 2H, *J* = 8.2, 2.0 Hz), 7.00 (d, 2H, *J* = 1.2 Hz), 6.98 (dd, 2H, *J* = 5.6, 3.6 Hz), 6.77 (dd, 2H, *J* = 5.8, 3.6 Hz), 6.20 (d, 2H, *J* = 8.8 Hz), 4.03 (t, 2H, *J* = 6.4 Hz), 1.82-1.88 (m, 2H), 1.50-1.54 (m, 2H), 1.386-1.394 (m, 4H), 0.93-0.96 (m, 3H). ^{13}C NMR (100 MHz, $CDCl_3$): 158.8, 144.7, 133.0, 132.2, 126.8, 126.5, 122.2, 119.6, 116.3, 115.6, 68.3, 31.6,

29.2, 25.8, 22.6, 14.0.

Compound 8

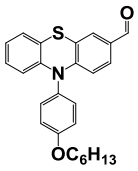

8

To a three-necked round bottom flask were added $POCl_3$ (0.6mL, 6.66 mmol) in anhydrous DMF (15.0 mL) under nitrogen at 0°C, after warming to room temperature. After 1 hour of stirring, compound **7** (0.5 g, 1.33 mmol) in anhydrous DMF (5.0 mL) was added slowly to the reaction solution, heating to 45°C and stirring 2 hours. Then the reaction was quenched by the solution of sodium bicarbonate and extracted with ethyl acetate. The organic layer was dried over anhydrous $MgSO_4$ and filtered. After removing the solvent, the crude product was purified by column chromatography on silica gel using CH_2Cl_2 : hexane (1 : 2) as an eluent, yielding a yellow solid (89.3%). Data: ^{1}H NMR (400 MHz, $CDCl_3$) : δ 9.68 (s, 1H), 7.44 (d, 1H, *J* = 1.6 Hz), 7.28 (dd, 1H, *J* = 8.2, 2.0 Hz), 7.26 (d, 2H, *J* = 8.8 Hz), 7.13 (d, 2H, *J* = 8.8 Hz), 6.96 (dd, 1H, *J* = 5.6, 3.6 Hz), 6.84 (dd, 2H, *J* = 5.8, 3.6 Hz), 6.22 (d, 1H, *J* = 8.8 Hz), 6.17-6.19 (m, 1H), 4.05 (t, 2H, *J* = 6.4 Hz), 1.84-1.88 (m, 2H), 1.51-1.55 (m, 2H), 1.38-1.42 (m, 4H), 0.93-0.97 (m, 3H). ^{13}C NMR (100 MHz, $CDCl_3$): 189.6, 159.2, 149.5, 142.8, 132.0, 131.6, 130.9, 129.9, 127.3, 127.1, 126.6, 123.5, 120.0, 118.9, 116.7, 116.4, 115.0, 68.4, 31.5, 29.2, 25.7, 22.6, 14.0.; HRMS calcd for $C_{25}H_{25}NO_2S$: 404.1684, found 404.1694.

Compound 9

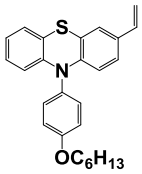

9

To a three-necked round bottom flask were added CH_3PPh_3I (6.1 g, 15.1 mmol) in anhydrous THF (40.0 mL) under nitrogen at 0°C, then *n*-BuLi (5.7 mL, 2.5 M in hexane) was added drop-wise. After 15 min of stirring, compound **8** (3.0 g, 7.4 mmol) in anhydrous THF was added slowly to the reaction solution at 0°C. The temperature of the solution was warmed to room temperature and

stirred overnight. Then, the reaction was quenched by cool water and extracted with ethyl acetate. The organic layer was dried over anhydrous $MgSO_4$ and filtered. After removing the solvent, the crude product was purified by column chromatography on silica gel using CH_2Cl_2 : hexane (1 : 4) as an eluent, yielding a yellow oil. Data: ^{1}H NMR (400 MHz, $CDCl_3$) : δ 9.68 (s, 1H), 7.44 (d, 1H, *J* = 1.6 Hz), 7.28 (dd, 1H, *J* = 8.2, 2.0 Hz), 7.26 (d, 2H, *J* = 8.8 Hz), 7.13 (d, 2H, *J* = 8.8 Hz), 6.96 (dd, 1H, *J* = 5.6, 3.6 Hz), 6.84 (dd, 2H, *J* = 5.8, 3.6 Hz), 6.22 (d, 1H, *J* = 8.8 Hz), 6.17-6.19 (m, 1H), 4.05 (t, 2H, *J* = 6.4 Hz), 1.84-1.88 (m, 2H), 1.51-1.55 (m, 2H), 1.38-1.42 (m, 4H), 0.93-0.97 (m, 3H). ^{13}C NMR (100 MHz, $CDCl_3$): 158.9, 144.2, 144.1, 135.3, 132.9, 132.0, 131.9, 126.8, 126.5, 125.0, 124.0, 122.2, 119.6, 119.2, 116.4, 115.6, 115.4, 111.8, 68.3, 31.6, 29.2, 25.7, 22.6, 14.0.

Compound 11

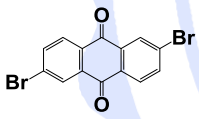

11

To a three-necked round bottom flask were added compound **10** (5.0 g, 21.0 mmol) and $CuBr_2$ (11.7 g, 52.5 mmol), *t*-BuONO (6.3 mL, 52.5 mmol), anhydrous acetonitrile (250.0 mL) under nitrogen. The reaction was refluxed overnight and then cooled down to room temperature. The mixture was washed by 20% HCl and acetonitrile sequentially, then compound **11** was obtained without any purification, yielding a brown solid (97%). Data: ^{1}H NMR (300 MHz, CDCl3): *δ* 8.43 (s, 2H), 8.17 (d, 2H, *J* = 8.4 Hz), 7.95 (d, 2H, *J*= 8.4 Hz); ^{13}C NMR (75 MHz, $CDCl_3$): *δ* 137.4, 130.4, 129.1; HRMS (*m/z*) (FAB): 363.8744 (M^+) (calcd for $C_{14}H_6Br_2O_2$: 363.8734).

Compound 13

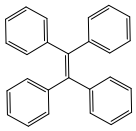

13

To a three-necked round bottom flask were added $TiCl_4$ (15.0 mL, 136.8 mmol) and anhydrous THF (75.0 mL) under nitrogen at 0°C. After stirring for 30 min, Zn powder (17.6 g, 274.5 mmol) was added to the reaction solution and refluxed for 2 hours. Then added pyridine (11.1 mL, 137.3 mmol) to the reaction solution and refluxed for one hour. After cooling down to room temperature, the solution of compound **12** (5.0 g, 27.5 mmol) in anhydrous THF was added to the reaction solution. The reaction was refluxed overnight and then cooled down to room temperature. The mixture was filtered by celatom then extracted with ethyl acetate. The organic layer was dried over anhydrous $MgSO_4$ and filtered. After removing the solvent, the crude product was purified by column chromatography on silica gel using CH_2Cl_2 : hexane (1 : 4) as an eluent, yielding a white solid (57.3%). Data: ^{1}H NMR (400 MHz, $CDCl_3$) : δ 7.11-7.09 (dd, 12H, *J* = 2.0 and 2.0 Hz), 7.04-7.02 (dd, 8H, *J* = 4.0 and 2.4 Hz). ^{13}C NMR (100 MHz, $CDCl_3$): 143.7, 141.0,131.3, 127.6, 126.4.

Compound 14

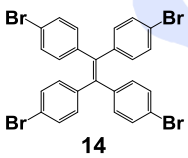

14

To a single-necked round bottom flask were added compound **13** (5.0 g, 15.1 mmol) and iodine (0.08 g, 0.3 mmol), bromine (3.5 mL, 68.0 mmol) and chloroform (100 mL) under nitrogen and stirred overnight. The resulting precipitate was filtered and washed with methanol, then compound **16** was obtained without any purification, yielding a white solid (97.3%). Data: ^{1}H NMR (400 MHz, $CDCl_3$) : δ 7.26 (d, 1H, *J* = 8.4 Hz), 6.84 (d, 1H, *J* = 8.4 Hz). ^{13}C NMR (100 MHz, $CDCl_3$): 141.5, 139.6, 132.7, 131.3, 121.3.

Compound 16

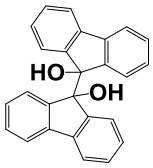

16

To a single-necked round bottom flask were added compound **15** (10.0 g, 55.5 mmol) and zinc powder (25.4 g, 388.5 mmol), zinc chloride (5.2 g, 38.2), water (10.0 mL) and THF (100.0 mL) under nitrogen and stirred 30 min. The mixture was dried over anhydrous $MgSO_4$, filtered and washed by ethyl acetate. After removing the solvent, the crude product was recrystallized by methanol, yielding a white solid (67.3%). Data: ^{1}H NMR (400 MHz, $CDCl_3$) : δ 7.37 (d, 4H, *J* = 7.2 Hz), 7.24 (s, 2H), 7.07 (s, 2H), 3.18 (s, 2H). ^{13}C NMR (100 MHz, $CDCl_3$): 145.2, 140.6, 129.1, 127.0, 125.2, 119.2, 86.5.

Compound 17

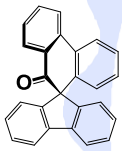

17

To a single round bottom flask were added compound **16** (9.7 g, 26.8 mmol) dissolved in dichloromethane and added toluene (100.0 mL), then CF_3SO_3H (30.0 mL, 339.0 mmol) was added drop-wise at 0°C. After 15 min of stirring, the reaction was quenched by cool water and extracted with ethyl acetate. The organic layer was dried over anhydrous $MgSO_4$ and filtered. After removing the solvent, the crude product was recrystallized by methanol, yielding a white solid (98.5%). Data: ^{1}H NMR (400 MHz, $CDCl_3$) : δ 8.20 (d, 1H, *J* = 7.2 Hz), 8.10 (d, 1H, *J* = 7.2 Hz), 7.99 (d, 1H, *J* = 7.2 Hz), 7.80 (d, 3H, *J* = 7.2 Hz), 7.47-7.41 (m, 1H), 7.39-7.34 (m, 3H), 7.20-7.16 (m, 2H), 7.10-7.03 (m, 3H), 6.63-6.61 (dd, 1H, *J* = 1.2 and 1.5 Hz). ^{13}C NMR (100 MHz, $CDCl_3$): 197.16, 147.1, 141.6, 139.3, 138.1, 134.9, 130.5, 130.1, 129.2, 128.5, 128.3, 128.1, 128.0, 127.9, 124.7, 124.1, 123.2, 120.5, 68.7.

Compound 18

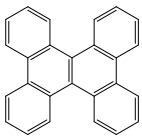

18

To a single round bottom flask were added compound **16** (5.0 g, 26.8 mmol) dissolved in dichloromethane and added toluene (300.0 mL), then CF_3SO_3H (50.0 mL, 339.0 mmol) was added drop-wise at 0°C. After 2 days of stirring, the reaction was quenched by cool water and extracted with ethyl acetate. The organic layer was dried over anhydrous $MgSO_4$ and filtered. After removing the solvent, the crude product was purified by column chromatography on silica gel using CH_2Cl_2 : hexane (1 : 2) as an eluent, yielding a white solid (33%). Data: ^{1}H NMR (400 MHz, $CDCl_3$) : δ 8.73-8.70 (m, 2H), 7.71-7.62 (m, 2H). ^{13}C NMR (100 MHz, $CDCl_3$): 130.9, 129.2, 128.9, 127.5, 126.6, 123.6.

Compound 19

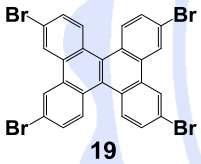

19

Compound **19** was synthesized following the procedure similar to that we used for compound **14**, except that compound **18** (5.0 g, 15.2 mmol) was used in place of compound **13**. Yielding a white solid (99.2%). Data: ^{1}H NMR (400 MHz, $CDCl_3$) : δ 8.73 (d, 1H, *J* = 2.0 Hz), 8.42 (d, 1H, *J* = 8.8 Hz), 7.75 (dd, 1H, *J* = 2.0 and 2.0 Hz). ^{13}C NMR (100 MHz, $CDCl_3$): 131.3, 130.6, 130.2, 127.7, 126.9, 126.6, 121.6.

Compound 20

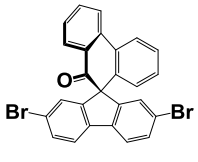

20

Compound **20** was synthesized following the procedure similar to that we used for compound **14**, except that compound **17** (8.5 g, 15.2 mmol) and dichloromethane was used in place of compound **13** and chloroform. Yielding a white solid (95.3%). Data: ^{1}H NMR (400 MHz, $CDCl_3$) : δ 8.22 (d, 1H, *J* = 8.12 Hz), 8.14 (d, 1H, *J* = 7.8 Hz), 8.03 (dd, 1H, *J* = 7.76 and 1.32 Hz), 7.84 (t, 1H, *J* = 7.92 Hz), 7.66 (s, 1H), 7.64 (s, 1H), 7.49-7.55 (m, 3H), 7.43 (t, 1H, *J* = 7.86

Hz), 7.13-7.17 (m, 3H), 6.59 (dd, 1H, *J* = 7.88 and 1.12 Hz). ^{13}C NMR (100 MHz, $CDCl_3$): 195.7, 149.1, 139.6, 137.7, 137.5, 135.4, 131.7, 130.3, 129.5, 129.3, 128.8, 128.7, 128.6, 128.2, 127.9, 124.3, 123.4, 121.9, 121.8.

Compound 21

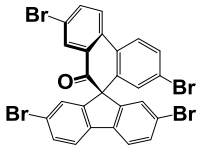

21

Compound **21** was synthesized following the procedure similar to that we used for compound **14**, except that compound **17** (5.0 g, 14.5 mmol) was used in place of compound **13**. Yielding a white solid. Data: ^{1}H NMR (400 MHz, $CDCl_3$) : δ 8.47 (d, 1H, *J* = 8.0 Hz), 8.11 (d, 1H, *J* = 0.4 Hz), 8.02 (dd, 1H, *J* = 1.6 and 1.2 Hz), 7.96-7.91 (m, 2H), 7.76 (d, 1H, *J* = 1.6 Hz), 7.61-7.55 (m, 2H), 7.05 (dd, 2H, *J* = 1.6 and 1.6 Hz), 6.66 (d, 2H, *J* = 2.0 Hz). ^{13}C NMR (100 MHz, $CDCl_3$): 192.9, 150.1, 148.5, 139.1, 139.0, 138.6, 138.3, 136.6, 135.6, 132.3, 132.0, 131.8, 131.2, 130.0, 128.5, 127.4, 126.8, 125.8, 125.5, 125.2, 124.2, 123.5, 123.0, 121.9, 117.8, 67.3.

Material Yih-1

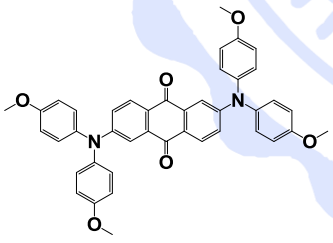

Yih-1

Material **Yih-1** was synthesized following the procedure similar to that we used for compound **2**, except that compound **2** (5.0 g, 21.8 mmol) and compound **13** (4.0 g, 10.9 mmol) was used in place of 4-methoxyaniline and 4-bromoanisole. Yielding a red solid (38.0%). Data: ^{1}H NMR (400 MHz, $CDCl_3$) : δ 7.26 (d, 2H, *J* = 8.8 Hz), 7.59 (d, 2H, *J* = 2.8 Hz), 7.13 (d, 8H, *J* = 8.8 Hz), 7.01 (dd, 2H, *J* = 2.8 and 2.8 Hz), 6.89 (d, 8H, *J* = 8.8 Hz), 3.82 (s, 12H). ^{13}C NMR (100 MHz, $CDCl_3$): 182.0, 157.4, 153.6, 138.6, 135.6, 129.0, 128.0, 124.8, 120.6, 115.2, 114.1, 55.5.

Material Yih-2

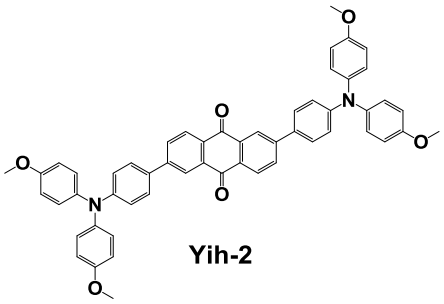

To a single-necked round bottom flask were added compound **5** (6.0 g, 13.9mmol) and compound **13** (1.8 g, 4.9mmol), $Pd(PPh_3)_4$ (4.8 g, 4.2 mmol), K_2CO_3 aqueous solution(2.0 M, 50 mL) and THF (50.0 mL). After stirring overnight, the reaction was extracted with ethyl acetate. The organic layer was dried over anhydrous $MgSO_4$ and filtered. After removing the solvent, the crude product was purified by column chromatography on silica gel using CH_2Cl_2 : hexane (2 : 1) as an eluent, yielding a red solid. Data: ^{1}H NMR (500 MHz, $CDCl_3$) : δ 8.49 (s, 1H), 8.33 (d, 1H, *J* = 8.5 Hz), 7.95 (d, 1H, *J* = 8.5 Hz), 7.56 (d, 2H, *J* = 3.0 Hz), 7.12 (d, 4H, *J* = 9.0 Hz), 7.01 (d, 2H, *J* = 8.5 Hz), 8.67 (d, 4H, *J* = 9.0 Hz), 3.82 (s, 6H). ^{13}C NMR (125 MHz, $CDCl_3$): 183.1, 160.3, 156.4, 149.6, 146.4, 140.3, 134.2, 131.4, 131.0, 129.9, 128.1, 127.9, 127.1, 124.4, 119.8, 114.9, 55.5, 30.9.

Material Yih-3

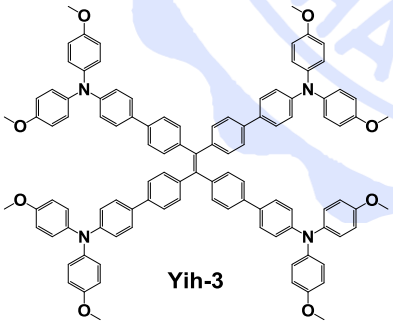

Material **Yih-3** was synthesized following the procedure similar to that we used for material **Yih-2**, except that compound **16** (3.0 g, 4.7 mmol) was used in place of compound **13**. Yielding a yellow solid. Data: ^{1}H NMR (400 MHz, $CDCl_3$) : δ 7.38 (d, 8H, *J* = 8.8 Hz), 7.31 (d, 8H, *J* = 8.4 Hz), 7.11 (d, 8H, *J* = 8.4 Hz), 7.04 (d, 16H, *J* = 1.6 Hz), 6.94 (d, 8H, *J* = 8.8 Hz), 6.82 (d, 16H, *J* = 2.0 Hz), 3.79 (s, 24H). ^{13}C NMR (100 MHz, $CDCl_3$): 155.7, 147.8, 141.9, 141.0, 138.1, 132.8, 128.9, 127.2, 126.4, 126.2, 120.9, 114.7, 55.5.

Material Yih-4

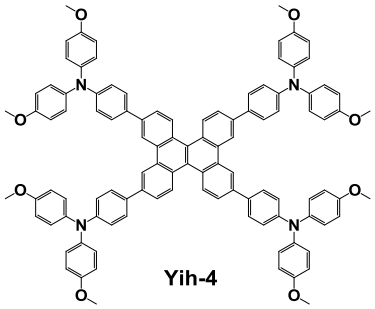

Material **Yih-4** was synthesized following the procedure similar to that we used for material **Yih-2**, except that compound **21** (3.0 g, 4.7 mmol) was used in place of compound **13**. Yielding a yellow solid. Data: ^{1}H NMR (400 MHz, $CDCl_3$) : δ 8.89 (s, 4H), 8.74 (d, 4H, *J* = 8.4 Hz), 7.84 (d, 4H, *J* = 8.4 Hz), 7.66 (d, 8H, *J* = 8.4 Hz), 7.14 (d, 16H, *J* = 8.4 Hz), 7.09 (d, 8H, *J* = 8.0 Hz), 6.87 (d, 16H, *J* = 8.8 Hz), 3.829 (s, 24H). ^{13}C NMR (100 MHz, $CDCl_3$): 156.0, 148.4, 140.9, 138.7, 132.8, 131.2, 129.3, 128.1, 127.8, 126.7, 125.2, 120.9, 114.8, 55.5.

Material Yih-5

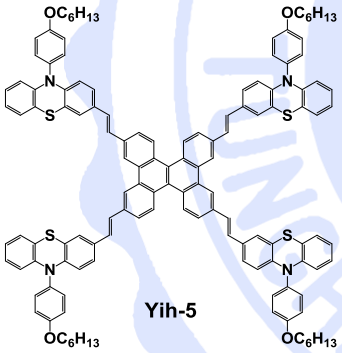

To a single-necked round bottom flask were added compound **11** (1.0 g, 2.5mmol) and compound **21** (0.3 g, 4.9mmol), $Pd(OAc)_2$ (0.06 g, 0.3 mmol), K_2CO_3 (excess) TBAB (excess) and DMF (20.0 mL). The reaction was refluxed overnight and then cooled down to room temperature. The mixture was filtered by celatom then extracted with ethyl acetate. The organic layer was dried over anhydrous $MgSO_4$ and filtered. After removing the solvent, the crude product was purified by column chromatography on silica gel using CH_2Cl_2 : hexane (2 : 1) as an eluent, yielding a yellow solid. Data: ^{1}H NMR (400 MHz, $CDCl_3$) : δ 8.49 (s, 1H), 8.45 (d, 1H, *J* = 8.68 Hz), 7.66 (d, 1H, *J* = 8.52 Hz), 7.28 (s, 1H), 7.21 (s, 1H), 7.08 (dd, 4H, *J* = 8.8 and 6.84 Hz), 7.00 (dd, 1H, *J* = 1.52 and 1.48 Hz), 6.97 (d, 1H, *J* = 8.24 Hz), 6.86-6.78 (m, 2H), 6.17 (t, 2H *J* = 6.0 Hz), 4.03 (t, 2H, *J* = 6.38 Hz), 1.89-1.81 (m, 2H), 1.39-1.37 (m, 4H), 1.25 (s, 1H), 0.95 (t, 3H, *J* = 6.9 Hz). ^{13}C NMR (100 MHz, $CDCl_3$): 158.9, 144.2, 143.9, 135.4, 132.9,132.1, 131.7, 130.8, 129.1,

128.5, 127.7, 126.8, 126.6, 125.7, 124.1, 123.8, 122.3, 122.0, 119.9, 119.3, 116.4, 115.7, 68.4, 31.6, 29.3, 25.8, 22.6, 14.1.

Material Yih-6

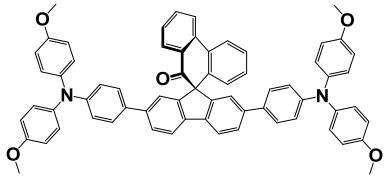

Yih-6

Material **Yih-6** was synthesized following the procedure similar to that we used for material **Yih-2**, except that compound **22** (1.0 g, 2.0mmol) was used in place of compound **13**. Yielding a yellow solid. Data: ^{1}H NMR (400 MHz, $CDCl_3$) : δ 8.18 (d, 1H, *J* = 8.0 Hz), 8.08 (d, 1H, *J* = 8.0 Hz), 8.02 (dd, 1H, *J* = 1.2 and 1.2 Hz), 7.81 (d, 2H, *J* = 4.8 Hz), 7.58 (dd, 2H, *J* = 1.2 and 1.6 Hz), 7.45 (t, 1H, *J* = 14.8), 7.37-7.33 (m, 1H), 7.23 (d, 8H, *J* = 8.4 Hz), 7.19 (d, 8H, *J* = 0.8 Hz), 7.03 (dd, 8H. *J* = 2.0 and 2.0 Hz), 6.84 (d, 4H, *J* = 8.8 Hz), 6.81 (dd, 8H, *J* = 2.0 and 2.4 Hz), 6.71 (d, 1H, *J* = 8.0 Hz). ^{13}C NMR (100 MHz, $CDCl_3$): 197.1, 155.9, 148.1, 148.0, 140.8, 140.1, 139.9, 139.4, 138.2, 134.9, 132.7, 130.5, 130.0, 129.3, 128.6, 128.5, 128.3, 128.0, 127.4, 126.7, 126.5, 124.0, 123.3,122.6, 120.7, 120.6, 114.7, 68.6, 55.5.

Material Yih-7

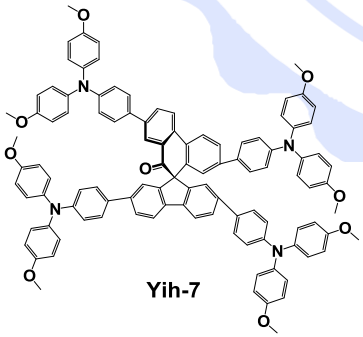

Yih-7

Material **Yih-7** was synthesized following the procedure similar to that we used for material **Yih-2**, except that compound **23** (1.0 g, 1.5mmol) was used in place of compound **13**. Yielding a yellow solid. Data: ^{1}H NMR (400 MHz, $CDCl_3$) δ 8.24 (d, 1H, *J* = 1.84 Hz), 8.21 (d, 1H, *J* = 8.6 Hz), 8.12 (d, 1H, *J* = 8.44 Hz), 7.98 (dd, 1H, *J* = 1.84 and 1.88 Hz), 7.55 (d, 1H, *J* = 10.12 Hz), 7.51 (d, 1H, *J* = 8.72 Hz), 7.42 (d, 2H, *J* = 1.2 Hz), 7.36 (dd, 2H, *J* = 1.24 and 1.12 Hz), 7.28 (d, 2H, *J* = 8.4 Hz), 7.23 (d, 2H, *J* = 2.68 Hz), 7.21 (s, 2H), 7.19 (s, 2H), 7.17 (s, 2H), 7.13 (d, 2H, *J* = 8.64 Hz), 7.10-7.06 (m, 6H), 7.03-7.00 (m,

12H), 6.90-6.78 (m, 22H), 3.81 (d, 12H, *J* = 9.08 Hz), 3.78 (s, 12H). ^{13}C NMR (100 MHz, $CDCl_3$): 197.4, 156.1, 156.0, 155.9, 155.8, 149.1, 148.8, 148.7, 148.4, 148.2, 148.0, 147.9, 141.2, 141.0, 140.9, 140.7, 140.2, 140.1, 139.8, 139.7, 138.2, 137.0, 136.1, 132.8, 132.6, 132.5, 131.5, 130.8, 130.0, 128.9, 128.7, 127.5, 127.3, 127.3, 127.2, 126.8, 126.7, 126.5, 126.5, 126.2, 126.1, 125.8, 124.3, 123.7, 123.5, 122.4, 121.1, 120.7, 120.6, 120.5, 120.3, 120.2, 114.8, 114.7, 114.6, 55.5.

REFERENCES

[1] World energy consumption by fuel type, 1990‐2040 (quadrillion Btu)

[2] Chapin, D. M.; Fuller, C. S.; Pearson, G. L. *J. Appl. Phys.* **1954**, *25*, 676

[3] http://en.wikipedia.org/wiki/Solar_cell

[4] http://auo.com/?sn=49&lang=zh-TW

[5] Zhao, J.; Wang, A.; Green, M. A.; Ferrazza, F. *Appl. Phys. Lett.* **1998**, *73*, 1991-1993.

[6] pv.energytrend.com.tw/news/20150305-10701.html

[7] Schultz, O.; Glunz, S. W.; Willeke, G. P. *Prog. Photovolt. Res. Appl.* **2004**, *12*, 553-558.

[8] Fardi, H. *ISRN Renewable Energy* **2012**, 859519

[9] Sasaki, K.; Agui, T.; Nakaido, K.; Takahashi, N.; Onitsuka, R.; Takamoto, T. *AIP Conf. Proc.* **2013**, *1556*, 22

[10] http://www.semiconductor-today.com/news_items/2012/DEC/SHARP_101212.html

[11] Bernede, J.C.; Derouiche, H.; Jara, V. D. *Solar Energy Materials & Solar Cells*. **2005**, *87*, 261

[12] Petritsch, K.; Friend, R.; Lux, H. A. *Synthetic Metals*. **1999**, *102*, 1776

[13] (a) M. Sun, L. Wang, B. Du, Y. Xiong, R. Liu, Y. Cao, *Synth. Met*. **2008**, *158*, 125 (b) M. Sun, L. Wang, Y. Cao, *Synth. Met*. **2009**, *159*, 556

[14] (a) Braun, D.; Heeger, A. J.; Koremer, H. J. *Electronic Material*. **1991**, *20*, 945 (b) Braun, D.; Heeger, A. J. *Appl. Phys. Lett.* **1991**, *58*, 1982

[15] C. W. Tang, *Appl. Phys. Lett.* **1986**, *48*, 183

[16] Günes, S.; Neugebauer, H.; Sariciftci, N. S. *Chem. Pev.* **2007**, *107*, 1324

[17] http://www.worldcommunitygrid.org/help/viewTopic.do?shortName=cep2

[18] Tsubomura, H.; Matsumura, M.; Nomura, Y.; Amamiya, T. *Nature* **1976**, *261*, 402-403

[19] O'Regan, B.; Grätzel, M. *Nature* **1991**, *353*, 737-740

[20] Hanaya, M. *Chem. Commun* **2015**, *54*, 15894

[21] K. Rakstys, S. Paek, P. Gao, P. Gratia, T. Marszalek, G. Grancini, K. T. Cho, K. Genevicius, V. Jankauskas, W. Pisula, M. K. Nazeeruddin *Journal Mater. Chem. A* **2017**, DOI: 10.1039/C7TA01718A

[22] http://en.wikipedia.org/wiki/Perovskite

[23] M. Grätzel, *Nat. Mater.*, **2014**, *13*, 838

[24] M. A. Green, A. Ho-Baillie and H. J. Snaith, *Nat. Photonics*, **2014**, *8*, 506

[25] T. C. Sum and N. Mathews, *Energy Environ. Sci.*, **2014**, *7*, 2518

[26] K. Liu, Y. Yao, J. Wang, L. Zhu, M. Sun, B. Ren, L. Xie, Y. Luo, Q. Meng, X. Zhan, *Mater. Chem. Front.*, **2017**, *1*, 100-110

[27] A. Kojima, K. Teshima, Y. Shirai, T. Miyasaka, *J. Am. Chem. Soc.*, **2009**, *131*, 6050

[28] H. S. Kim, C. R. Lee, J. H. Im, K. B. Lee, T. Moehl, A. Marchioro, S. J. Moon, R. Humphry-Baker, J. H. Yum, J. E. Moser, M. Grätzel, N. G. Park, *Sci. Rep.* **2012**, *2*, 591

[29] N. R. E. L. National Renewable Energy Laboratory, 2016

[30] J. A. Christians, P. A. Miranda Herrera and P. V. Kamat, *J. Am. Chem. Soc.*, **2015**, *137*, 1530-1538

[31] National Renewable Energy Laboratory (NREL), Golden, CO-United States Department of Energy

[32] http://www.greenrhinoenergy.com/solar/radiation/spectra.php

[33] Soalr.ofweek.com/2016-06/ART-260009-8140-29107172_2.html

[34] Cho, I.; Jeon, N. J.; Kwon, O. K.; Kim, D. W.; Jung, E. H.; Noh, J. H.; Seo, J. W.; Il Seok, S.; Park, S. *Chem. Sci.* **2017**, *8*, 734-741

[35] Bi, D.; Tress, W.; Dar, M. I.; Gao, P.; Luo, J.; Renevier, C.; Schenk, K.; Abate, A.;

Giordano, F.; Correa-Baena, J.-P.; Decoppet, J.-D.; Zakeeruddin, S. M.; Nazeeruddin, M. K.; Grätzel, M.; Hagfeldt, A. *Sci. Adv.* **2016**, *2*, 1501170

[36] Garcia-Benito, I.; Zimmermann, I.; Urieta-Mora, J.; Arago, J.; Molina-Ontoria, A.; Orti, E.; Martin, N.; Nazeeruddin, M. K. *J. Mater. Chem. A.* **2017**, *5*, 8317-8324

[37] Gao, P.; Grätzel, M.; Nazeeruddin, M. K. *Energy Environ. Sci.* **2014**, *7*, 2448

[38] Rakstys, K.; Abate, A.; Dar, M. I.; Gao, P.; Jankauskas, V.; Jacopin, G.; Kamarauskas, E.; Kazim, S.; Ahmad, S.; Grätzel, M.; Nazeeruddin, M. K. *J. Am. Chem. Soc.* **2015**, *137*, 16172-16178

[39] Christians, J. A.; Fung, R. C.; Kamat, P. V. *J. Am. Chem. Soc.* **2013**, *136*, 758

[40] Liu, Z.; Zhang, M.; Xu, X.; Cai, F.; Yuan, H.; Bu, L.; Li, W.; Zhu, A.; Zhao, Z.; Wang, M. *J. Mater. Chem. A.* **2015**, *3*, 24121

[41] Wang, K. C.; Shen, P. S.; Li, M. H.; Chen, S.; Lin, M. W.; Chen, P.; Guo, T. F. *ACS Appl. Mater. Interfaces.* **2014**, *6*, 11851

[42] Chen, W.; Wu, Y.; Liu, J.; Qian, C.; Yang, X.; Islam, A.; Cheng, Y. B.; Han, L. *Energy Environ. Sci.* **2015**, *8*, 629

[43] Qin, P.; Tanaka, S.; Ito, S.; Tetreault, N.; Manabe, K.; Nishino, H.; Nazeeruddin, M. K.; Grätzel, M. *Nat. Commun.* **2014**, *5*, 3834

[44] Ito, S.; Tanaka, S.; Vahlman, H.; Nishino, H.; Manabe, K.; Lund, P. *ChemPhysChem* **2014,** *15*, 1194

[45] Chavhan, S.; Miguel, O.; Grande, H. J.; Gonzalez-Pedro, V.; Sánchez, R. S.; Barea, E. M.; Mora-Seró, I.; Tena-Zaera, R. *J. Mater. Chem. A.* **2014**, *2*, 12754

[46] Subbiah, A. S.; Halder, A.; Ghosh, S.; Mahuli, N.; Hodes, G.; Sarkar, S. K. *J. Phys. Chem. Lett.* **2014**, *5*, 1748

[47] Ito, S.; Tanaka, S.; Manabe, K.; Nishino, H. *J. Phys. Chem. C.* **2014**, *118*, 16995

[48] Ye, S.; Sun, W.; Li, Y.; Yan, W.; Peng, H.; Bian, Z.; Liu, Z.; Huang, C. *Nano Lett.* **2015**, *15*, 3723

[49] Kim, J. H.; Liang, P. W.; Williams, S. T.; Cho, N.; Chueh, C. C.; Glaz, M. S.; Ginger, D. S.; Jen, A. K. Y. *Adv. Mater.* **2015**, *27*, 695

[50] Wang, Y.; Xia, Z.; Liang, J.; Wang, X.; Liu, Y.; L, C.; Zhang, S.; Zhou, H. *Semicond. Sci. Technol.* **2015**, *31*, 4004

[51] Chen, W.; Wu, Y.; Yue, Y.; Liu, J.; Zhang, W.; Yang, X.; Chen, H.; Bi, E.; Ashraful, I. Grätzel, M. *Science* **2015**, *350*, 944

[52] Li, Y.; Zhu, J.; Huang, Y.; Wei, J.; Liu, F.; Shao, Z.; Hu, L.; Chen, S.; Yang, S.; Tang, J. *Nanoscale* **2015**, *7*, 9902

[53] Lv, M.; Zhu, J.; Huang, Y.; Li, Y.; Zhao, Z.; Xu, Y.; Dai, S. *ACS Appl. Mater. Interfaces.* **2015**, *7*, 17482

[54] Yang, W. S.; Noh, J. H.; Jeon, N. J.; Kim, Y. C.; Ryu, S.; Seo, J.; Seok, S. I. *Science* **2015**, *384*, 1234

[55] Jeon, N. J.; Noh, J. H.; Yang, W. S.; Kim, Y. C.; Ryu, S.; Seo, J.; Seok, S. I. *Nature* **2015**, *517*, 476

[56] Conongs, B.; Baeten, L.; De Dobbelaere, C.; D′Haen, J.; Manca, J.; Boyen, H. G. *Adv. Mater*. **2014,** *26*, 2041.

[57] Guo, Y.; Liu, C.; Inoue, K.; Harano, K.; Tanaka, H.; Nakamura, E. *J. Mater. Chem. A* **2014,** *2*, 13827

[58] Conings, B.; Baeten, L.; Jacobs, T.; Dera, R.; D′Haen, J.; Manca, J.; Boyen, H. G. *APL Mater*. **2014,** *2*, 081505

[59] Matteocci, F.; Razza, S.; Di Giacomo, F.; Casaluci, S.; Mincuzzi, G.; Brown, T. M.; D′Epifanio, A.; Licoccia, S.; Di Carlo, A. *Phys. Chem. Chem. Phys.* **2014,** *16*, 3918

[60] Di Giacomo, F.; Razza, S.; Matteocci, F.; D'Epifanio, A.; Licoccia, S.; Brown, T. M.; Di Carlo, A. *J. Power Sources* **2014,** *251*, 152

[61] Guo, Y.; Liu, C.; Tanaka, H.; Nakamura, E. *J. Phys. Chem. Lett.* **2015,** *6*, 535

[62] Chiang, C. H.; Tseng, Z. L.;Wu, C. G. *J. Mater. Chem. A* **2014,** *2*, 15897

[63] Jeng, J. Y.; Chiang, Y. F.; Lee, M. H.; Peng, S. R.; Guo, T. F.; Chen, P.;Wen, T. C. *Adv. Mater.* **2013,** *25*, 3727

[64] Malinkiewicz, O.; Yella, A.; Lee, Y. H.; Espallargas, G. M.; Graetzel, M.; Nazeeruddin, M. K.; Bolink, H. J. *Nat. Photonics* **2014,** *8*, 128

[65] Chiang, Y. F.; Jeng, J. Y.; Lee, M. H.; Peng, S. R.; Chen, P.; Guo, T. F.;Wen, T. C.; Hsu, Y. J.; Hsu, C. M. *Phys. Chem. Chem. Phys.* **2014,** *16*, 6033

[66] Sun, S.; Salim, T.; Mathews, N.; Duchamp, M.; Boothroyd, C.; Xing, G.; Sum, T. C.; Lam, Y. M. *Energy Environ. Sci.* **2014,** *7*, 399

[67] Ryu, S.; Noh, J. H.; Jeon, N. J.; Kim, Y. C.; Yang,W. S.; Seo, J.; Seok, S. I. *Energy Environ. Sci.* **2014,** *7*, 2614

[68] Xiao, Y.; Han, G.; Chang, Y.; Zhou, H.; Li, M.; Li, Y. *J. Power Sources* **2014,** *267*, 1

[69] Zhao, D.; Sexton, M.; Park, H. Y.; Baure, G.; Nino, J. C.; So, F. *Adv. Energy Mater.* **2014,** *5*, 1401855

[70] Zhu, Z.; Bai, Y.; Lee, H. K. H.; Mu, C.; Zhang, T.; Zhang, L.; Wang, J.; Yan, H.; So, S. K.; Yang, S. *Adv. Funct. Mater.* **2014,** *24*, 7357

[71] Yan,W.; Li, Y.; Li, Y.; Ye, S.; Liu, Z.;Wang, S.; Bian, Z.; Huang, C. *Nano Res.* **2015,** *8*, 2474

[72] Conings, B.; Baeten, L.; De Dobbelaere, C.; D′Haen, J.; Manca, J.; Boyen, H. G. *Adv. Mater.* **2014,** *26*, 2041

[73] Heo, J. H.; Han, H. J.; Kim, D.; Ahn, T. K.; Im, S. H. *Energy Environ. Sci.* **2015,** *8*, 1602

[74] Liu, J.; Pathak, S.; Stergiopoulos, T.; Leijtens, T.; Wojciechowski, K.; Schumann, S.; Kausch-Busies, N.; Snaith, H. J. *J. Phys. Chem. Lett.* **2015,** *6*, 1666

[75] Cai, B.; Xing, Y.; Yang, Z.; Zhang,W. H.; Qiu, J. *Energy Environ. Sci.* **2013,** *6*, 1480

[76] Kwon, Y. S.; Lim, J.; Yun, H. J.; Kim, Y. H.; Park, T. *Energy Environ. Sci.* **2014,**

7, 1454

[77] Guo, Y.; Liu, C.; Inoue, K.; Harano, K.; Tanaka, H.; Nakamura, E. *J. Mater. Chem. A* **2014,** *2*, 13827

[78] Chen,W.; Bao, X.; Zhu, Q.; Zhu, D.; Qiu, M.; Sun, M.; Yang, R. *J. Mater. Chem. C* **2015,** *3*, 10070

[79] Wang, S.; Sina, M.; Parikh, P.; Uekert, T.; Shahbazian, B.; Devaraj, A.; Meng, Y. S. *Nano Lett.* **2016**, *16*, 5594-5600

[80] Juarez-Perez, E. J.; Leyden, M. R.; Wang, S.; Ono, L. K.; Hawash, Z.; Qi, Y. *Chem. Mater.* **2016**, *28*, 5702-5709

[81] Leijtens, T.; Giovenzana, T.; Habisreutinger, S. N.; Tinkham, J. S.; Noel, N. K.; Kamino, B. A.; Sadoughi, G.; Sellinger, A.; Snaith, H. J. *ACS Appl. Mater. Interfaces.* **2016**, *8*, 5981-5989

[82] Niu, G.; Guo, X.; Wang, L. *J. Mater. Chem. A.* **2015**, *3*, 8970-8980

[83] Deschler, F.; Price, M.; Pathak, S.; Klintberg, L. E.; Jarausch, D. D.; Higler, R.; Hüttner, S.; Leijtens, T.; Stranks, S. D.; Snaith, H. J. *J. Phys. Chem. Lett.* **2014,** *5*, 1421

[84] Xu, B.; Bi, D.; Hua, Y.; Liu, P.; Cheng, M.; Graetzel, M.; Kloo, L.; Hagfeldt, A.; Sun, L. *Energy Environ. Sci.* **2016,** *9*, 873-877

[85] Bi, D.; Xu, B.; Gao, P.; Sun, L.; Graetzel, M.; Hagfeldt, A. *Nano Energy* **2016**, *23*, 138-144

[86] Kojima, A.; Teshima, K.; Shirai, Y.; Miyasaka, T. *J. Am. Chem. Soc.* **2009,** *131*, 6050

[87] Yao, X.; Ding, Y. L.; Zhang, X. D.; Zhao, Y. *Acta Phys. Sin.* **2015,** *64*, 38805

[88] Yuan, H. L.; Li, J. P.;Wang, M. K. *Acta Phys. Sin.* **2015,** *64*, 38405

[89] Kim, H. S.; Lee, C. R.; Im, J. H.; Lee, K. B.; Moehl, T.; Marchioro, A.; Moon, S. J.; Humphry-Baker, R.; Yum, J. H.; Moser, J. E. *Sci. Rep-UK* **2012,** *2*, 591

[90] Qin, P.; Tanaka, S.; Ito, S.; Tetreault, N.; Manabe, K.; Nishino, H.; Nazeeruddin, M. K.; Grätzel, M. *Nat. Commun.* **2014,** *5*, 3834

[91] Ito, S.; Tanaka, S.; Vahlman, H.; Nishino, H.; Manabe, K.; Lund, P. *ChemPhysChem* **2014,** *15*, 1194

[92] Badia, L.; Mas-Marzá, E.; Sánchez, R. S.; Barea, E. M.; Bisquert, J.; Mora-Seró, I. *APL Mater.* **2014,** *2*, 081507

[93] Ahn, N.; Son, D. Y.; Jang, I. H.; Kang, S. M.; Choi, M.; Park, N. G. *J. Am. Chem. Soc.* **2015,** *13*, 8696

[94] Zhu, L.; Xiao, J.; Shi, J.;Wang, J.; Lv, S.; Xu, Y.; Luo, Y.; Xiao, Y.;Wang, S.; Meng, Q. *Nano Res.* **2014,** *8*, 1116

[95] Li, H.; Fu, K.; Hagfeldt, A.; Grätzel, M.; Mhaisalkar, S. G.; Grimsdale, A. C. *Angew. Chem. Int. Edit.* **2014,** *53*, 4085

[96] Choi, H.; Park, S.; Kang, M. S.; Ko, J. *Chem. Commun.* **2015,** *51*, 9305

[97] Krishnamoorthy, T.; Kunwu, F.; Boix, P. P.; Li, H.; Koh, T. M.; Leong,W. L.; Powar, S.; Grimsdale, A.; Grätzel, M.; Mathews, N. *J. Mater. Chem. A* **2014,** *2*, 6305

[98] Song, Y.; Lv, S.; Liu, X.; Li, X.;Wang, S.;Wei, H.; Li, D.; Xiao, Y.; Meng, Q. *Chem. Commun.* **2014,** *50*, 15239

[99] Abate, A.; Planells, M.; Hollman, D. J.; Barthi, V.; Chand, S.; Snaith, H. J.; Robertson, N. *Phys. Chem. Chem. Phys.* **2015,** *17*, 2335

[100] Kim, B. S.; Kim, T. M.; Choi, M. S.; Shim, H. S.; Kim, J. J. *Org. Electron.* **2015,** *17*, 102

[101] Liu, Y.; Hong, Z.; Chen, Q.; Chen, H.; Chang,W. H.; Yang, Y. M.; Song, T. B.; Yang, Y. *Adv. Mater*. **2016,** *28*, 440-446

[102] Zheng, L.; Chung, Y. H.; Ma, Y.; Zhang, L.; Xiao, L.; Chen, Z.; Wang, S.; Qu, B.; Gong, Q. *Chem. Commun.* **2014,** *50*, 11196

[103] Kumar, C. V.; Sfyri, G.; Raptis, D.; Stathatos, E.; Lianos, P. *RSC Adv.* **2015,** *5*, 3786

[104] Sfyri, G.; Kumar, C. V.;Wang, Y. L.; Xu, Z. X.; Krontiras, C.; Lianos, P. *Appl. Surf. Sci.* **2016,** *360*, 767

[105] Ke,W.; Zhao, D.; Grice, C. R.; Cimaroli, A. J.; Fang, G.; Yan, Y. *J. Mater. Chem. A* **2015,** *3*, 23888

[106] Seo, J.; Jeon, N. J.; Yang,W. S.; Shin, H.W.; Ahn, T. K.; Lee, J.; Noh, J. H.; Seok, S. I. *Adv. Energy Mater.* **2015,** *5*, 1501320

[107] Ramos, F. J.; Ince, M.; Urbani, M.; Abate, A.; Grätzel, M.; Ahmad, S.; Torres, T.; Nazeeruddin, M. K. *Dalton Trans.* **2015,** *44*, 10847

[108] Sfyri, G.; Kumar, C. V.; Sabapathi, G.; Giribabu, L.; Andrikopoulos, K. S.; Stathatos, E.; Lianos, P. *RSC Adv.* **2015,** *5*, 69813

[109] Lim, I.; Kim, E. K.; Patil, S. A.; Lee,W.; Shrestha, N. K.; Lee, J. K.; Seok,W. K.; Cho, C. G.; Han, S. H. *RSC Adv.* **2015,** *5*, 55321

[110] Kazim, S.; Ramos, F. J.; Gao, P.; Nazeeruddin, M. K.; Grätzel, M.; Ahmad, S. *Energy Environ. Sci.* **2015,** *8*, 1816

[111] Xiao, J.; Han, L.; Zhu, L.; Lv, S.; Shi, J.;Wei, H.; Xu, Y.; Dong, J.; Xu, X.; Xiao, Y. *RSC Adv.* **2014,** *4*, 32918

[112] Bi, D.; Yang, L.; Boschloo, G.; Hagfeldt, A.; Johansson, E. M. *J. Phys. Chem. Lett.* **2013,** *4*, 1532

[113] Sun, M.;Wang, S.; Xiao, Y.; Song, Z.; Li, X. *J. Energ. Chem.* **2015,** *24*, 756

[114] Liu, Y. S.; Chen, Q.; Duan, H.-S.; Zhou, H.; Yang, (M.) Y.; Chen, H.; Luo, S.; Song, T.-B.; Dou, L.; Hong, Z.; Yang, Y. *J. Mater. Chem. A.* **2015**, *3*, 11940-11947

[115] Zhang, F.; Yi, C.; Wei, P.; Bi, X.; Luo, J.; Jacopin, G.; Wang, S.; Li, X.; Xiao, Y.; Zakeerudin, S. M.; Grätzel, M. *Adv. Energy Mater.* **2016**, *6*, 1600401

[116] Huang, C.; Fu, W.; Li, C. Z.; Zhang, Z.; Qiu, W.; Shi, M.; Heremans, P.; Jen,

A. K.-Y.; Chen, H. *J. Am. Chem. Soc.* **2016**, *138*, 2528-2531

[117] Rakstys, K.; Paek, S.; Gao, P.; Gratia, P.; Marszalek, T.; Grancini, G.; Cho, K. T.; Genevicius, K.; Jankauskas, V.; Pisula, W.; Nazeeruddin, M. K. *J. Mater. Chem. A.* **2017**, *5*, 7811-7815

[118] Yang, W. S.; Noh, J. H.; Jeon, N. J.; Kim, Y. C.; Ryu, S.; Seo, J. Seok, S. I. *Science* **2015**, *348*, 1234-1237

[119] Ahn, N.; Son, D. Y.; Jang, I. H.; Kang, S. M.; Choi, M.; Park, N. G. *J. Am. Chem. Soc.* **2015**, *137*, 8696-8699

[120] Gratia, P.; Magomedov, A.; Malinauskas, T.; Daskeviciene, M.; Abate, A.; Ahmad, S.; Grätzel, M.; Getautis, V.; Nazeeruddin, M. K. *Angew. Chem. Int. Ed.* **2015**, *54*, 11409

[121] Rakstys, K.; Saliba, M.; Gao, P.; Gratia, P.; Kamarauskas, E.; Paek, S.; Jankauskas, V.; Nazeeruddin, M. K. *Angew. Chem. Int. Ed.* **2016**, *55*, 7464

[122] Park, S.; Heo, J. H.; Yun, J. H.; Jung, T. S.; Kwak, K.; Ko, M. J.; Cheon, C. H.; Kim, J. Y.; Im, S. H.; Son, H. J. *Chem. Sci.* **2016**, *7*, 5517

[123] Xu, B.; Bi, D.; Hua, Y.; Liu, P.; Cheng, M.; Grätzel, M.; Kloo, L.; Hagfeldt, A.; Sun, L. *Energy Environ. Sci.* **2016**, *9*, 873

[124] Malinauskas, T.; Saliba, M.; Matsui, T.; Daskeviciene, M.; Urnikaite, S.; Gratia, P.; Send, R.; Wonneberger, H.; Bruder, I.; Grätzel, M.; Getautis, V.; Nazeeruddin, M. K. *Energy Environ. Sci.* **2016**, *9*, 1681

[125] Bengs, H.; Ebert, M.; Karthaus, O.; Kohne, B.; Pracefcke, K.; Ringsdorf, H.; Wenforff, J. H.; Wustefeld, R. *Adv. Mater.* **1990**, *3*, 141-144

[126] Yamaguchi, S.; Swager, T. M. *J. Am. Chem. Soc.* **2001**,*123*, 12087-12088

[127] Herbstein, F. H. *Acta Cryst.* **1979**, *B35*, 1661-1670

[128] Pascal, R. A. *Chem. Rev.* **2006**, *106*, 4809-4819

[129] Ueda, Y.; Tsuji, H.; Tanaka, H.; Nakamura, E. *Chem. Asian J.* **2014**, *9*, 1623-

1628

[130] Huang, C.; Fu, W.; Li, C.-Z.; Zhang, Z.; Qiu, W.; Shi, M.; Heremans, P.; Jen, A. K.-Y.; Chen, H. *J. Am. Chem. Soc.* **2016**, *138*, 2528

[131] Rakstys, K.; Paek, S.; Gao, P.; Gratia, P.; Marszalek, T.; Grancini, G.; Cho, K. T.; Genevicius, K.; Jankauskas, V.; Pisula, W.; Nazeeruddin, M. K. *J. Mater. Chem. A.* **2017**, *5*, 7811-7815

[132] M. Saliba, S. Orlandi, T. Matsui, S. Aghazada, M. Cavazzini, J.-P. Correa-Baena, P. Gao, R. Scopelliti, E. Mosconi, K.-H. Dahmen, F. De Angelis, A. Abate, A. Hagfeldt, G. Pozzi, M. Grätzel and M. K. Nazeeruddin, *Nature Energy*, 2016, **1**, 15017

NMR Spectra

(a)

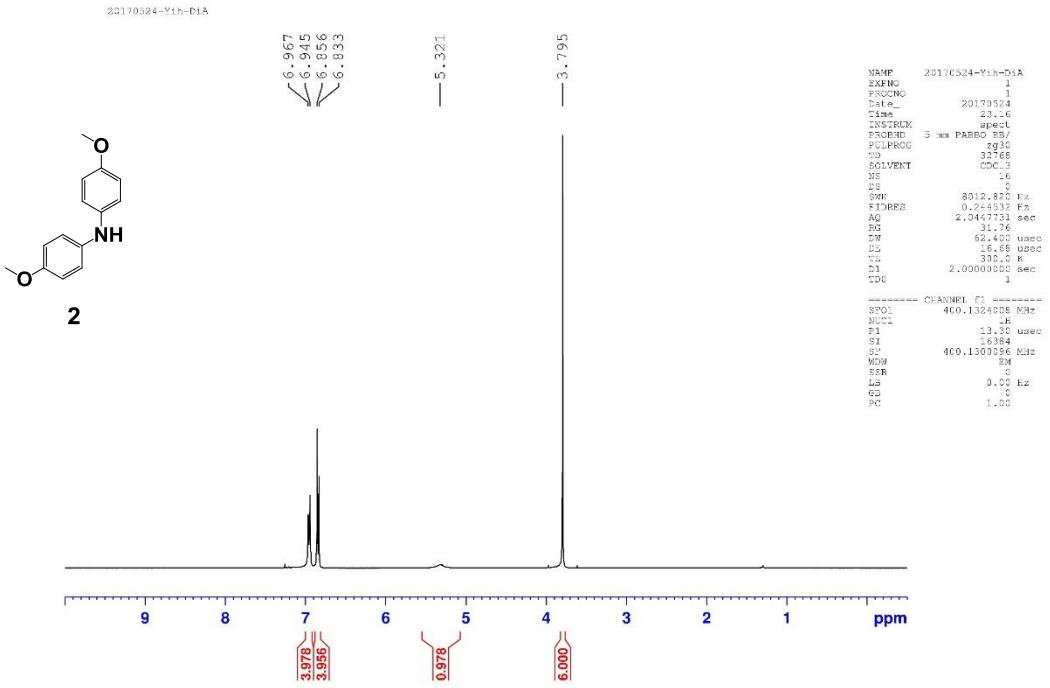

(b)

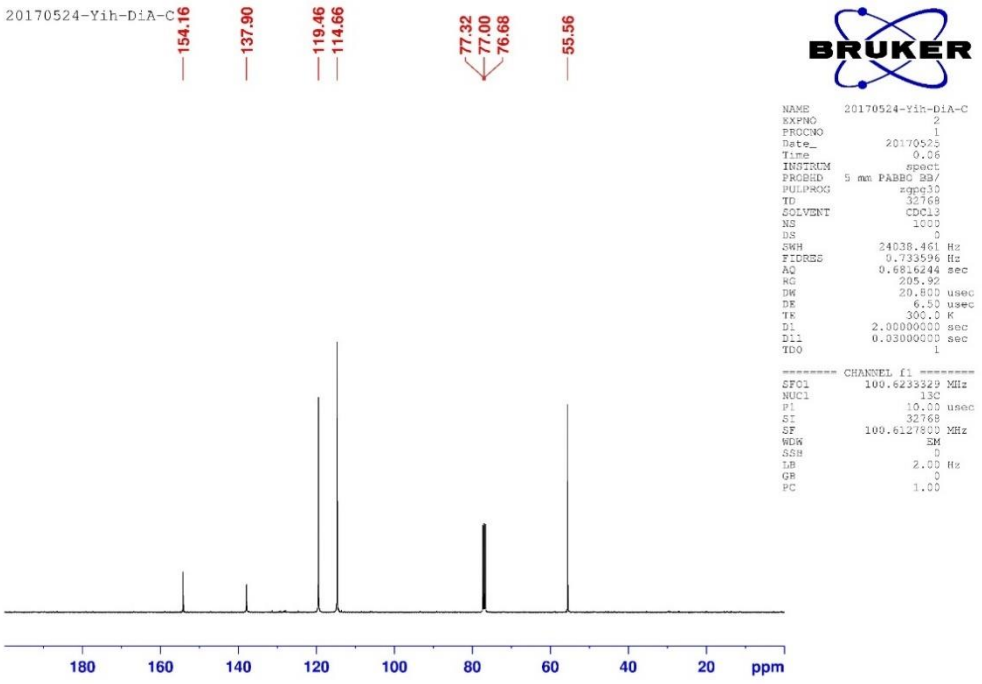

Spectra 1. (a) ^{1}H and (b) ^{13}C NMR spectra of compound **2**

(a)

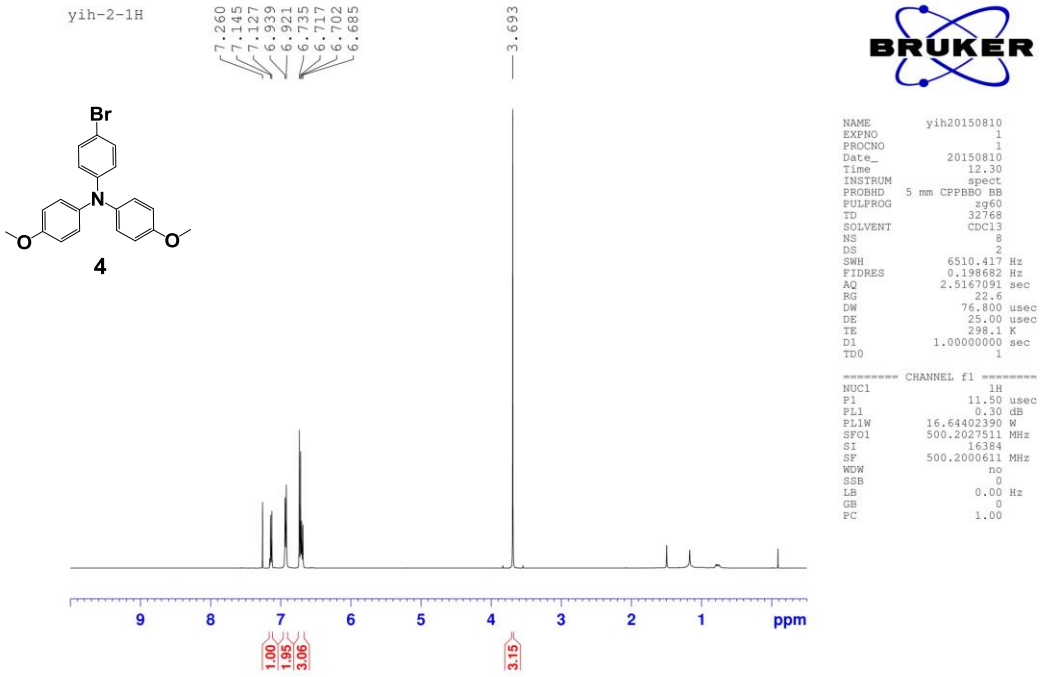

(b)

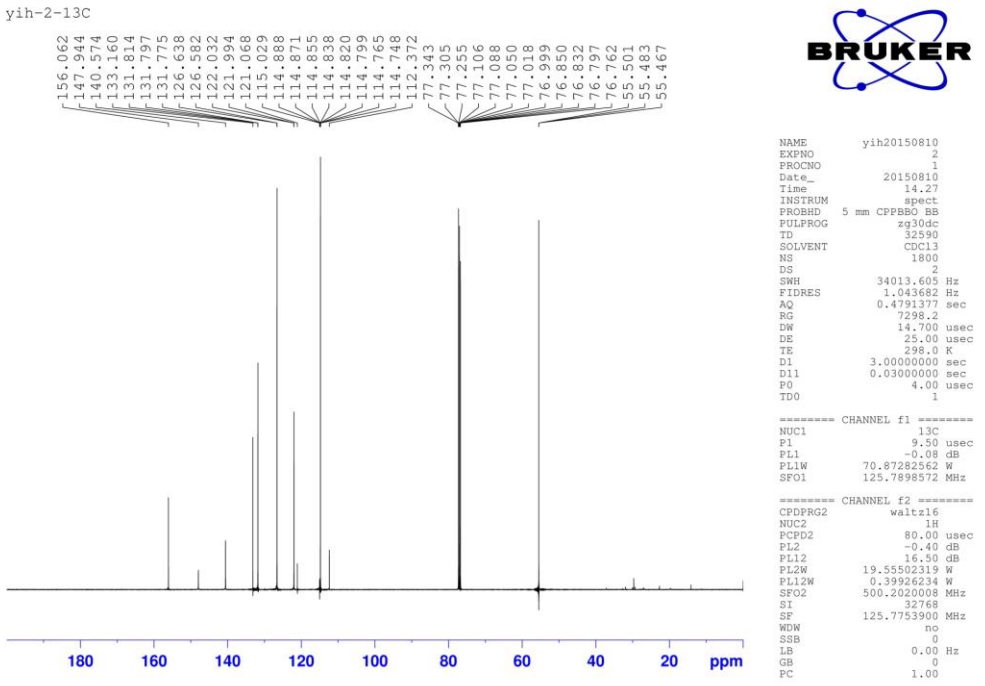

Spectra 2. (a) ^{1}H and (b) ^{13}C NMR spectra of compound **4**

(a)

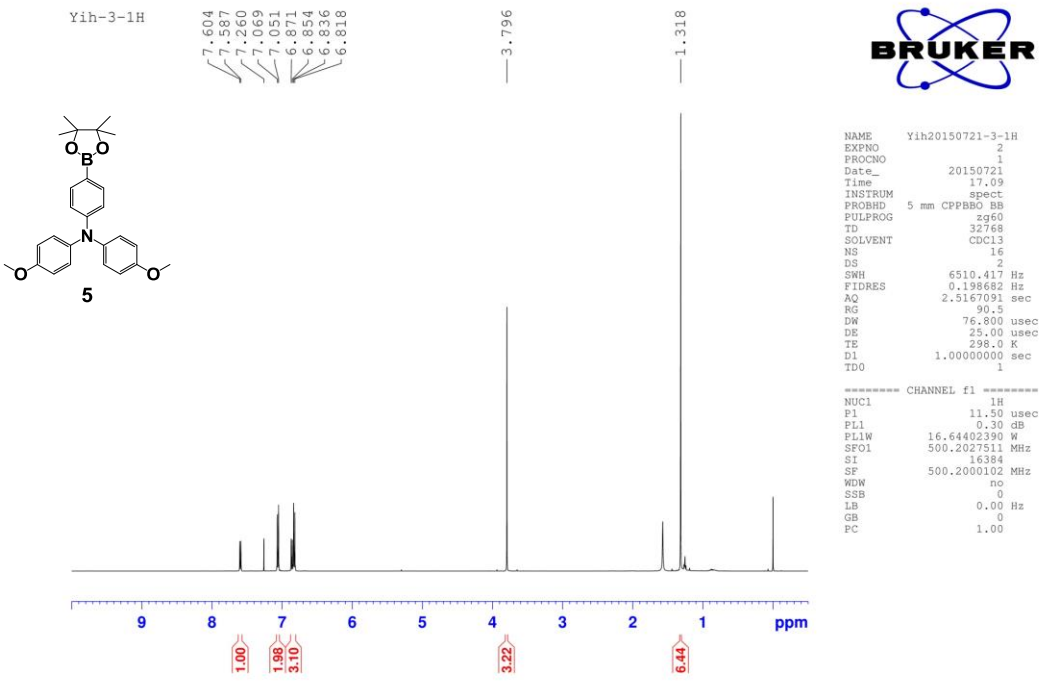

(b)

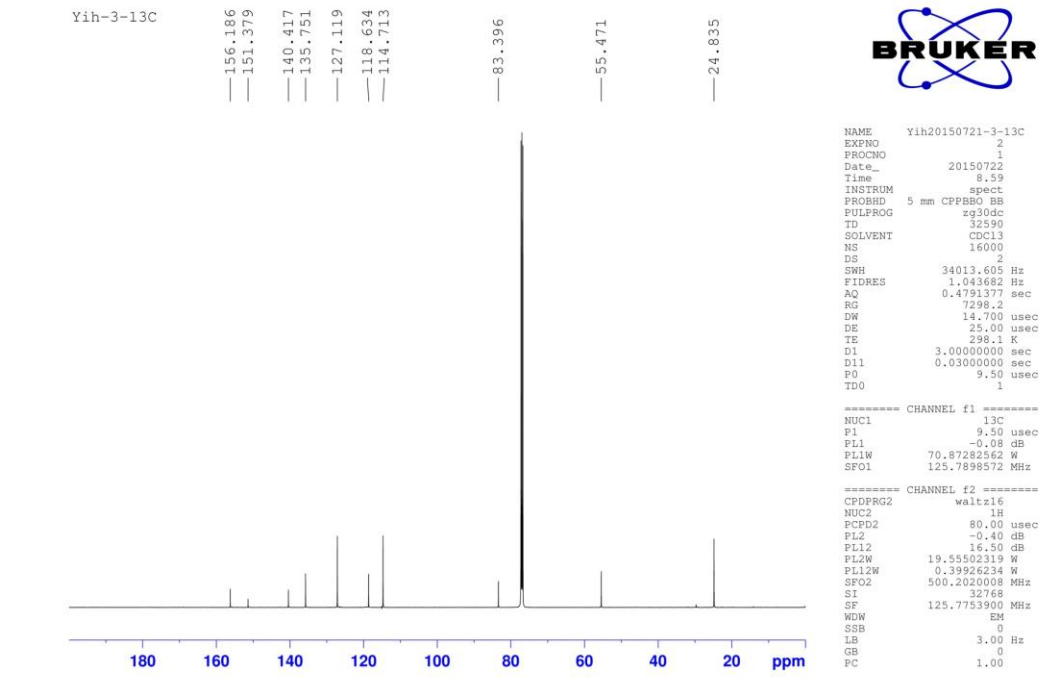

Spectra 3. (a) ^{1}H and (b) ^{13}C NMR spectra of compound **5**

(a)

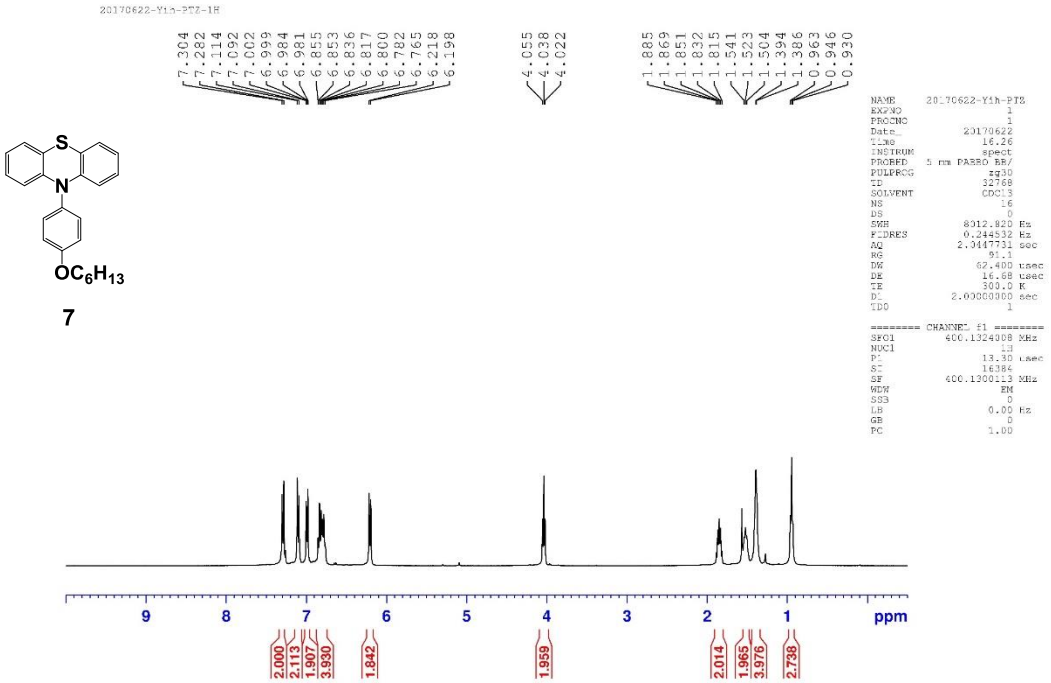

(b)

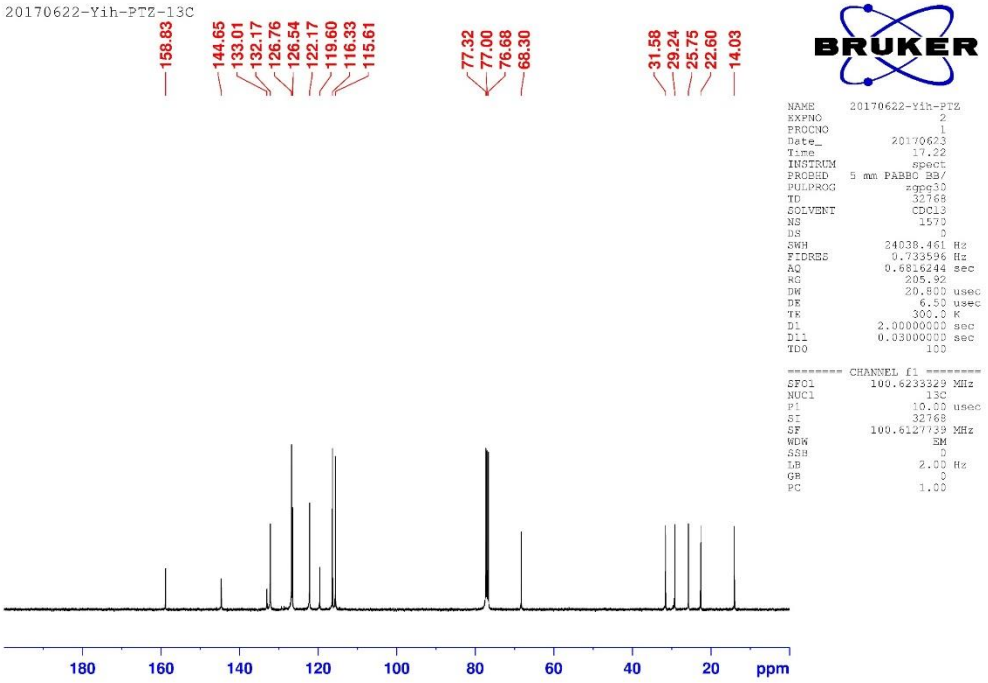

Spectra 4. (a) ^{1}H and (b) ^{13}C NMR spectra of compound **7**

(a)

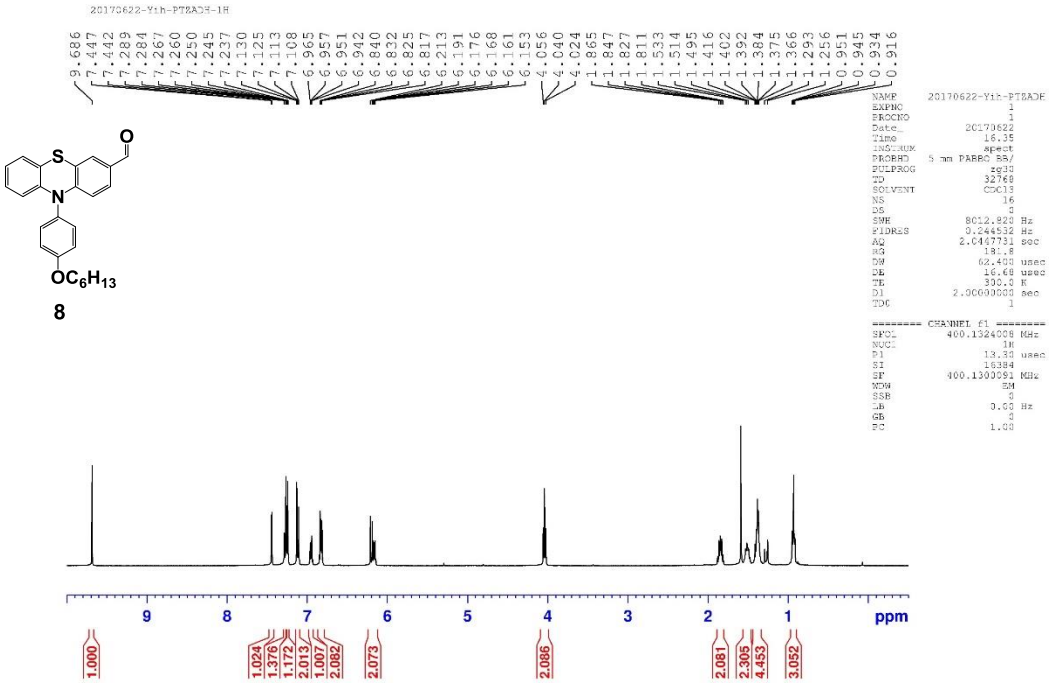

(b)

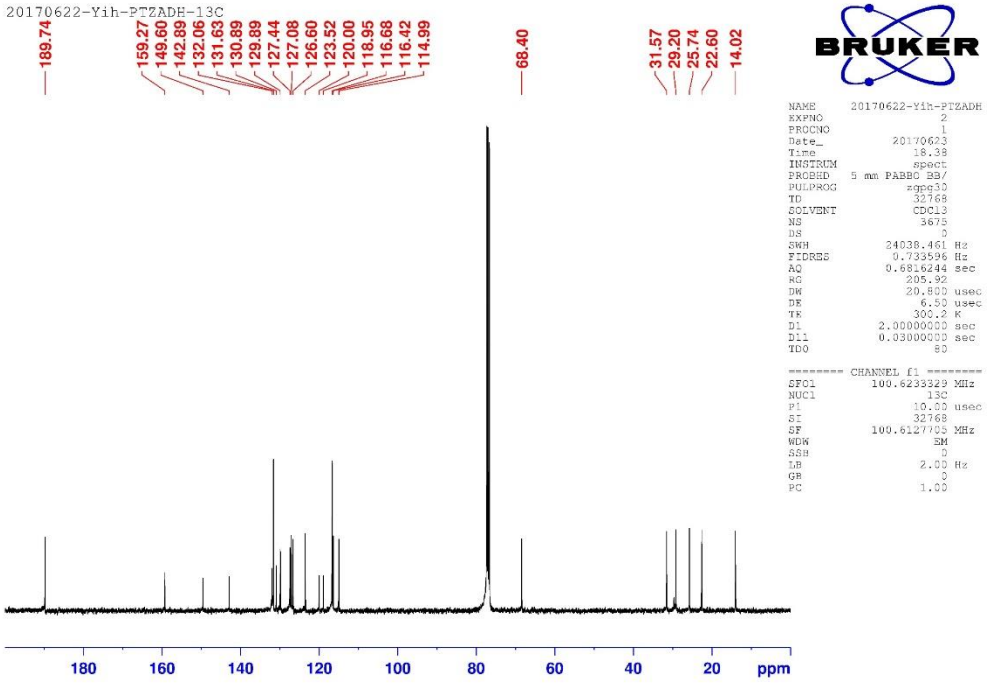

Spectra 5. (a) ^{1}H and (b) ^{13}C NMR spectra of compound **8**

(a)

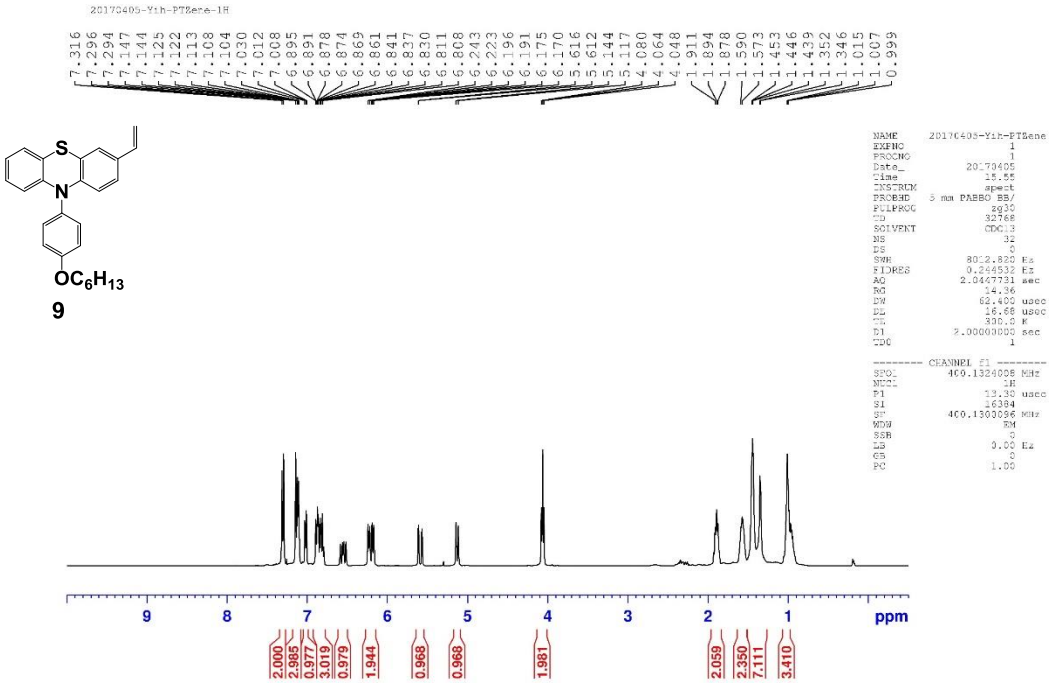

(b)

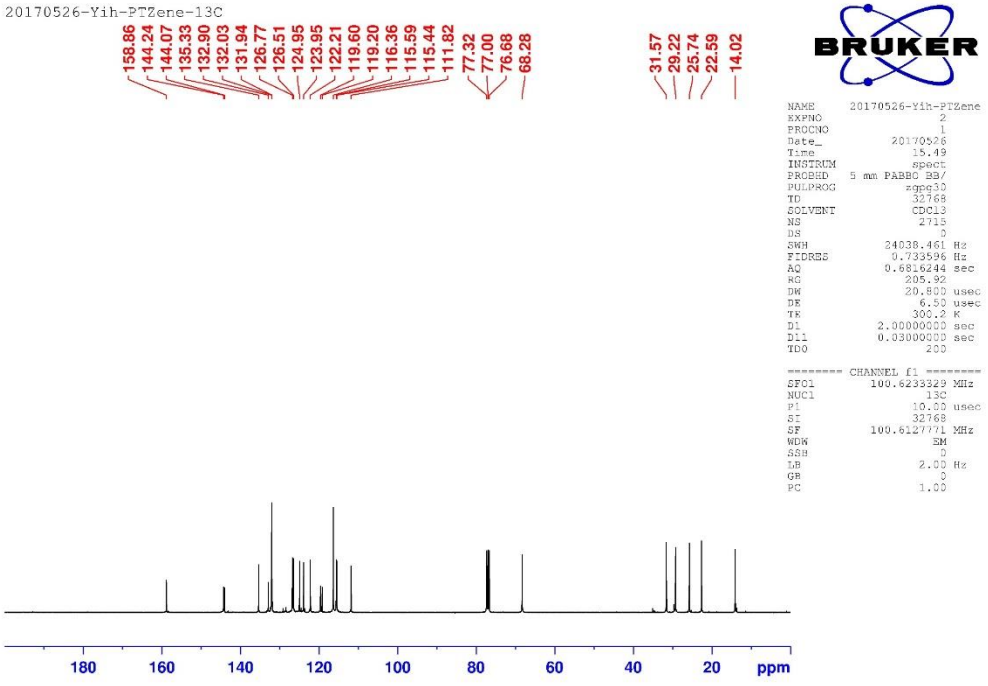

Spectra 6. (a) ^{1}H and (b) ^{13}C NMR spectra of compound **9**

(a)

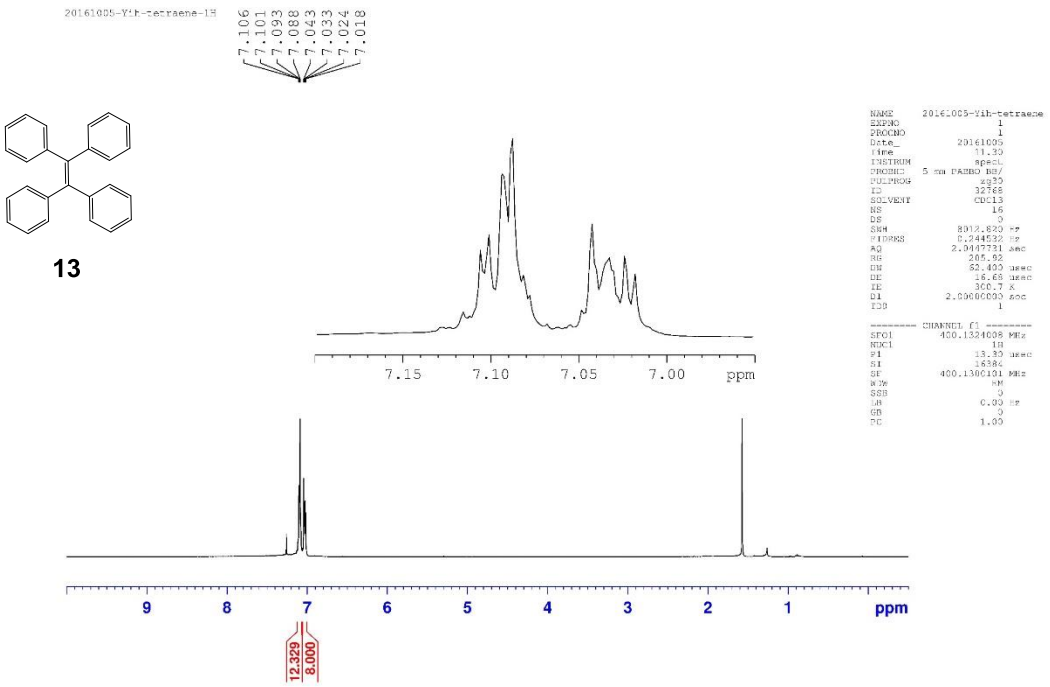

(b)

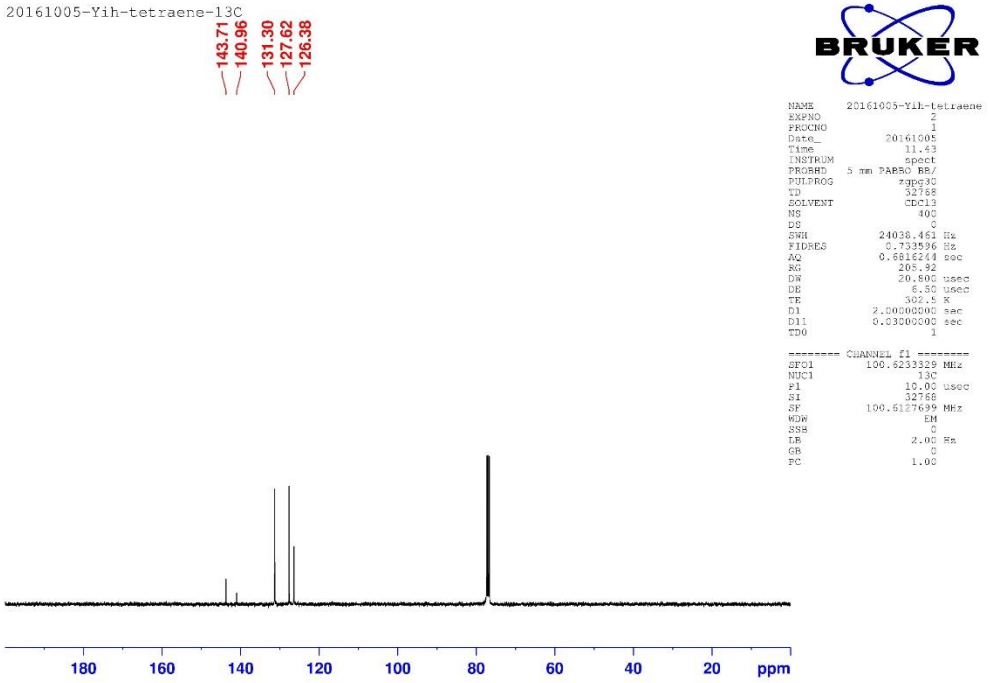

Spectra 7. (a) ^{1}H and (b) ^{13}C NMR spectra of compound **13**

(a)

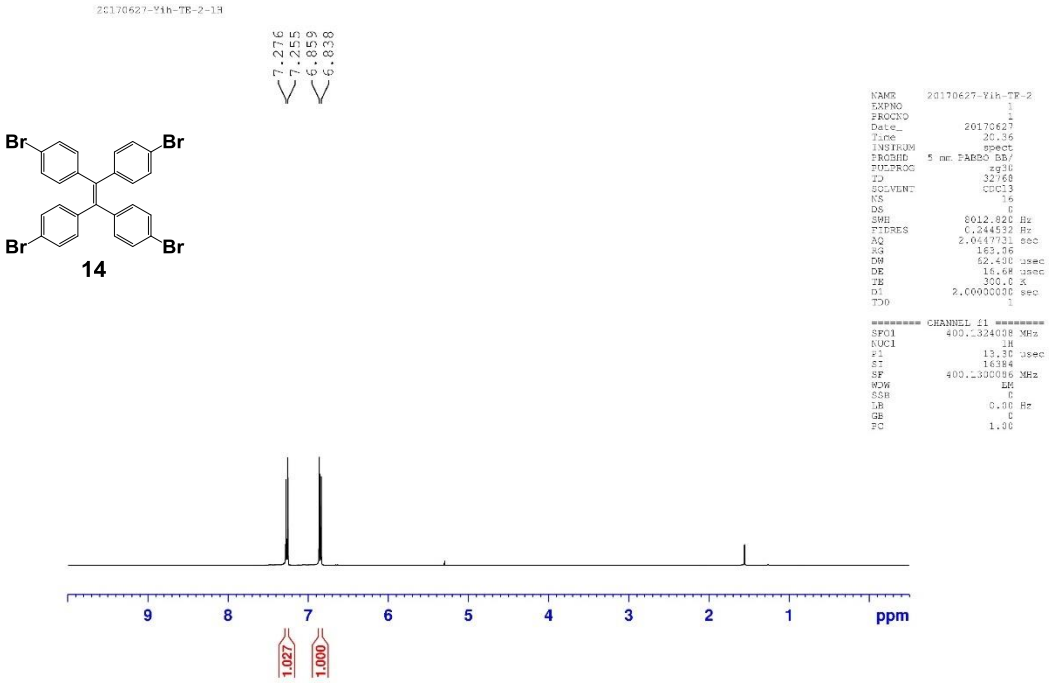

(b)

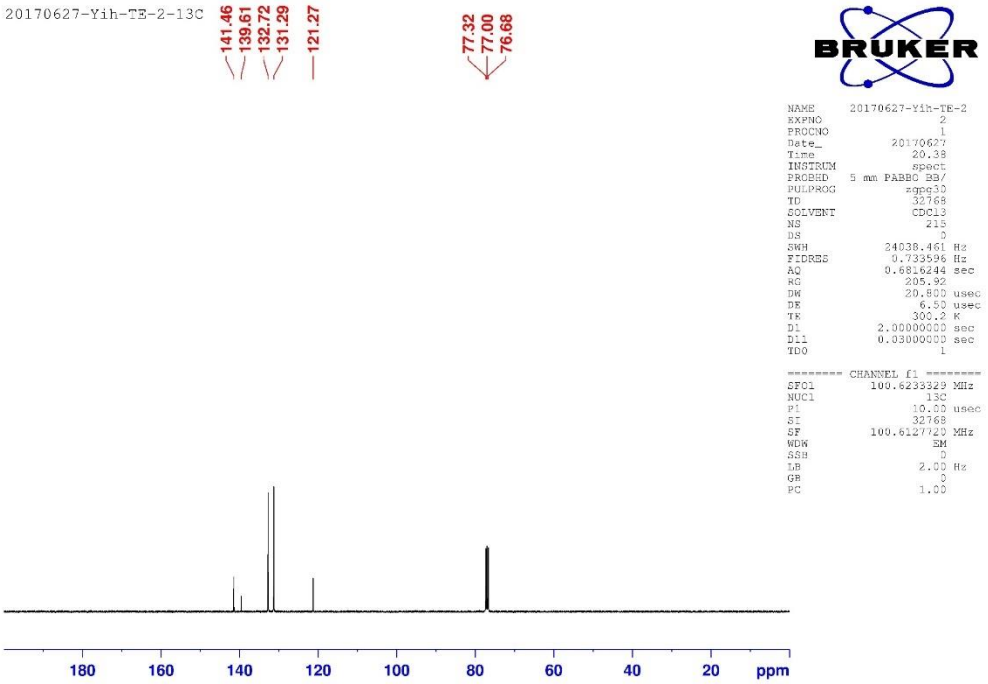

Spectra 8. (a) ^{1}H and (b) ^{13}C NMR spectra of compound **14**

(a)

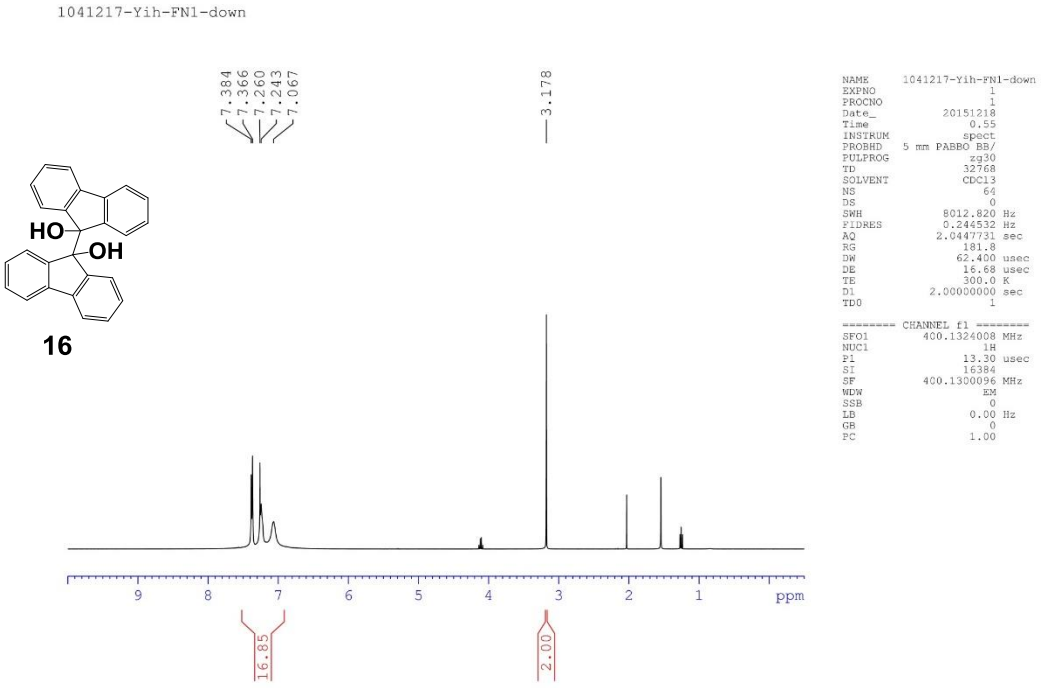

(b)

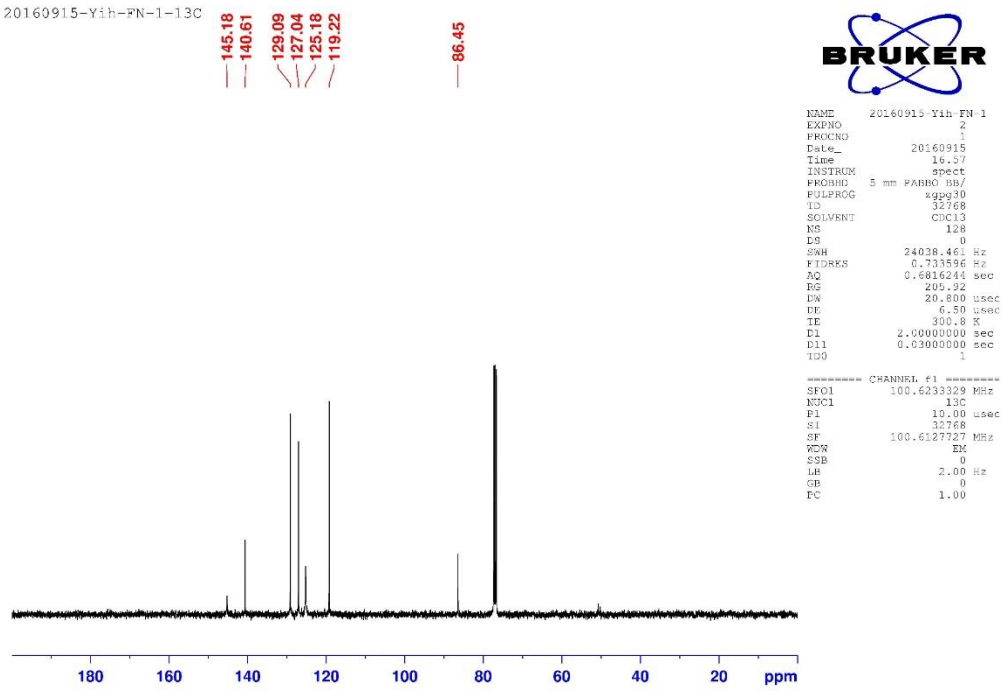

Spectra 7. (a) ^{1}H and (b) ^{13}C NMR spectra of compound **16**

(a)

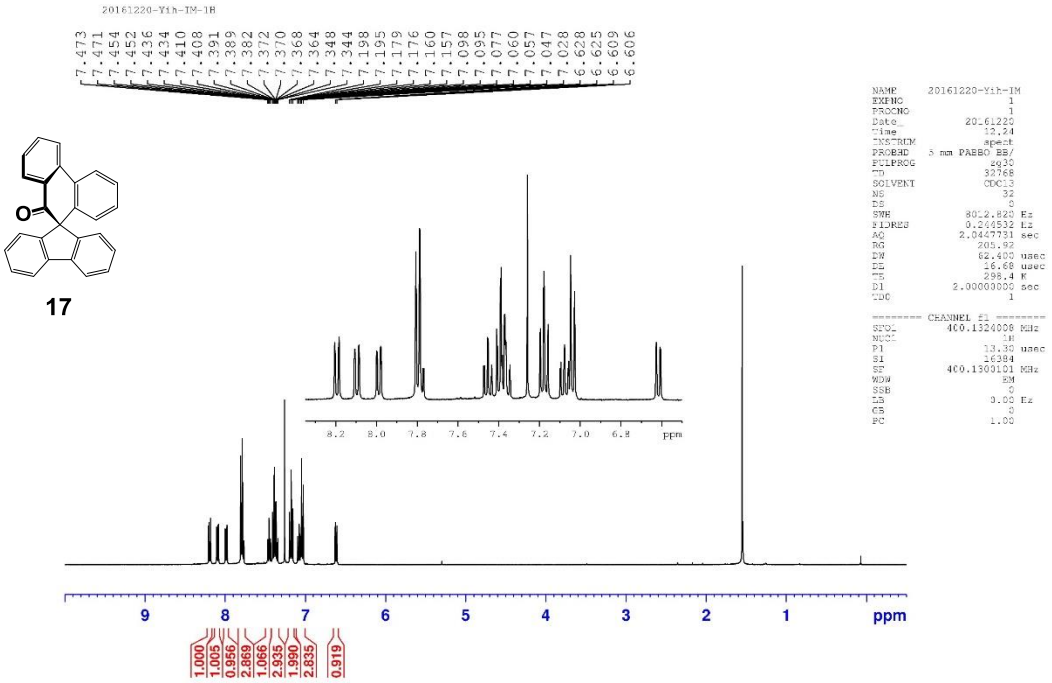

(b)

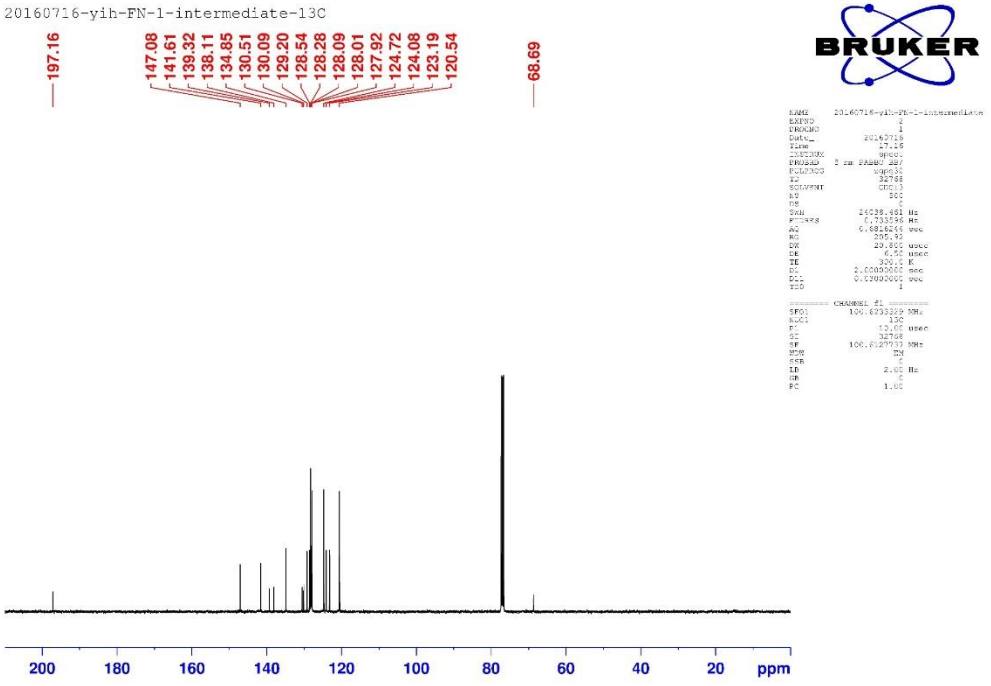

Spectra 8. (a) ^{1}H and (b) ^{13}C NMR spectra of compound **17**

(a)

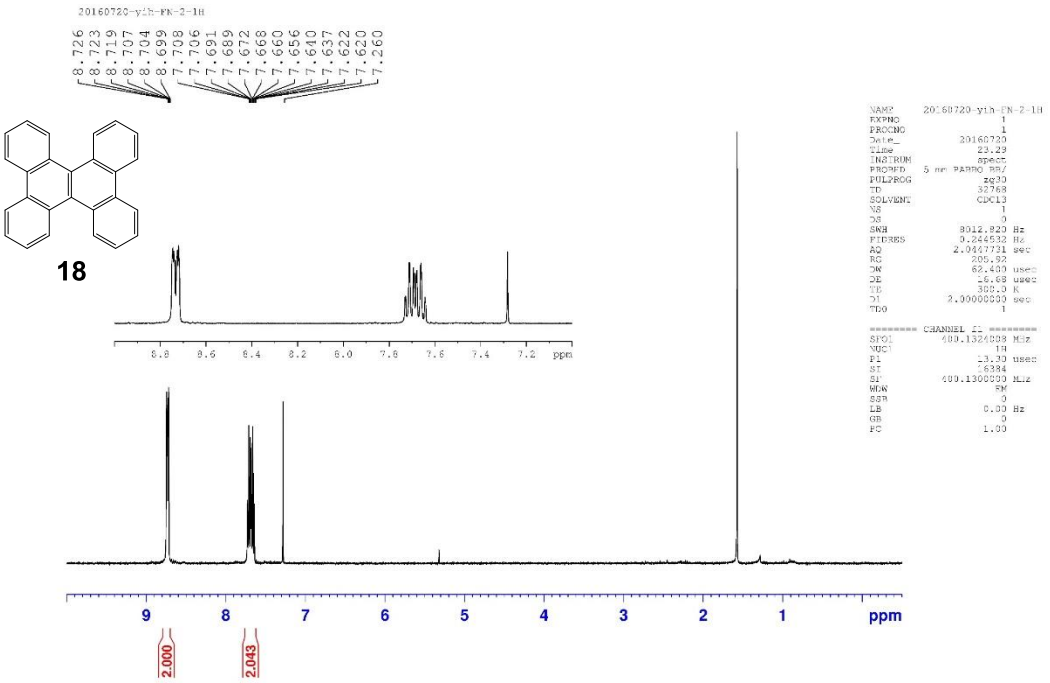

(b)

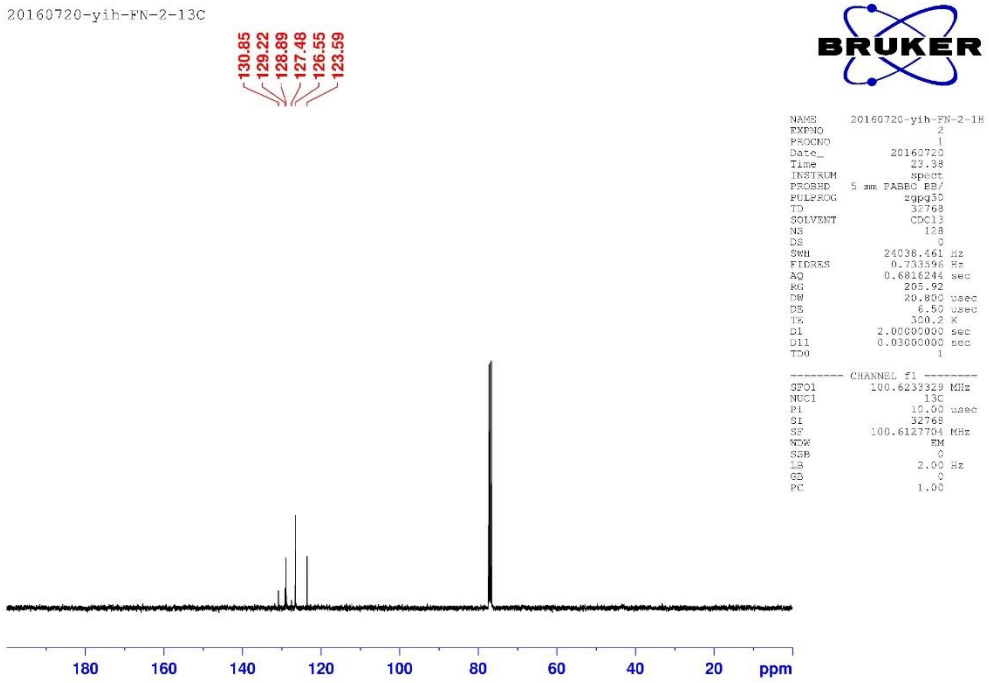

Spectra 9. (a) ^{1}H and (b) ^{13}C NMR spectra of compound **18**

(a)

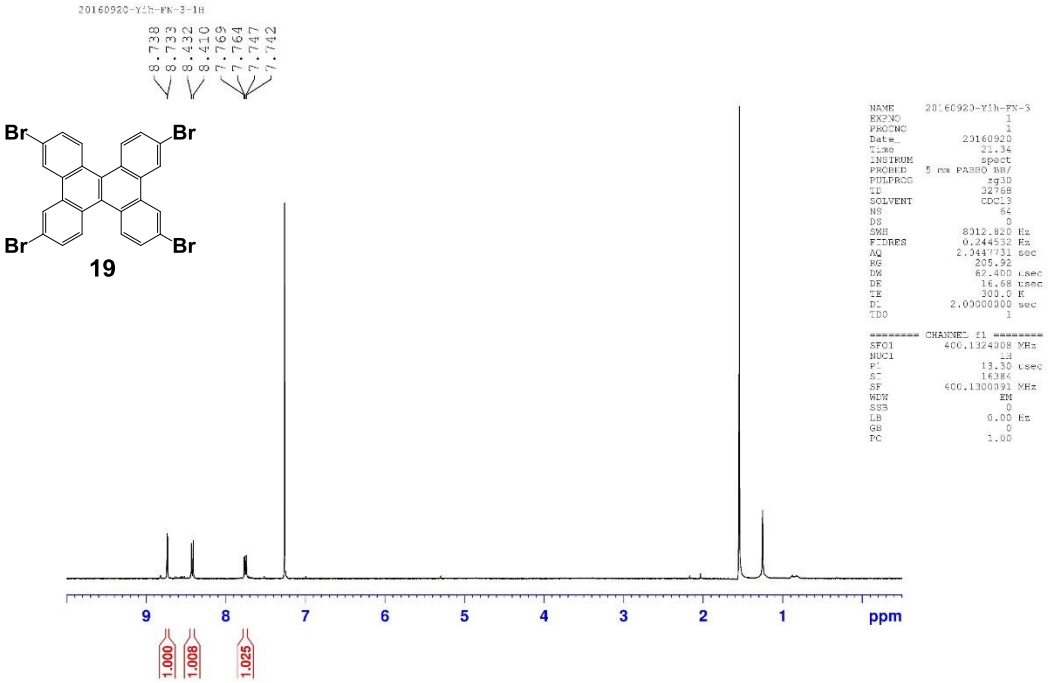

(b)

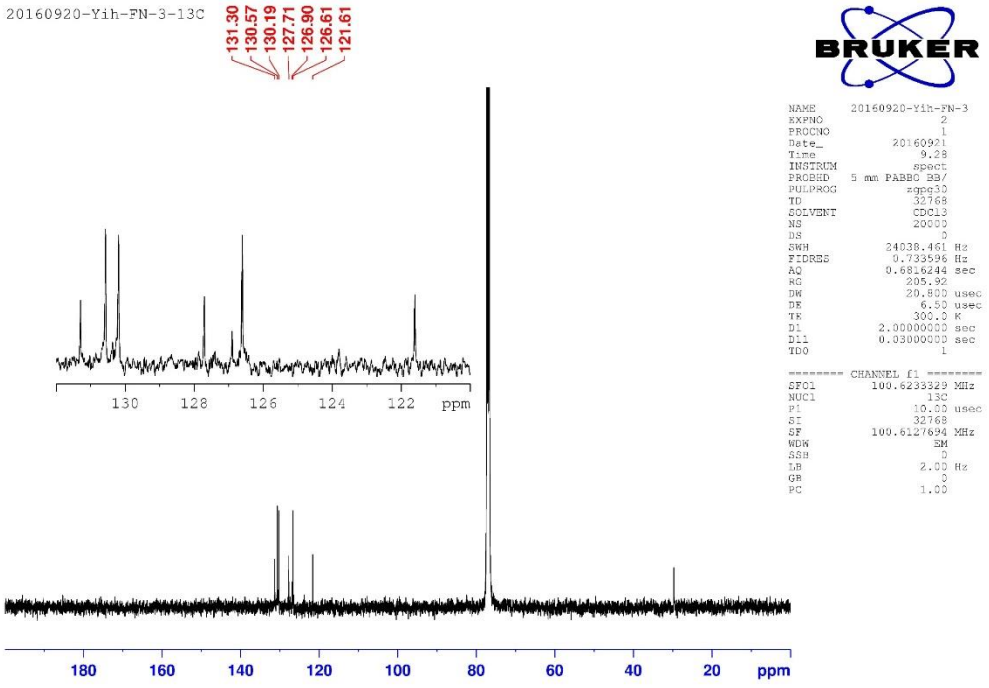

Spectra 10. (a) ^{1}H and (b) ^{13}C NMR spectra of compound **19**

(a)

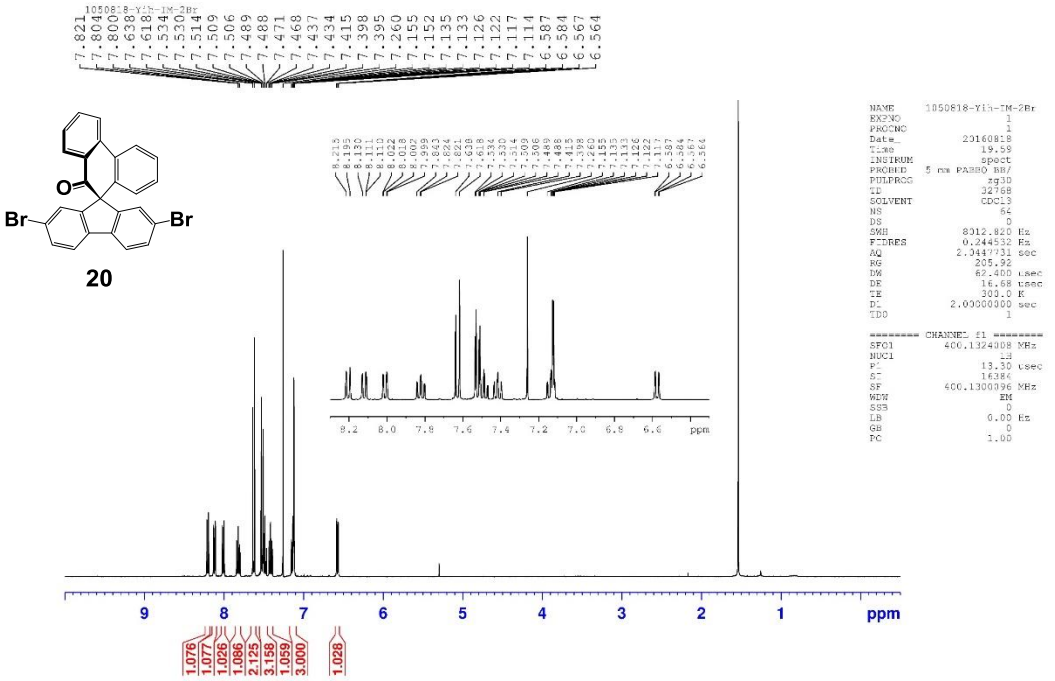

(b)

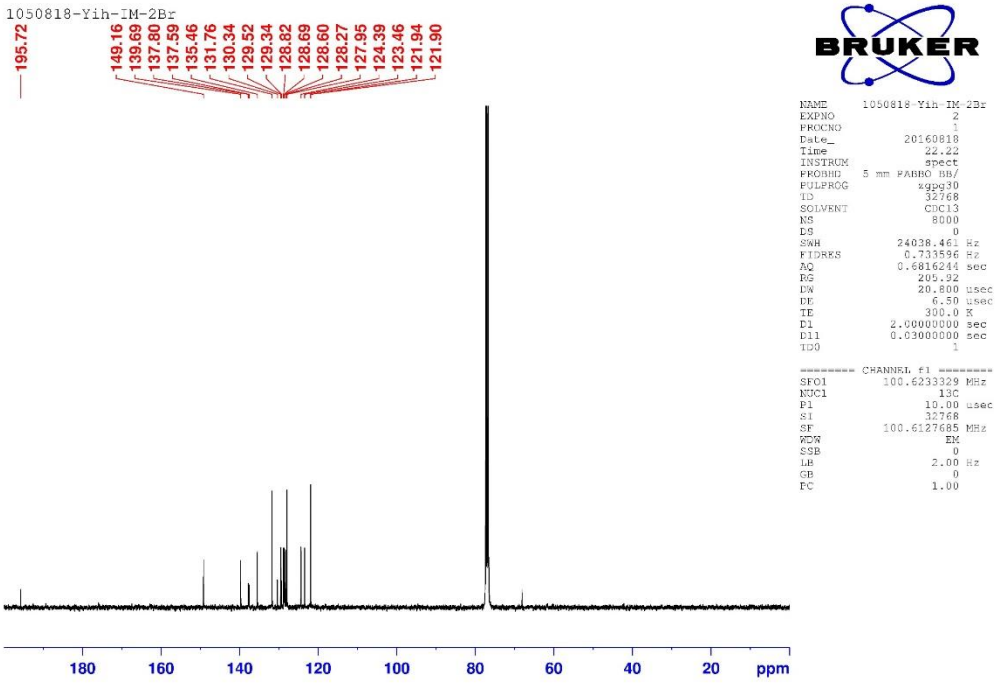

Spectra 11. (a) ^{1}H and (b) ^{13}C NMR spectra of compound **20**

(a)

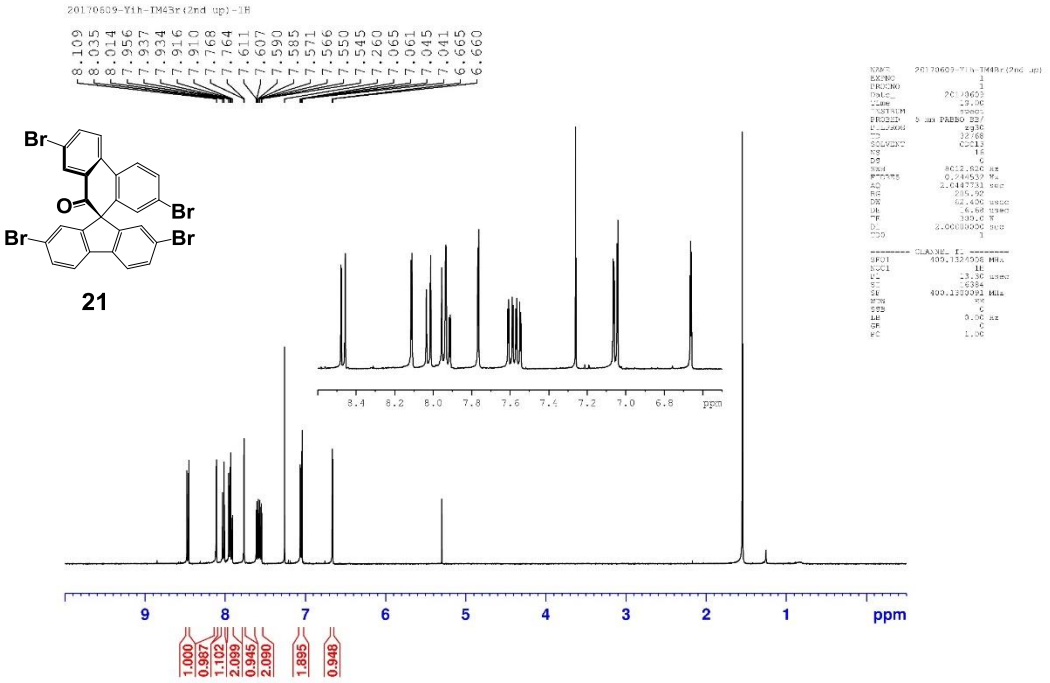

(b)

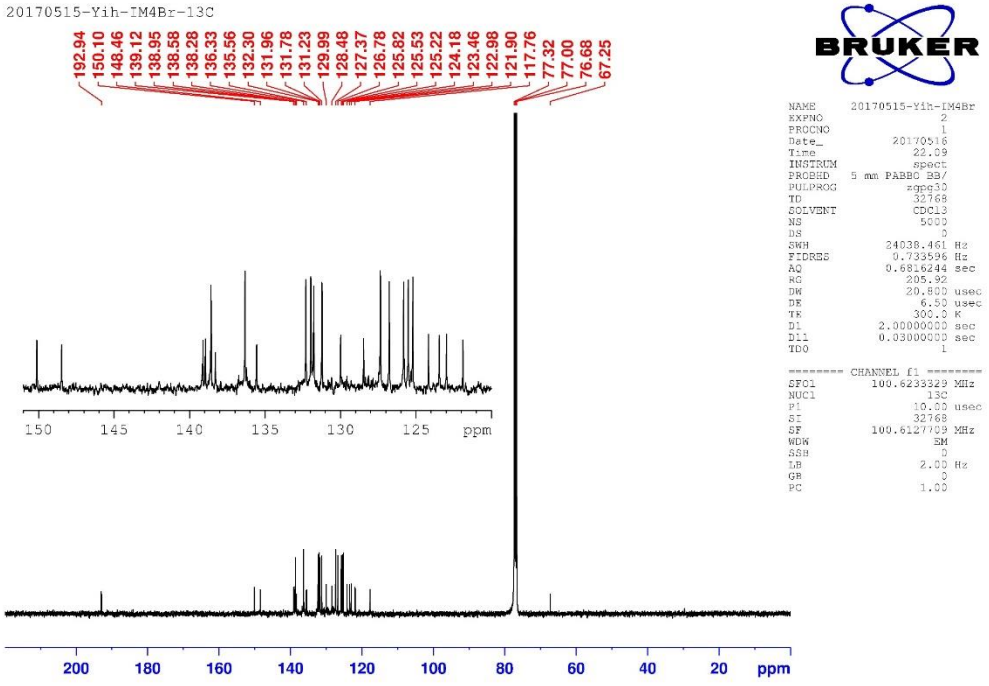

Spectra 12. (a) ^{1}H and (b) ^{13}C NMR spectra of compound **21**

(a)

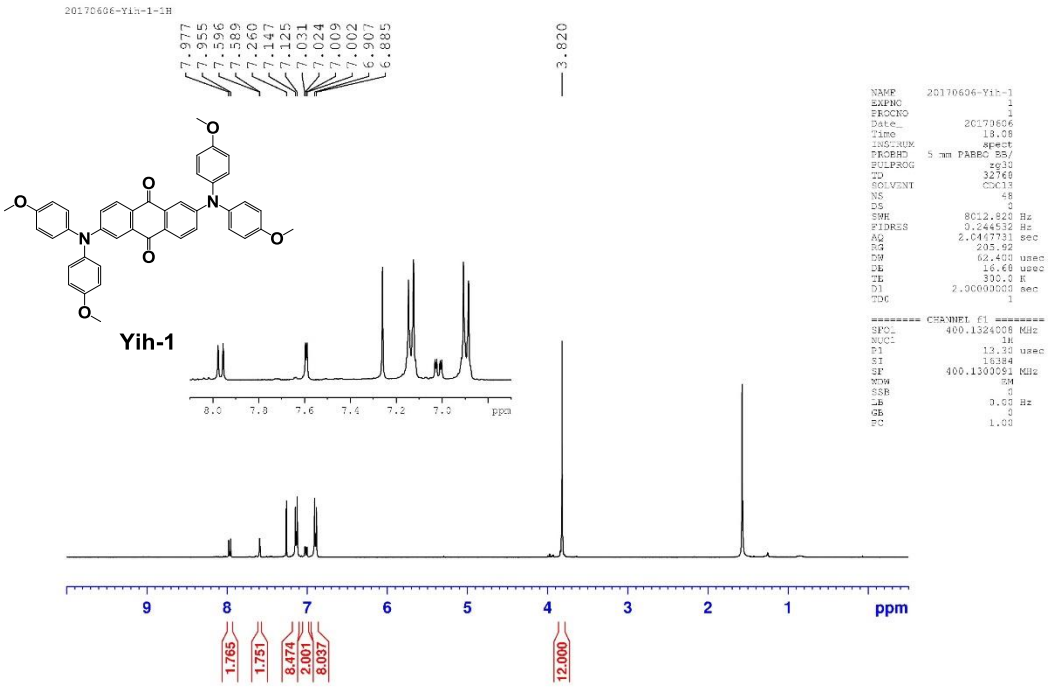

(b)

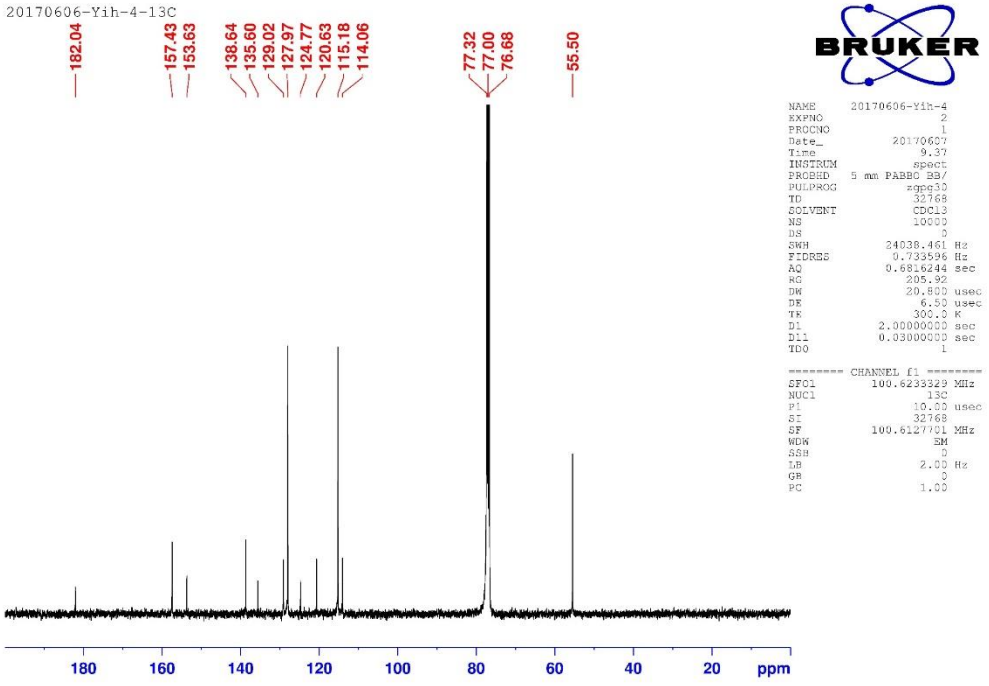

Spectra 135. (a) ^{1}H and (b) ^{13}C NMR spectra of **Yih-1**

(a)

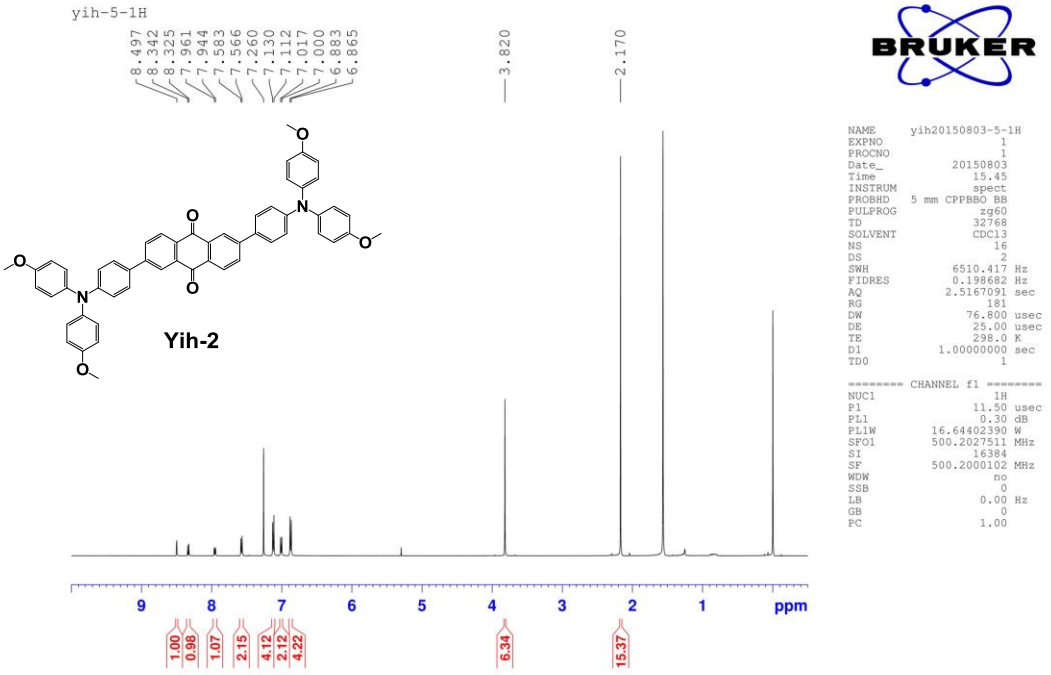

(b)

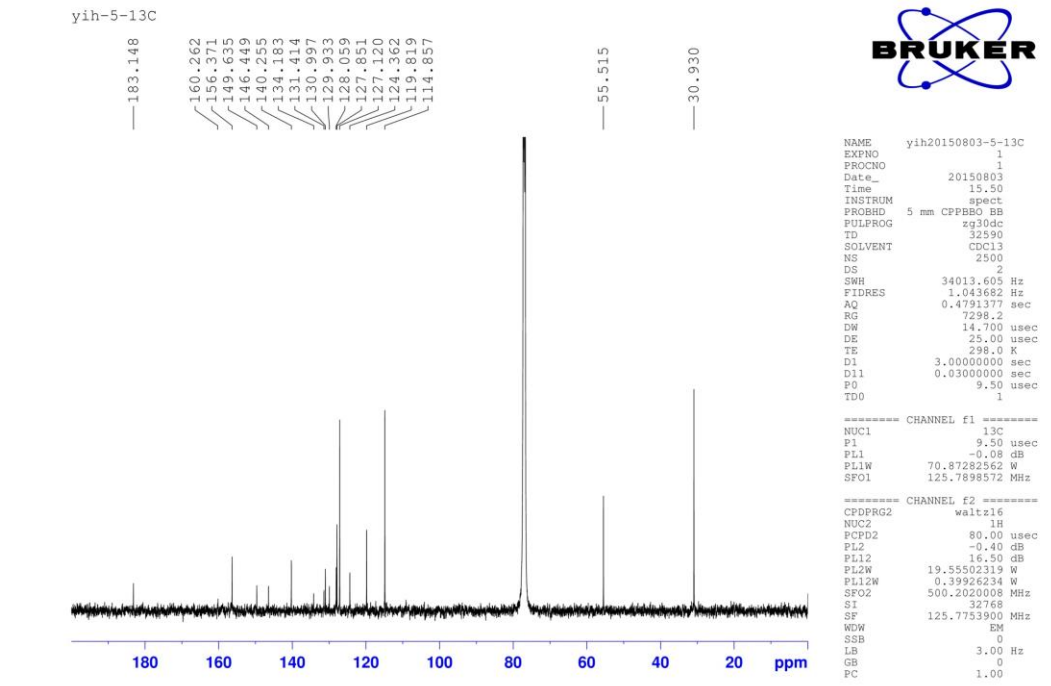

Spectra 146. (a) ^{1}H and (b) ^{13}C NMR spectra of **Yih-2**

(a)

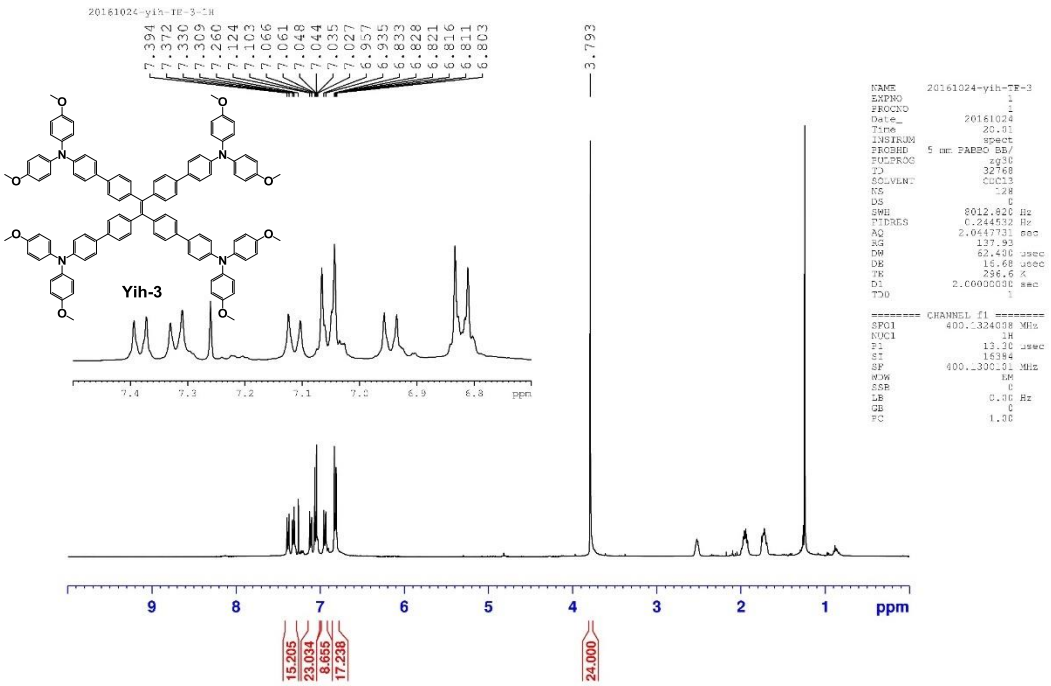

(b)

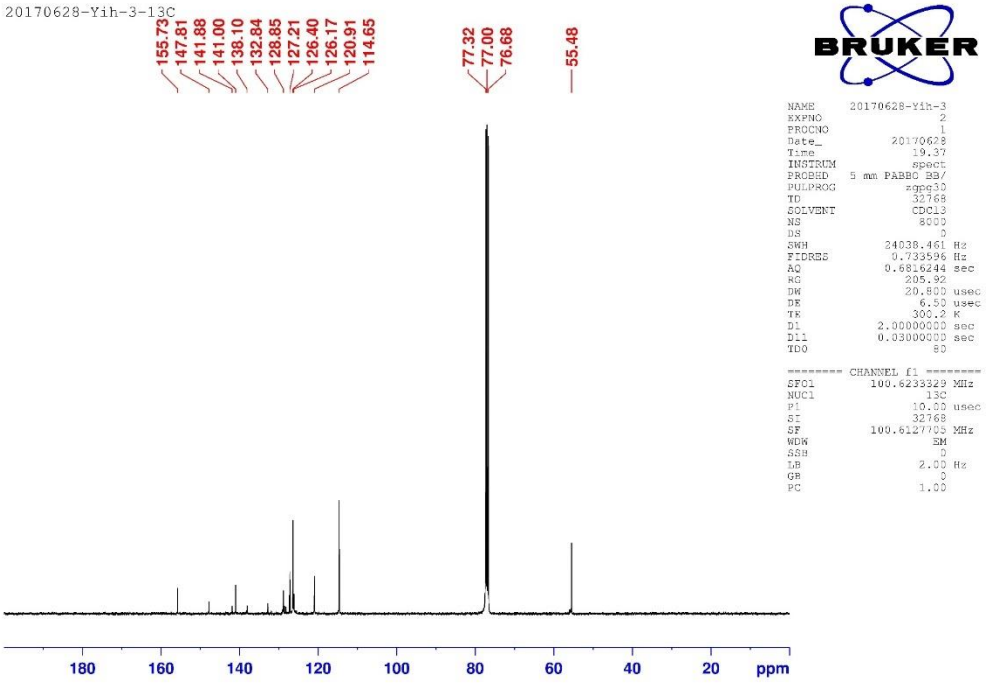

Spectra 157. (a) ^{1}H and (b) ^{13}C NMR spectra of **Yih-3**

(a)

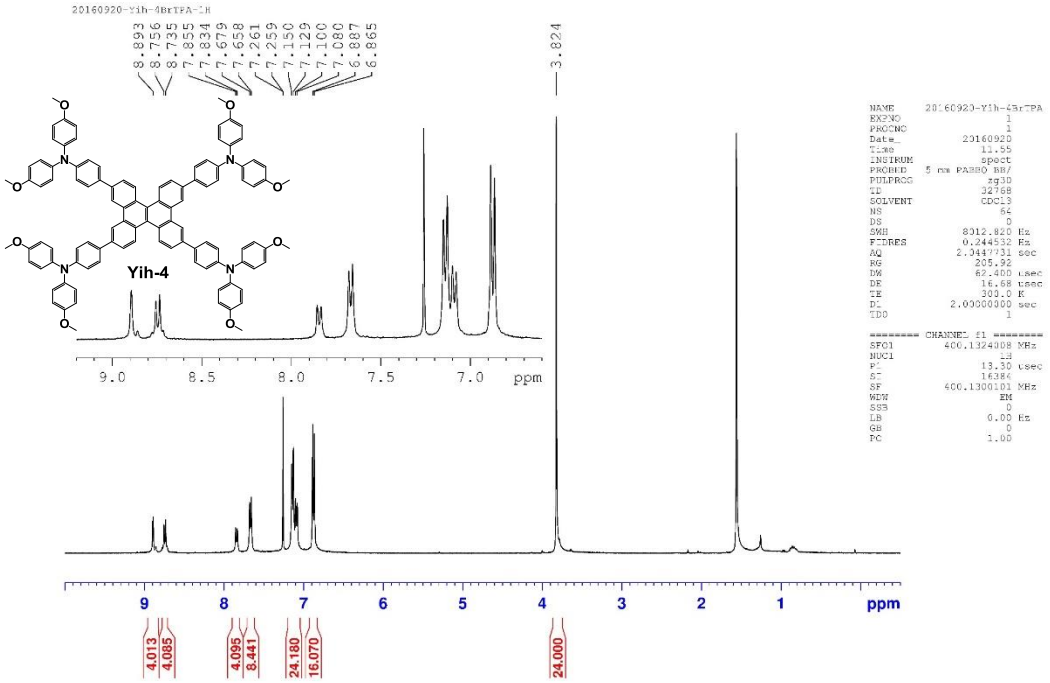

(b)

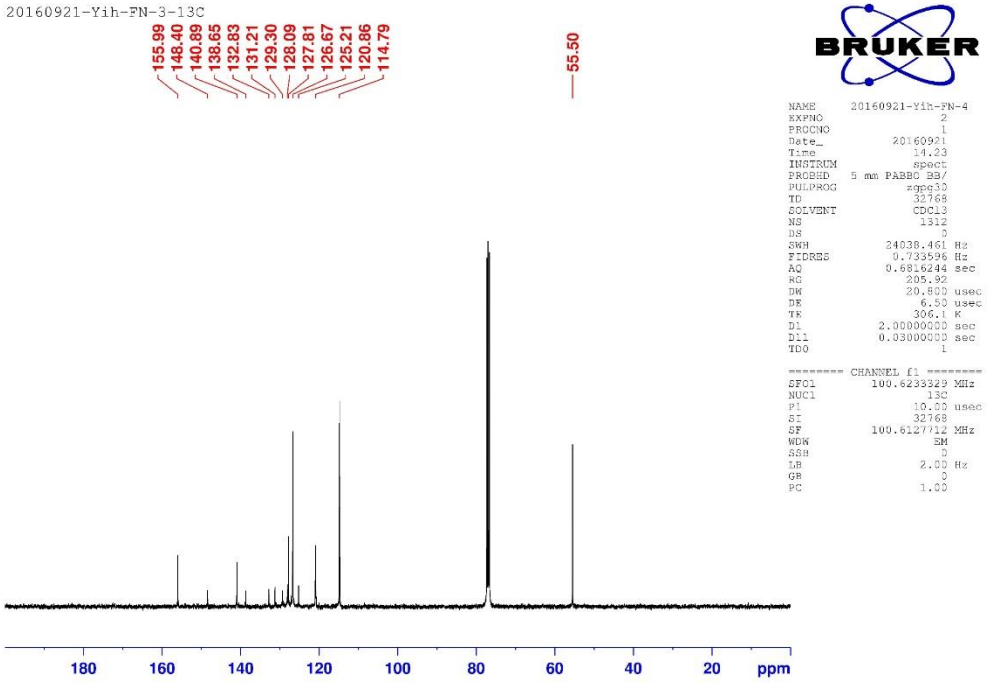

Spectra 168. (a) ^{1}H and (b) ^{13}C NMR spectra of **Yih-4**

(a)

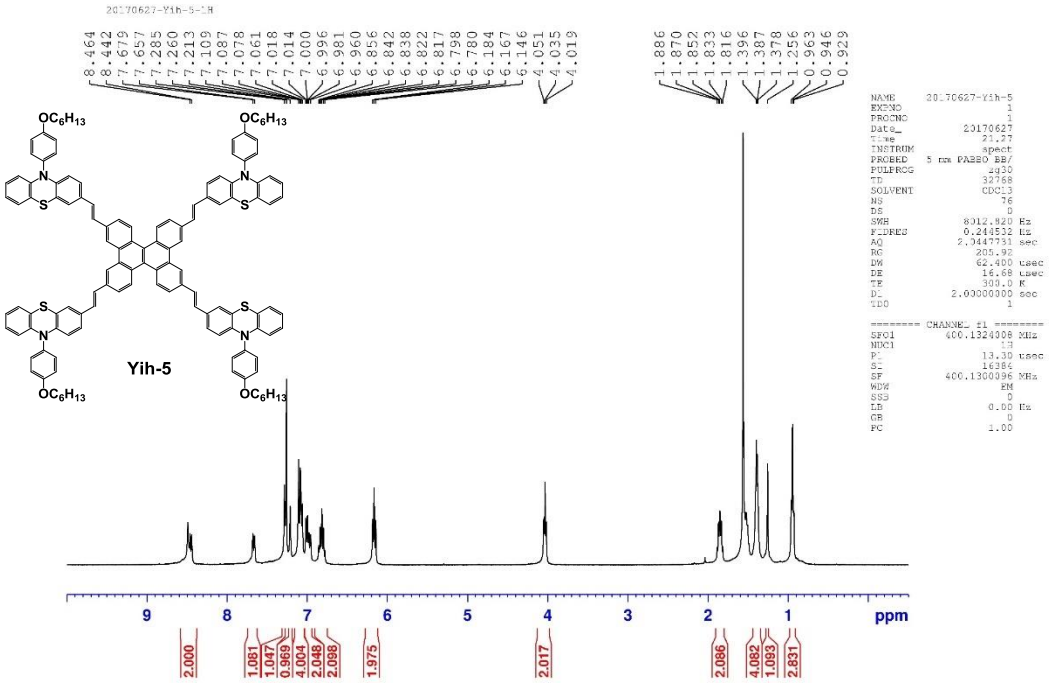

(b)

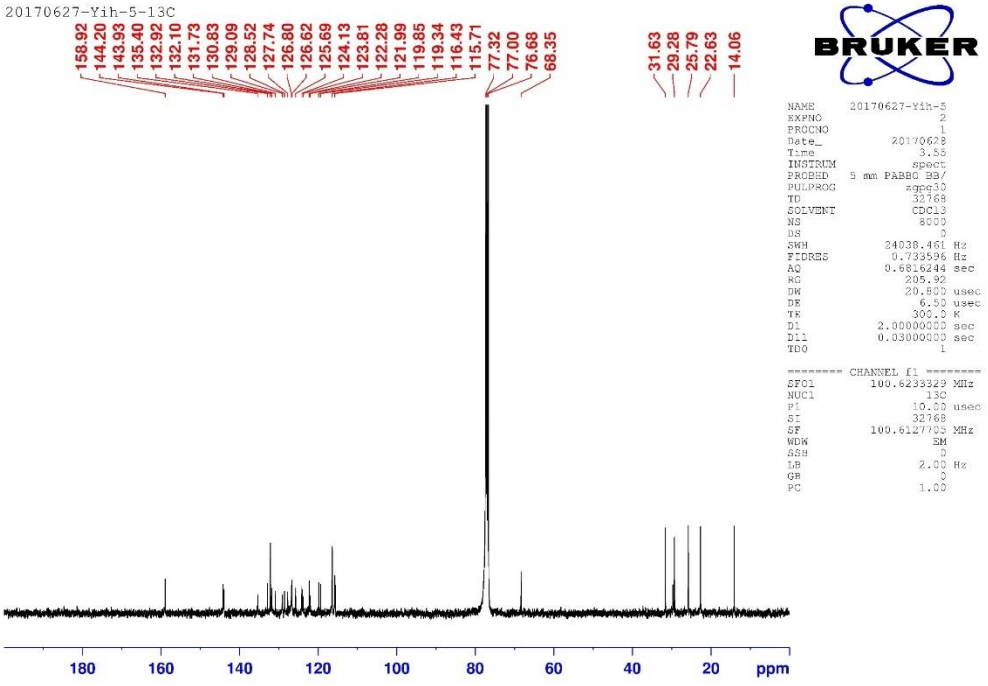

Spectra 17. (a) ^{1}H and (b) ^{13}C NMR spectra of **Yih-5**

(a)

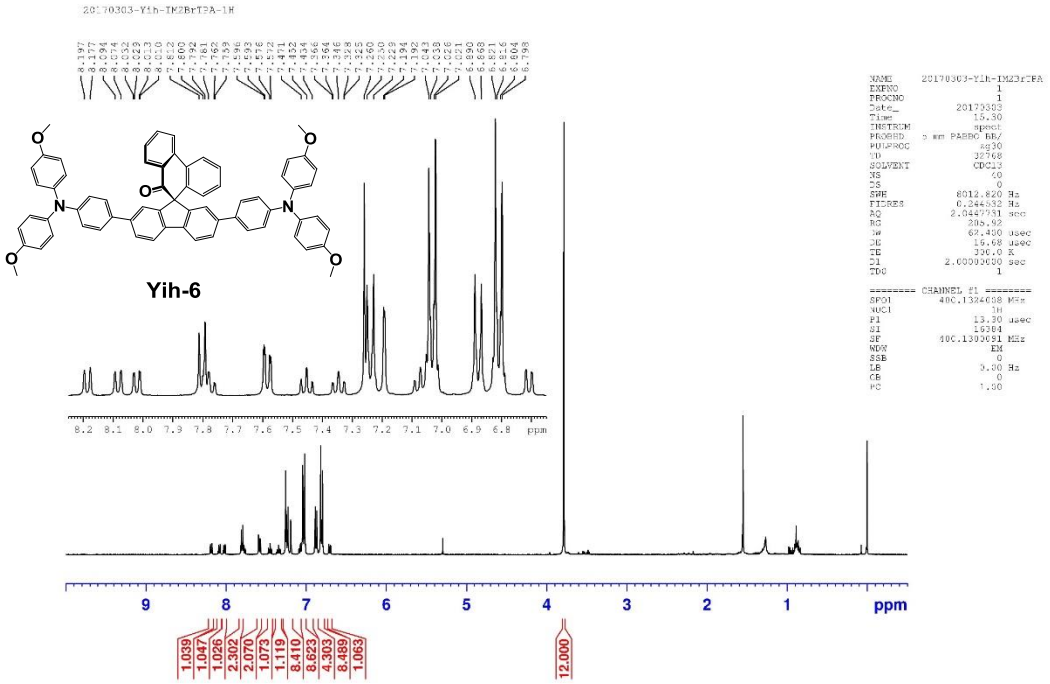

(b)

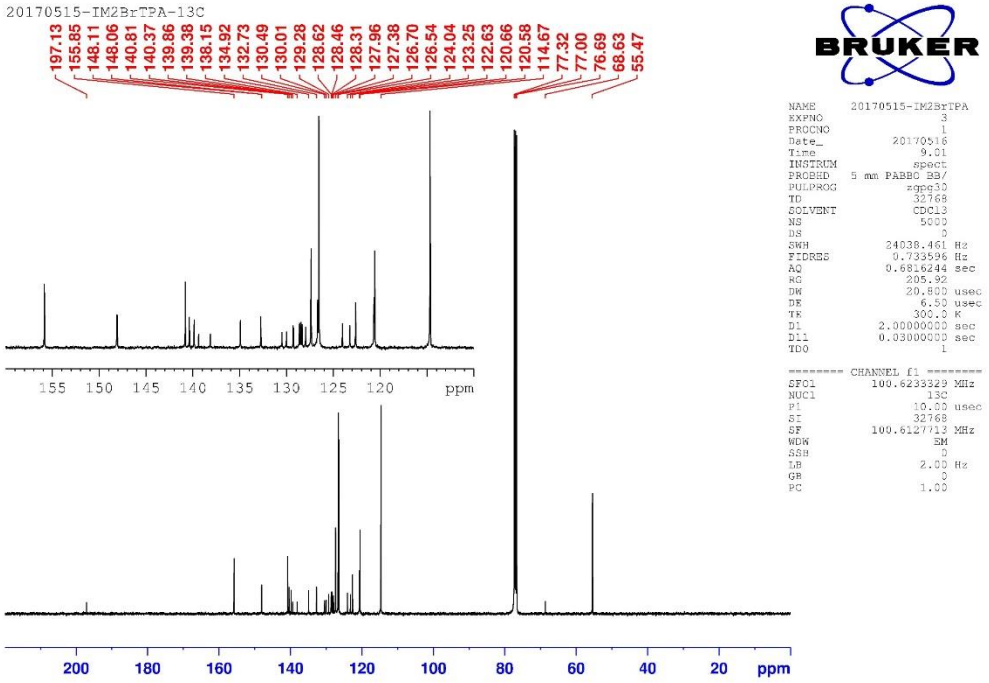

Spectra 18. (a) ^{1}H and (b) ^{13}C NMR spectra of **Yih-6**

(a)

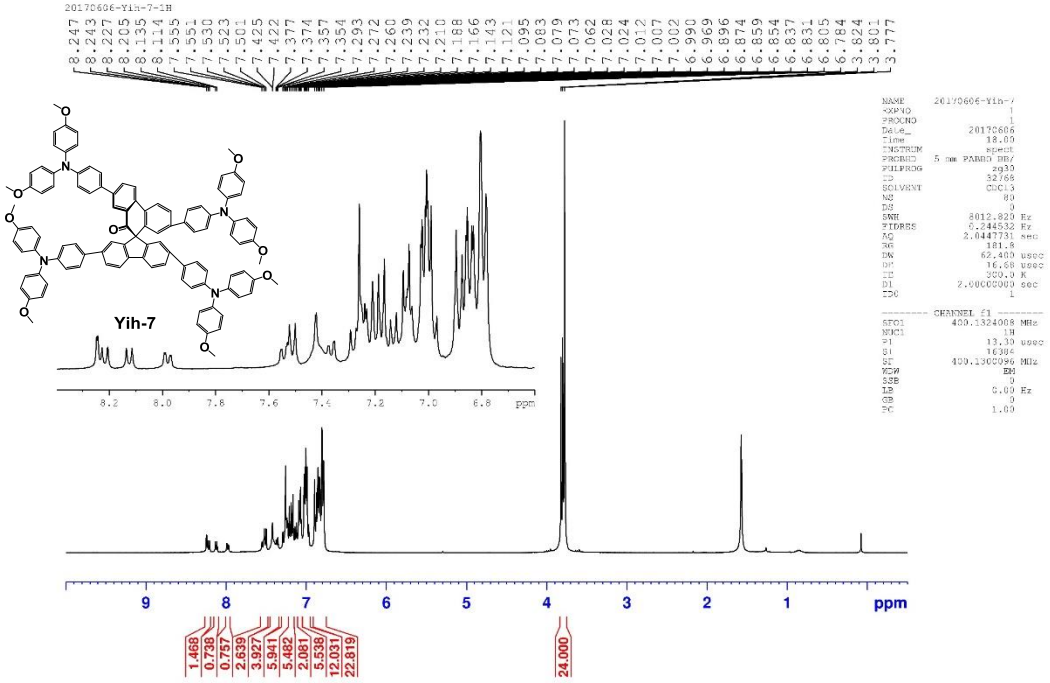

(b)

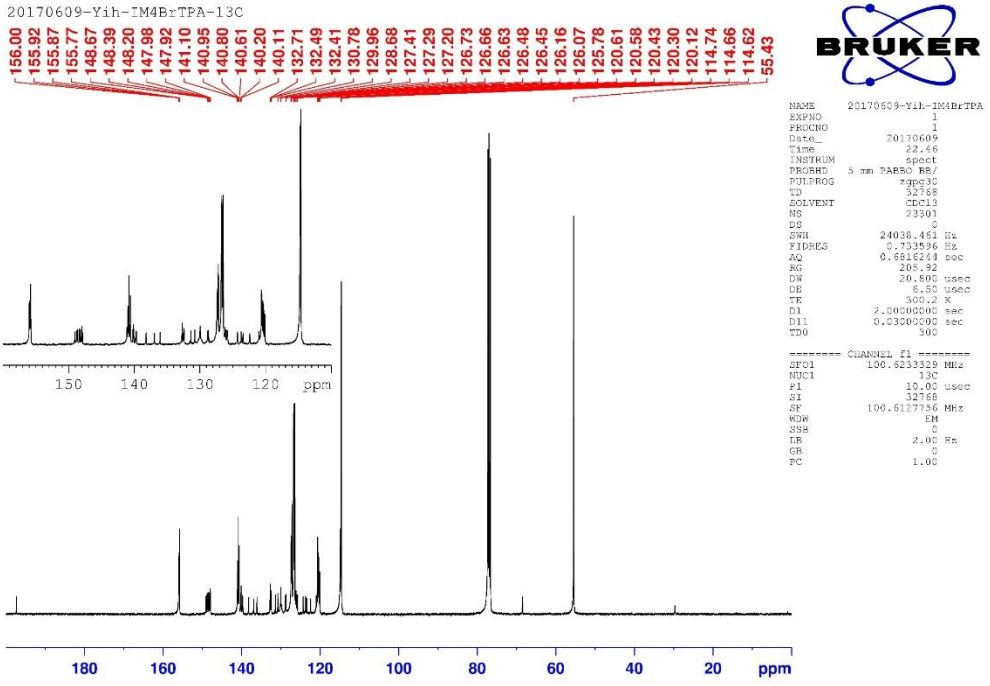

Spectra 19. (a) ^{1}H and (b) ^{13}C NMR spectra of **Yih-7**